TENDON MULTI-SCALE STRUCTURE,

MECHANICAL FUNCTION, AND DAMAGE

by

Andrea H. Lee

A dissertation submitted to the Faculty of the University of Delaware in partial fulfillment of the requirements for the degree of Doctor of Philosophy in Biomedical Engineering

Winter 2019

TENDON MULTI-SCALE STRUCTURE,

MECHANICAL FUNCTION, AND DAMAGE

by

Andrea H. Lee

Approved: _____
Dawn M. Elliott, Ph.D.
Chair of the Department of Biomedical Engineering

Approved: _____
Levi T. Thompson, Ph.D.
Dean of the College of Engineering

Approved: _____
Douglas J. Doren, Ph.D.
Interim Vice Provost for Graduate and Professional Education

I certify that I have read this dissertation and that in my opinion it meets the academic and professional standard required by the University as a dissertation for the degree of Doctor of Philosophy.

Signed: _____

Dawn M. Elliott, Ph.D.
Professor in charge of dissertation

I certify that I have read this dissertation and that in my opinion it meets the academic and professional standard required by the University as a dissertation for the degree of Doctor of Philosophy.

Signed: _____

Randall L. Duncan, Ph.D.
Member of dissertation committee

I certify that I have read this dissertation and that in my opinion it meets the academic and professional standard required by the University as a dissertation for the degree of Doctor of Philosophy.

Signed: _____

Megan Killian, Ph.D.
Member of dissertation committee

I certify that I have read this dissertation and that in my opinion it meets the academic and professional standard required by the University as a dissertation for the degree of Doctor of Philosophy.

Signed: _____

Michael H. Santare, Ph.D.
Member of dissertation committee

I certify that I have read this dissertation and that in my opinion it meets the academic and professional standard required by the University as a dissertation for the degree of Doctor of Philosophy.

Signed: _____

Abhyudai Singh, Ph.D.
Member of dissertation committee

ACKNOWLEDGMENTS

I would like to acknowledge my thesis advisor, Dr. Dawn Elliott, for her excellent mentorship and support of my research interest. I relied on Dawn for a personal, academic, and professional guidance. Her keen insight and depth of knowledge have been a great asset in guiding my dissertation, and I have learned to be an innovative, independent, and insightful scientist and engineer. She also thrived to create a friendly and collaborative space within the lab, where I always felt comfortable communicating my opinions and ideas. My decision to pursue my graduate degree at the University of Delaware was based on Dawn's reputation for her research excellence and mentorship that was well-known in the field, and it was indeed one of the best decisions I have made. Her ability to manage the lab, while leading the department and professional societies, is truly remarkable and impressive. I cannot thank her enough for the excellent training and mentorship I have received that will continue to shape my future professional career.

I would also like to thank several other people that positively influenced various stages of my academic journey. First and foremost, I am grateful to my thesis committee members for their advice and feedback in structuring this dissertation. The committee members made sure that they were available when I needed guidance, and they offered invaluable expertise in the field. They were always engaging and enthusiastic about my research, and this enthusiasm really helped me stay on track. I also thank Dr. Jeffrey Caplan and all the staff members at the Delaware Biotechnology Institute for their incredible depth

of knowledge and generosity. I am so grateful of the support they offered in all the imaging techniques that made this dissertation possible.

I want to thank my fellow colleagues who were a crucial part of my social and professional life. Specifically, I would like to thank the Elliott Lab members including John Peloquin, John DeLucca, Babak Safa, Kyle Meadows, and Ellen Bloom for engaging discussions of ideas, techniques, and concepts that were instrumental to my work. In addition, I would like to acknowledge that discussions of my research with Dr. Mary Boggs and Ryan Locke were extremely helpful. I would also like to thank the former lab members Dr. Spencer Szczesny, Dr. Woojin Han, Dr. Amy Cleason and Justin Hollenbeck for the continuous guidance and friendship. Finally, I want to thank Dr. Mark Buckley, Dr. Mike Zuscik, and Dr. Rob Mooney for giving me the opportunity to conduct my undergraduate research that shaped my initial interest in research.

Lastly, I thank my family and friends that supported my decision to pursue my Ph.D. While my choice to pursue a Ph.D. in biomedical engineering appeared untraditional to my family, they always provided an unconditional support and enthusiasm for my decision. Specifically, I want to thank my grandparents, mother, brother, and sister-in-law for their patience and love. I also want to thank Vincent Sayseng for his unwavering love and emotional support, and this dissertation would not have been possible without him. Lastly, I have to thank my closest friends including Charlie Dangio, Daniel Yu, Dae-Hee Lee, Jeffrey Tuteur, and Ioannis Zampetakis for their friendship and love.

This dissertation is dedicated to my mother.

TABLE OF CONTENTS

LIST OF TABLES

LIST OF FIGURES

ABSTRACT

TENDON MULTI-SCALE STRUCTURE,

MECHANICAL FUNCTION, AND DAMAGE

Andrea H. Lee

Dawn M. Elliott

Tendinopathy, degeneration of tendon that leads to pain and dysfunction, is common in both sports and occupational settings, but the mechanisms for tendinopathy are still unknown. Many studies attribute the initiation of tendinopathy to damage initiated by mechanical loading, leading to microstructural changes. Yet, the link between mechanical loading and microstructural changes, resulting in macroscopic changes, is not fully elucidated. Thus, the objective of the dissertation was to investigate the damage mechanisms and hierarchical structure of non-load- and load-bearing rat tendons, including the tail, plantaris, and Achilles tendons. Damage is defined as an irreversible change in micro-scale deformation that is observable in tissue-scale mechanical parameters. Multi-scale mechanical testing was conducted to investigate the damage mechanisms by simultaneously quantifying tissue-scale mechanical and microstructural changes. The hierarchical structures of these tendons were studied using multiple imaging methods including histology, scanning electron microscopy (SEM), and confocal microscopy.

At the tissue-scale, the transition strain, linear region modulus, and inflection point strain demonstrated strain-dependent changes in rat tail and plantaris tendons, suggesting that these metrics can be used to quantify the effect of damage. At the micro-scale, the micro-scale strain fully recovered following loading and unloading, yet the micro-scale sliding was only partially recoverable in all tendons. The non-recoverable sliding was strain-dependent in the tail and plantaris tendons, and the percentage of non-recoverable sliding was surprisingly similar between the tail and plantaris tendons. The non-recoverable sliding was related to the altered tissue-scale transition strain in the tail and plantaris tendons. Collectively, the micro-scale sliding is responsible for both loading and damage mechanisms for both non-load and load-bearing tendons. Achilles tendon demonstrated some of the mechanical responses observed in plantaris and tail tendons, yet the results were inconclusive due to its complex structure. Studying the hierarchical structure of these tendons demonstrated that fascicles are absent in rat tendons, and thus the fiber is the largest tendon subunit in rats, with the exception of rat tail tendon. We provided a structurally-based definition of fiber as a bundle of collagen fibrils that is surrounded by elongated cells, and the fiber diameters were consistently 10-50 μm, which is conserved across larger species. Understanding the mechanisms responsible for the pathogenesis and progression of tendinopathy can improve prevention and rehabilitation strategies and guide therapies and design of engineered constructs.

Chapter 1

INTRODUCTION

Tendon is a fiber-reinforced load-bearing soft tissue that connects muscle to bone and provides mechanical functions and stability. Tendon is required to withstand large repetitive mechanical forces and deformations and, therefore, is vulnerable to tendon pathologies such as tendinopathy, a clinical presentation of pathology resulting in pain, tenderness, swelling, and functional weakness. [1–4] An incidence rate of tendinopathy is steadily rising and is common in both sports and occupational settings. [3,5–7] Yet, tendon has a poor healing capacity and treatment options are limited. [8–11] The current rehabilitation strategies are not sufficient to completely reverse pathology once initiated, [2,12] leaving disorganized scar collagen with inferior mechanical properties, [3,5,9] and thus prevention of tendinopathy is important.

Many studies attribute the initiation of tendinopathy to damage initiated by mechanical loading that leads to microstructural changes. [1,2,4,13–17] Still, the specific mechanism of tendon damage, spanning multiple length scales, is unknown. Specifically, the relationship between micro-scale structural changes and tissue-scale functional changes is not well understood. In addition, a quantification of tendon damage remains challenging, in part because a precise definition with appropriate engineering context and multi-scale understanding of tendon structure and mechanics have not been applied to study tendon damage.

Thus, this thesis will investigate the damage mechanisms by studying the multi-scale mechanics of tendons and hierarchical structure with varying mechanical functions. **Chapter 2** will include pertinent background information to demonstrate the significance of the dissertation. **Chapter 3** will study the damage mechanisms of non-load-bearing tendon using the multi-scale mechanical testing and will establish a method of tendon damage quantification that will be used throughout the thesis. The effects of freezing on tendon mechanical properties and damage mechanisms at multi-scale will be presented in **Chapter 4**. **Chapter 5** will focus on the hierarchical structure of tendons by using multiple imaging methods to provide definitions of each hierarchical scale based on the characteristic features. **Chapter 6** will demonstrate the damage mechanisms of load-bearing tendons using a similar approach used in Chapter 3. **Chapter 7** will briefly discuss a pilot study that investigated the effect of aging on the damage mechanisms. Finally, in **Chapter 8**, a summary and conclusion of this dissertation are provided, and future studies based on the findings of the dissertation are proposed. This knowledge can improve prevention and rehabilitation strategies and identify structural targets for functional regeneration, repair, and replacement. In addition, the experimental design of the dissertation can also be applied to other fiber-reinforced tissues (e.g., ligament, meniscus, annulus fibrosis) in the future.

Chapter 2

BACKGROUND

2.1 Tendon Structure

Tendon is mostly composed of fibrous collagens (65%-80% of dry weight) that are mostly aligned in one direction, [18–20] and it is assembled into a complex hierarchical organization, spanning multiple length scales (Figure 2.1). In addition, it is composed of 1-2% of elastin [21,22], ~1% proteoglycans (PGs), [23] other minor collagens, proteins, and water. [24] The majority of the collagen is type I with small quantities of type III collagen and other types of collagen. [25,26] Collagen is a main structural protein that constitutes various connective tissues in the human body. At the molecular-scale, collagen is composed of three peptide chains (i.e., α-helices), which wrap into a tight triple helix. [27,28] Each triple helix is made of repetitious amino acid, and the three peptide chains are stabilized by hydrogen bond. [29,30] At either end of the collagen chain, there is a specialized amino acid, hydroxylysine, that can form cross-links of collagen molecules to create a structure with high loading capacity. [31,32] This structural packing allows type I collagen to be stronger than steel, gram for gram, [31] and withstand high-magnitude and/or repetitive loading.

At the nano-scale, the collagen molecules spontaneously assemble with regularly staggered ends, and adjacent collagen molecules displace from one another by 67 nm to form a fibril. This particular staggering of collagen molecule gives rise to a characteristic feature of a striation of collagen fibrils, which is often observed by electron micrographs.

[33,34] At the micro-scale, it is widely accepted that the collage fibrils assemble to form a fiber, and fibers form a fascicle at the tissue-scale, which is the largest subunit in tendon. [19,35,36] However, it is important to point out that there is currently a disagreement on the absence/presence of fiber, and the definitions of these structures vary among published studies. [36]

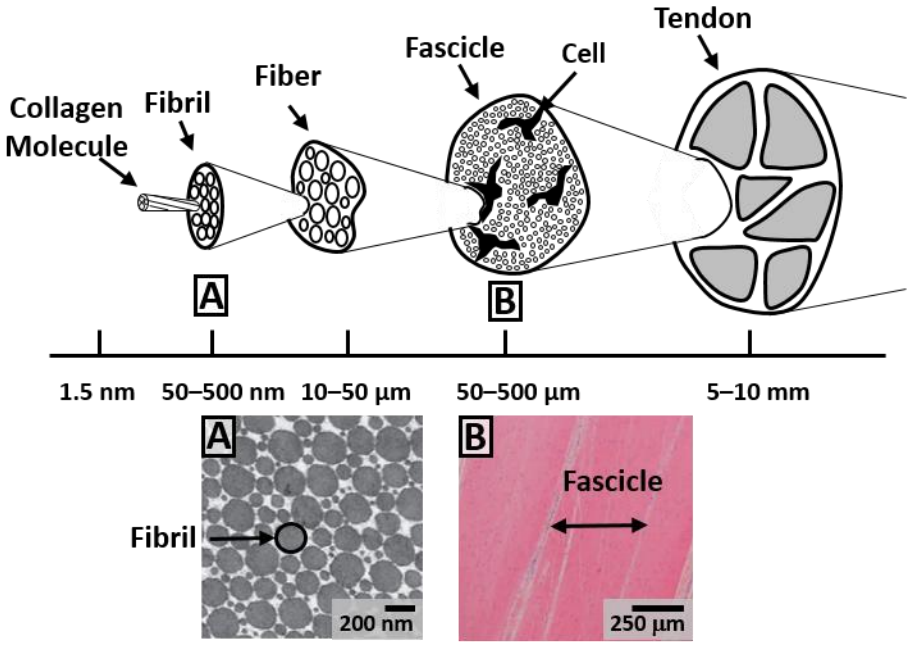

Figure 2.1: Hierarchical structure of tendon. Collagen molecules assemble with regularly staggered ends to form a fibril. Collage fibrils assemble to form a fiber, and fibers form a fascicle at the tissue-scale, which is the largest subunit in tendon. A) Electron micrographs of fibrils of rat tail tendon and B) H&E staining of the equine tendon are shown. [37] This schematic is adapted from: [19,38]

2.2 Tendon Mechanical Function

Tendon connects muscle to bone and can withstand high and/or repetitive mechanical forces and deformations in uniaxial tension, which is a primary direction that

is loaded *in vivo*. [39] Due to its intricate assembly of hierarchical collagen structure, tendon exhibits a non-linear mechanical response under tension (Figure. 2.2). At low strain, a stress-strain response of tendon is highly non-linear, and this region is called a toe-region (Figure 2.2). This toe-region is associated with uncrimping, realignment, and elongation of collagen at multiple length scales. [40–42] At higher strain, after the initial non-linear region, the stress-strain response of tendon is more linear with an apparent modulus being relatively constant, and this region is called a linear-region. Once tendon is loaded to a higher load and becomes damaged, the load-bearing capacity of tendon can gradually decrease and completely fail or rupture.

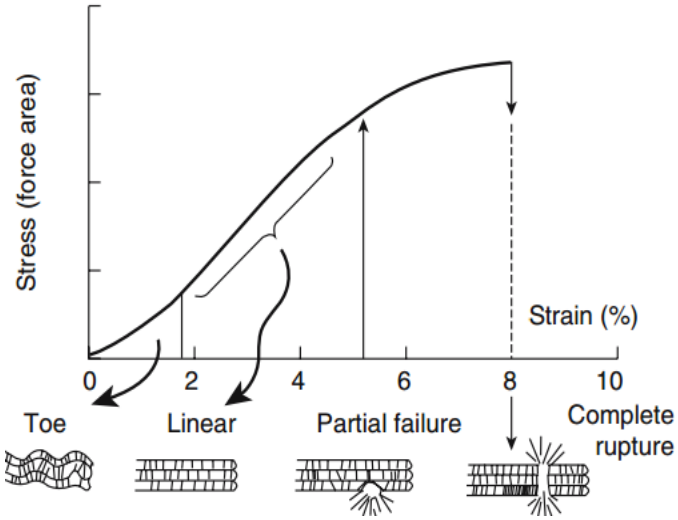

Figure 2.2: Schematic showing stress-strain curve. The stress-strain curve is associated with structural deformation at the micro-scale, where an accumulation of damage can lead to complete rupture at high strain. [43]

2.3 Tendon Structure-Function (S/F) Relationships

The mechanical function of tendon is closely related to the hierarchical structure that spans multiple length scales, and thus a structure-function (S/F) relationship is

important in addressing loading mechanisms of healthy tendon as well as injury, degeneration, and aging of tendon. The collagen structure of healthy tendon is densely packed and is highly aligned. However, the structure of tendinopathic tendon has an abnormal collagen structure and arrangement, in addition to an altered level of PGs, collagen, vascularity, and cell viability. [2,44] A replacement of collagen type I to type III, [26] decrease in accumulation non-enzymatic cross-links, and increase in cross-sectional area (CSA) were also observed in tendinopathic tendons. [2,5,45] These structural changes lead to mechanical changes including lower tendon stiffness, modulus, and peak stress. [46,47] Thus, tendinopathy affects structures at multi-scale, which leads to inferior mechanical properties.

2.4 Initiation of Tendinopathy and Damage

Mechanical loading is one of the primary factors that regulate tendon life-cycle. In healthy tendon, mechanical loading is required to maintain tendon homeostasis and preserve tendon integrity. [12,48–50] However, high magnitude and/or cycles of mechanical loading is speculated to cause tendon damage, [51,52] which is supported by an increase in the number of patients suffering from tendinopathy in sports [5,9,15] and occupational settings that require repetitive tasks. [6,7] Thus, overloading, mechanical loading that exceeds homeostatic loading, that leads to damage is theorized to be the major contributor to tendinopathy initiation. This thesis will investigate the damage mechanism by studying the relationship between micro-scale structural change and tissue-scale functional changes after mechanical loading.

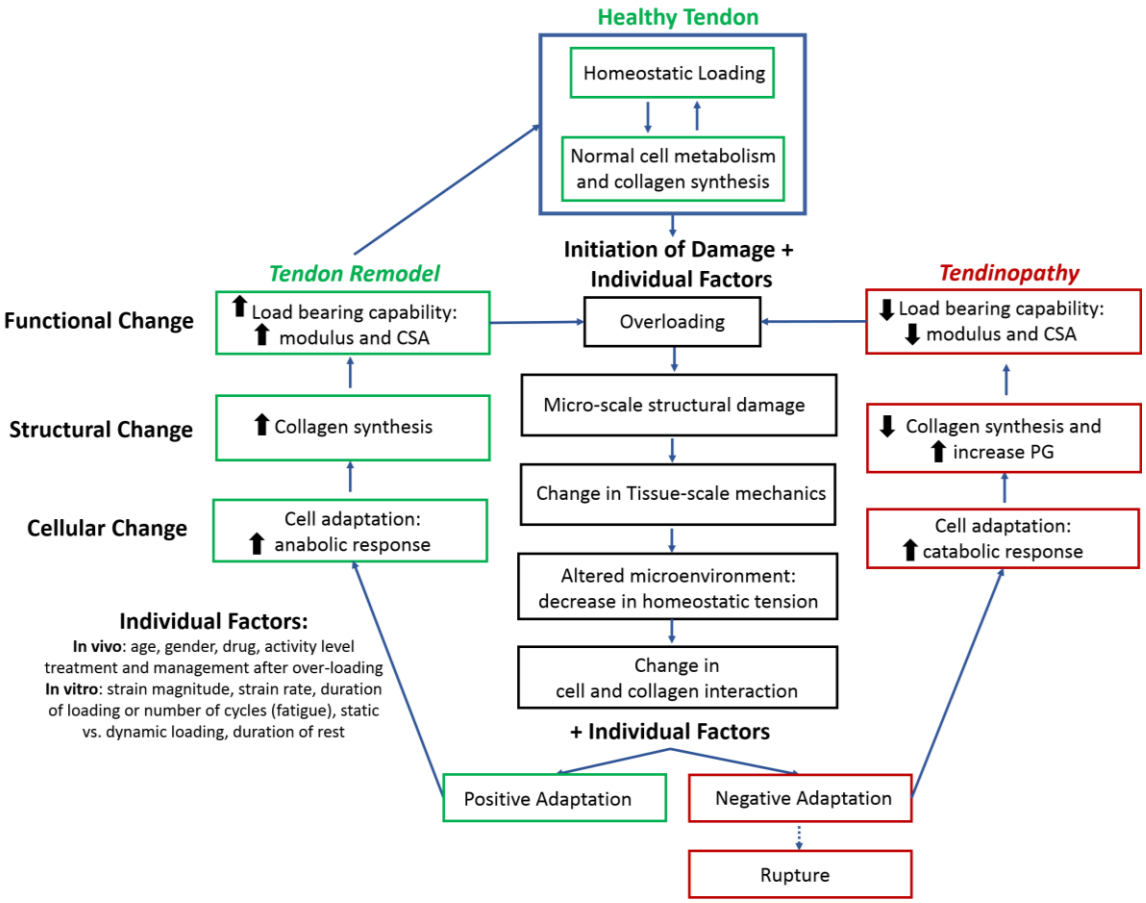

Figure 2.3: Model of initiation of tendinopathy. This dissertation focuses on the critical gap, early mechanical contribution immediately after overloading, that is outlined in black.

As a part of the thesis, a novel model on tendinopathy initiation was developed and the thesis will address a gap in knowledge shown in the model (Figure 2.3). Tendon remodeling and tendinopathy have been widely studied in advance stages, after either positive or negative adaptation has taken place (i.e., green and red boxes). [12,50] Previous studies demonstrated rehabilitation and exercise increase anabolic response observed in protein and gene expression changes, [53–55], leading to superior structural and functional

changes (i.e., green boxes). [4,56–58] On the other hand, tendinopathy increases catabolic response, [49,59,60] leading to inferior structural and functional changes (i.e., red boxes). [46,47,61] Yet, the gap in knowledge is that the process that leads to either negative or positive adaptation is largely speculative (i.e., black boxes). This thesis will investigate the effect of over-loading on the micro-scale structural damage that is observable as a change in tissue-scale mechanics (i.e., black boxes), which can potentially lead to tendon remodel or tendinopathy.

The general assumption of the model is that damage is a part of tendon life-cycle, and mechanical loading is a primary factor that initiates damage. For tendon to undergo any function change, whether that is a positive or negative adaptation, I hypothesize that mechanical loading is needed to deviate from homeostasis and cannot be achieved without damage. To support this, mechanical and structural changes were observed after fatigue loading at a low-load that only reached a toe-region [62] and no cell death was observed after loading to a strain magnitude that has been shown to alter micro-scale structure. [63,64] In addition, a previous study has shown that cells can detect collagen kinks that are produced by overloading and migrate to the site. [65] Note that the thresholds that distinguish homeostatic loading from overloading and positive adaptation from negative adaptation are likely to be dependent on multiple factors observed in vitro and in vivo settings (Figure 2.3).

2.5 Definition of Damage

One of the hurdles in addressing the gap in knowledge is due to a lack of a precise definition of tendon damage with appropriate engineering context. In this study, we define damage, consistent with the definition established in engineering and applied to other materials, as an irreversible change in the microstructure that is related to a change in macroscopic mechanical parameters. [66] Examples of the microstructural changes include microcracks in metals, [66–69], interlamellar debonding in polymers, [70,71] matrix microcracking in composites, [72,73] and voids in ceramics [74]; all of these irreversible rearrangements in microstructure produced impaired macroscopic mechanical properties, such as lowered modulus. In tendon, histological [75] and microscopic [52,76] studies have shown microstructural changes that appear to represent damage; however, these were not directly linked to mechanics. Similarly, changes to tissue-scale mechanical behavior, such as reduced modulus and decreased failure stress and strain, are well-studied when tendon is loaded to high stresses and/or for multiple cycles. [3,14,51,77,78] As mentioned above, while these are likely in response to microstructural damage, the link to microstructural change is not fully elucidated. Thus, evaluation of tendon at multiple length scales to identify the microstructural source is a critical aspect in the study of tendon damage.

Another key feature in the definition of damage, in addition to microstructural changes described above, is that it must be irreversible. Tendon, due to its viscoelastic properties, can partially recover its tissue-scale mechanical properties after loading. [21,25] However, many studies attempted to quantify the tissue-scale mechanical response immediately after loading, without decoupling the effects of time-dependent recovery from

the permanent change. [26,27] Quantification of damage must distinguish between the irreversible (non-recoverable, permanent) and recoverable changes in mechanical parameters (strictly related to mechanical effects, separate from cell contributions to healing).

Rodent tendons are widely used to study tendinopathy and to address fundamental physiological questions about development, growth, and remodeling. While larger animals may better represent human tendons, it is difficult to simultaneously analyze the whole tendon structure and mechanics at multi-scale. Most commonly, parts of the tendon are excised from large animal tendons to characterize only limited aspects of the S/F relationship. [51,76,79] Rodent tendons, on the other hand, are small enough to study the whole tendon S/F relationship. This thesis will focus on rat tendons to address the tendon damage mechanisms and the effect of on S/F relationship of the whole tendon at multiple length scales.

2.6 Functionally Distinct Tendon

Tendon hierarchical structure depends on the mechanical function of tendon. Specifically, there are key differences between non-load- and load-bearing tendons in equine and bovine tendons. These differences include tendon mechanics, [80–82] fascicle and interfascicular mechanics, [80,81,83] interfascicular matrix composition, [84] cross-link density, [82] and fibril deformation. [82,85] It is well-accepted that mechanical function dictates the hierarchical organizations, [36] and thus the damage mechanisms between functionally distinct tendon may differ. To study the S/F relationship and damage

mechanisms of rat tendons, the hierarchical organization and damage mechanisms must be studied in tendons with varying mechanical functions.

2.7 Research Objectives

The objectives of this dissertation were to investigate the damage mechanisms and hierarchical structure of non-load and load-bearing rat tendons. Damage is defined as an irreversible change in the micro-scale deformation that is observable in tissue-scale mechanical parameters. Multi-scale mechanical testing was conducted on rat tendons to investigate the damage mechanisms by simultaneously quantifying tissue-scale mechanical and microstructural changes. The hierarchical structure of these tendons was studied using multiple imaging methods including histology, scanning electron microscopy (SEM), and confocal microscopy. Collectively, shear measured at the micro-scale, which was measured as a micro-scale sliding, was a load transfer mechanism, and a non-recoverable sliding, which indicates a residual sliding remaining after mechanical loading, was a damage mechanism for both non-load and load-bearing tendons. Analysis of the hierarchical structure of these tendons demonstrated that rat tendons do not contain fascicles and thus a fiber is the largest tendon subunit, with the exception of rat tail tendon.

Chapter 3

INVESTIGATING TENDON DAMAGE MECHANISM IN RAT TAIL TENDON BY MEASURING MULTI-SCALE RECOVERY FOLLOWING TENSILE LOADING

Based on published work: Lee, AH.; Szczesny SE.; Santare, MH.; Elliott, DM. "Investigating Mechanisms of Tendon Damage by Measuring Multi-scale Unloaded Recovery Following Tensile Loading,": Acta Biomaterialia, **2017** 57:363-372.

3.1 Introduction

Damage in tendon at the tissue-scale has been proposed to initiate when tendon is loaded beyond a strain threshold, [86–89] but metrics to define the damage threshold are not well established. While some studies use a non-recoverable length (i.e., laxity) to identify the threshold, [17,90,91] others use the beginning of strain-softening behavior. [51,92] A recent study hypothesized that the inflection point in the stress-strain curve, which marks the point where the stress-strain response shifts from strain-stiffening to strain-softening, may mark the damage threshold in fibrous tissue. [93] Thus, we investigated if the inflection point in the stress-strain curve represents the damage threshold or onset of damage.

The effect of mechanical loading on microstructure that leads to damage is unknown. Specifically, the microstructural location for tendon damage is unclear. Some studies have identified structural changes of fibrils in the form of collagen kinking and discontinuities [51,52] or increase in D-period, [94] while other studies suggest damage is

localized to the structure that connects adjacent collagen fibrils together. [38,80] It is possible that both occur or that damage on one location may precede the other. Mathematical shear lag modeling of tendon has suggested that plastic deformation of the structure that allows micro-scale sliding replicates the tissue-scale mechanical behavior of tendon fascicles (matching the equilibrium stresses and predicting fibril strain); however, elastic deformation of fibrils cannot replicate this tissue-scale mechanical behavior. [38,95] Thus, shear lag modeling suggests that microstructural damage is localized to the structure that allows micro-scale sliding and produces the observed changes in mechanical response at the tissue-scale. In this study, we aim to experimentally identify the microstructural source of damage by investigating tendon structure and deformation at the micro-scale.

In summary, the objective of this study was to elucidate the tendon damage mechanisms. The key definitions of damage, an irreversible change in the microstructure that is observable in the macroscopic mechanical parameters, were applied. Microstructural changes were quantified at the micro-scale and mechanical changes were simultaneously quantified at the tissue-scale. Experiments were designed to ensure damage was measured only as a non-recoverable change in mechanical behavior by allowing the tissue to recover after potentially overloading, and the threshold for damage initiation was determined.

3.2 Materials and Methods

3.2.1 Sample Preparation

Rat tail tendon fascicles were harvested from eleven 6-8 month old Sprague-Dawley male rats. The entire tail was excised, and we further dissected an 8 cm long

segment of the tail from the proximal end with its skin intact. These tails were previously frozen at -20^{o}C, where the maximum number of freeze-thaw cycle was limited to three. [96] On the day of the experiment, each fascicle was pulled from the tail for mechanical testing using forceps. We stained each sample with 10 μ g/ml 5-DTAF (5-(4,6-Dichlorotriazinyl) aminofluorescein, Life Technologies) to minimize the effect of DTAF on mechanics. [97] We tested on a custom-made uniaxial testing device with a PBS bath mounted on an inverted confocal microscope (LSM 5 LIVE, objective Plan-Apochromat 10x/0.45) as previously described. [38] Each sample was soaked in PBS to stabilize pH at room temperature for at least 3 hours before testing to allow the sample to reach equilibrium. [98] All the samples were kept at room temperature from the beginning of DTAF staining to the end of mechanical testing.

3.2.2 Mechanical Testing Protocol

Mechanical testing on a total of 8 groups with n=7 fascicles per group was performed. Each fascicle was randomly assigned to a grip strain of 2, 4, 6, or 8%, while also randomizing the number of freeze-thaw cycles for each strain group (the average freeze-thaw cycles were 2 per group). In addition, within each strain level, each fascicle was randomly assigned to either ‘No Rest’ or ‘Rest’ group. We preloaded each fascicle to 0.5g (~5mN) to define the reference length and preconditioned with 5 cycles of 4% grip strain (i.e., grip-to-grip displacement). After ramping to the strain level, we held the strain level constant for 15 min to reach an equilibrium followed by unloading to the reference length. The ‘No Rest’ or ‘Rest’ group was used to compare the effect of 60-minute

unloaded rest on tissue-level parameters and separate the recoverable from non-recoverable deformation (Figure 3.1a). The No Rest group was immediately loaded to failure after unloading, whereas the Rest group was held at its reference length for 60 minutes before loading to failure.

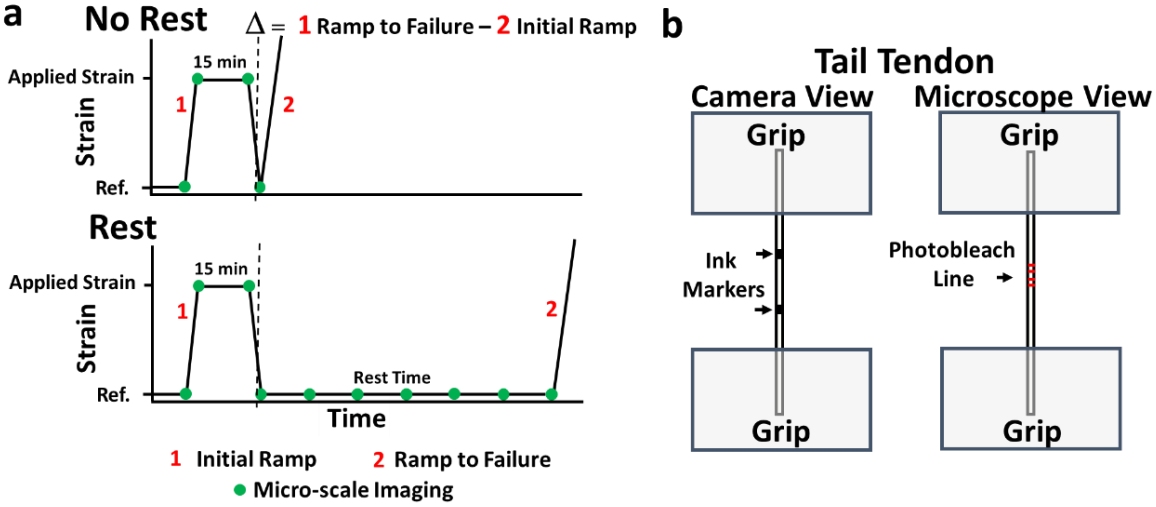

Figure 3.1: Mechanical loading profile schematic. (a) Definition of Δ = Ramp to Failure – Initial Ramp was used to quantify damage when loaded to applied strain (i.e., strain levels 2, 4, 6 or 8%). For the No Rest group, fascicle was loaded to failure immediately after unloading, whereas the Rest group was allowed to rest for 60 minutes at the reference length before loading to failure. The green dots represent when confocal images were taken to quantify micro-scale deformation. Dashed line represents when tendon was unloaded to the reference length. All the loading and unloading rates were 1%/s. (b) Ink markers were applied to tail tendon to optically measure the applied strain using a CCD camera. On the other side of the tendon, four photobleached lines were applied using a confocal microscope to measure the micro-scale deformations. The photobleach lines are not to scale and enlarged for visualization.

The tissue-scale parameters calculated from the initial ramp were defined as 'Initial Ramp' and the parameters calculated from the ramp-to-failure were defined as 'Ramp to Failure' (Figure 3.1a). The strain rate for all loading and unloading was 1%/s, and only the

fascicles that failed in the mid-substance were included in the following analysis. We excluded samples that failed at the grip (n=2) or slipped during preconditioning (n=3) from this study and additional fascicles were added to achieve our target sample size based on a power analysis. Thus, all the samples failed at mid-substance.

3.2.3 Data Acquisition

To measure the tissue strain, we applied two ink markers directly on the tendon using a permanent marker and imaged with CCD camera to track displacement of markers using a digital image correlation (Figure 3.1b; Vic 2D, Correlated Solutions). The optically calculated strain is referred to as tissue strain, and this is different from the grip strain (e.g., 2, 4, 6, or 8%). The tissue strain quantified at the end of Initial Ramp was labeled as 'applied strain', and this is the maximum tissue strain measured during the Initial Ramp. In addition, we quantified the transverse strain and micro-scale parameters (i.e., micro-scale strain and sliding) using the confocal microscope. The confocal image stacks (15 fps; $0.53 \times 0.53 \times 1.24$ μm pixel−1) were taken after preconditioning to reconstruct the cross-sectional profile of each sample. This profile was fitted with an ellipse to determine the sample cross-sectional area by measuring both the major and minor axes. We acquired images at 10 time points, represented by green dots (Figure 3.1a): after preconditioning (i.e., reference image), at the beginning and end of the relaxation period, and every 10 minutes during the 60-minute rest period. Note that data for No Rest groups can only be quantified after preconditioning, at the beginning and end of the relaxation period. Thus,

we only report data acquired using the confocal microscope for Rest groups, but we have carried out identical staining and imaging procedure for both No Rest and Rest groups.

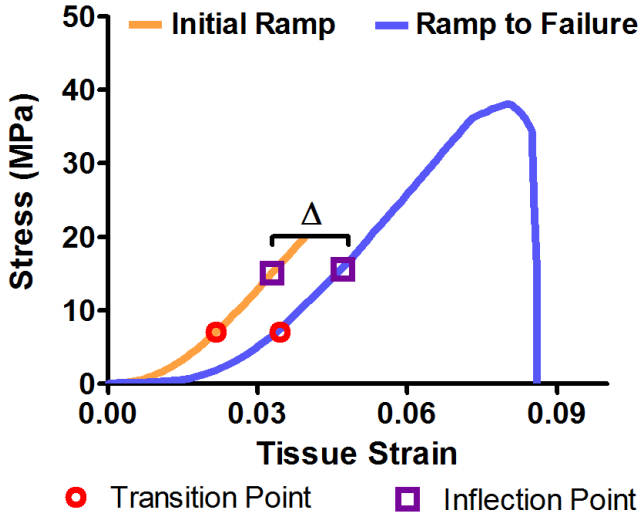

Figure 3.2: Tissue-scale parameter quantification. The representative σ-ε response of the tail tendons is shown, where Initial Ramp is represented as an orange and Ramp to Failure is represented as a blue line. The stress relaxation and unloading are not shown in the graph. Transition point (red open circle), inflection point (purple open square), and linear region modulus (linear line between transition and inflection points) were quantified for both ramps.

3.2.4 Data Analysis – Tissue-scale parameters

The tissue-scale stress-strain (σ-ε) data was constructed by dividing the tensile force by the original cross sectional area to calculate stress and tracking marker displacement to calculate tissue strain. The σ-ε data up to an inflection point, defined as a point where the stress-strain curve shifts from strain-stiffening to strain-softening, [93] was used to determine transition point and modulus. This was to ensure that we were quantifying the modulus of the linear region before strain-softening (Figure 3.2). The

inflection point, was calculated by fitting a cubic smoothing spline using the *csaps* function in Matlab and finding the first zero crossing point of the second derivative.

The σ-ε data from zero to the inflection point was then fit with a nonlinear constitutive model (Eq. 1) to simultaneously calculate linear region modulus (E), transition strain (p), and transition stress (q), where the transition point was defined as the end of the nonlinear toe-region (Figure 3.2) [99]:

$$\sigma = \begin{cases} A * (exp(B\varepsilon) - 1), & \forall \varepsilon \leq p \\ E * (\varepsilon - p) + q, & \forall \varepsilon > p \end{cases} \quad (3.1)$$

This equation was fully defined by three parameters: p and the constants A and B. From algebraic evaluation of Equation 1, at the transition point (i.e., $\varepsilon = p$) the transition stress can be expressed as $q = \sigma(p) = A * (exp(Bp) - 1)$.

Using the Matlab function *fmincon*, the parameter values (A, B, and p) were simultaneously optimized to minimize a mean square error. To describe the nonlinear behavior, we chose a widely used exponential model. By using the constitutive model and optimization, the continuity between the toe and linear region is enforced and the quantification of parameters is objective and reproducible.

The tissue-scale parameters including the linear region modulus, transition strain, transition stress, inflection point strain, and inflection point stress were calculated for both Initial Ramp (i.e., pre-damage state) and Ramp to Failure (i.e., post-damage state). To quantify the effect of damage, we calculated the change in each parameter (Δ), defined as Δ= Ramp to Failure – Initial Ramp (Figure 3.1a). In case of no damage, the values of the parameters for the Initial Ramp and Ramp to Failure are the same and the Δ is zero. In contrast, the Δ is a non-zero value if there is an observable damage. The linear region and

inflection point occur above the 2% grip strain, so we excluded the Initial Ramp 2% strain group data for the linear region modulus, inflection point strain, and inflection point stress (Table 3.1).

Table 3.1: Initial Ramp and Ramp to Failure values for tissue-scale parameters. Table includes parameters for both No Rest and Rest groups (average ± SD).

	2%		**4%**		**6%**		**8%**	
	No Rest	**Rest**	**No Rest**	**Rest**	**No Rest**	**Rest**	**No Rest**	**Rest**
Transition Strain								
Initial Ramp	0.013 ± 0.006	0.010 ± 0.006	0.014 ± 0.006	0.015 ± 0.006	0.017 ± 0.009	0.017 ± 0.005	0.020 ± 0.009	0.016 ± 0.009
Ramp to Failure	0.015 ± 0.006	0.014 ± 0.006	0.021 ± 0.003	0.021 ± 0.005	0.064 ± 0.089	0.026 ± 0.004	0.042 ± 0.009	0.030 ± 0.016
Transition Stress (MPa)								
Initial Ramp	4.39 ± 1.22	2.26 ± 0.50	4.40 ± 1.2	5.02 ± 1.15	5.48 ± 1.99	5.30 ± 1.28	6.32 ± 2.63	4.89 ± 1.61
Ramp to Failure	4.57 ± 4.52	4.70 ± 1.60	5.86 ± 1.39	6.49 ± 1.25	6.99 ± 1.84	6.83 ± 1.69	6.71 ± 1.80	6.68 ± 2.25
Linear Reg. Mod (MPa)								
Initial Ramp			973 ± 176	976 ± 233	1010 ± 172	872 ± 170	895 ± 120	984 ± 220
Ramp to Failure	1315 ± 356	1082 ± 115	923 ± 185	936 ± 217	771 ± 263	736 ± 126	526 ± 155	653 ± 156
Inflection Pt. Strain								
Initial Ramp			0.021 ± 0.004	0.022 ± 0.002	0.025 ± 0.008	0.024 ± 0.005	0.028 ± 0.007	0.022 ± 0.009
Ramp to Failure	0.024 ± 0.006	0.024 ± 0.007	0.033 ± 0.004	0.032 ± 0.005	0.050 ± 0.010	0.047 ± 0.006	0.063 ± 0.007	0.051 ± 0.020
Inflection Pt. Stress (MPa)								
Initial Ramp			13.4 ± 2.24	16.0 ± 2.73	14.0 ± 3.82	12.3 ± 2.75	13.9 ± 3.51	14.3 ± 6.02
Ramp to Failure	16.7 ± 11.1	16.0 ± 7.98	16.5 ± 2.85	16.3 ± 3.11	22.7 ± 3.53	22.6 ± 2.46	20.7 ± 6.28	24.8 ± 10.7
Peak Strain	0.081 ± 0.038	0.078 ± 0.020	0.088 ± 0.019	0.082 ± 0.017	0.100 ± 0.019	0.092 ± 0.010	0.107 ± 0.009	0.097 ± 0.019
Peak Stress (MPa)	61.6 ± 9.11	50.0 ± 7.04	47.7 ± 11.1	45.7 ± 9.80	49.7 ± 11.1	49.3 ± 2.76	32.0 ± 9.34	52.4 ± 20.9

The peak stress and strain were also quantified for the fascicles that failed within the load cell limit of 10 N. The fascicles that did not fail were excluded in the peak stress and strain analyses but included in all the other analyses. In total, the number of fascicles excluded in the peak stress and strain analyses were n=3, n=1, n=1, and n=2 for No Rest groups and n=2, n=1, n=2, and n=0 for Rest groups for the 2, 4, 6, and 8% strain levels, respectively.

The transverse strain (ε_t) was calculated by measuring the change in fascicle width (w), where w was the major axis of the cross-sectional profile acquired from confocal images, as $\varepsilon_t = (w_o - w_i)/w_o)$, where w_o is the reference width and w_i is width at the time of interest. The confocal images were used instead of CCD camera images to quantify transverse strain since the resolution of confocal images was higher than that of CCD images. In addition, we fitted an exponential decay function, $f(t) = C * exp(-t/\tau)$, where C is a constant, to quantify the transverse strain recovery response by quantifying the time constant (τ_t).

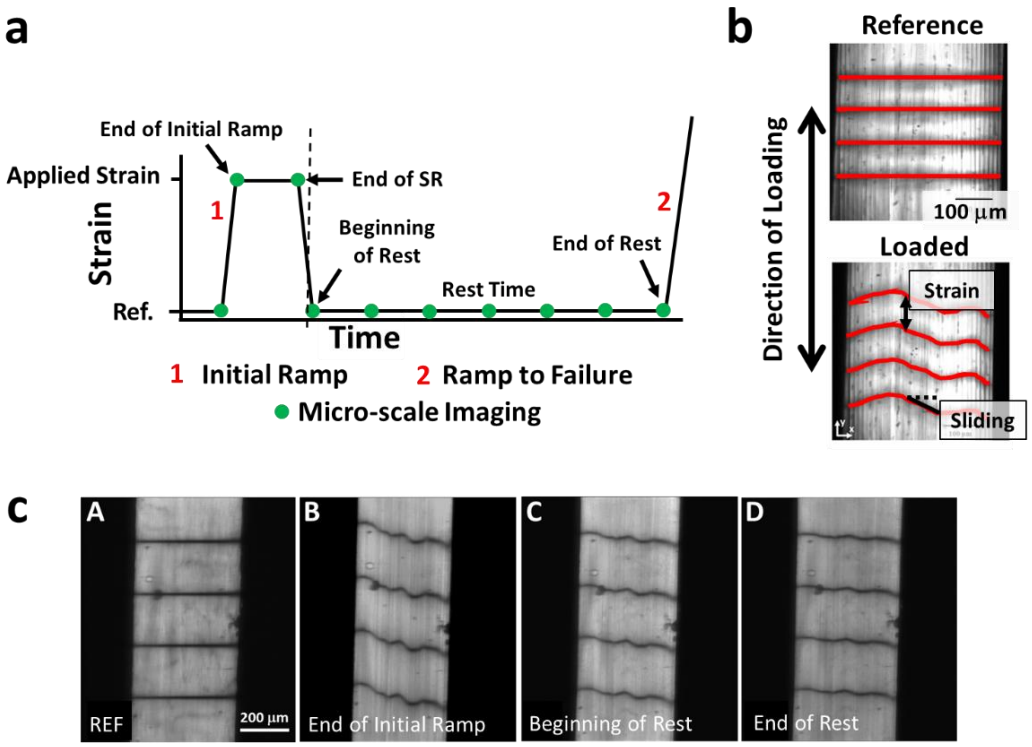

Figure 3.3: Micro-scale parameter quantification. (a) Parameters measured at End of Initial Ramp, End of Stress Relaxation (SR), Beginning of Rest, and End of Rest were quantified and used for further analysis. (b) The micro-scale strain and sliding, a measurement of micro-scale deformation of averaged fibril and fiber structures, were quantified using deformed photobleached lines. (c) Representative image of tendon used to measure micro-scale mechanics. The image corresponds to: (A) the reference state before loading; (B) at End of Initial Ramp, where the micro-scale strain and sliding increased compared with the reference image; (C) Beginning of Rest, or immediately after unloading, where the sliding partially recovered; and, (D) at End of Rest, where the sliding was not fully recovered after loading to 6%.

3.2.5 Data Analysis – Micro-scale parameters

Using a confocal microscope, four lines were photobleached perpendicular to the fibril direction and separated by 200µm to measure the micro-scale deformations (Figure 3.3b). The lines were tracked to calculate the micro-scale strain and sliding as previously

described. [38] The micro-scale strain represents an axial deformation, and the micro-scale sliding represents a relative shear deformation of collagen fibers and fibrils. The micro-scale strain was defined as the change in distance between pairs of photobleached lines, and the micro-scale sliding was defined as the average tortuosity (i.e., waviness) of all four lines (Figure 3.3b, c).

The sliding was decomposed into recoverable (i.e., elastic and viscoelastic) and non-recoverable portions from the values for sliding at the End of Stress Relaxation (SR), Beginning of Rest, and End of Rest, (Figure 3.3a). The elastic sliding recovery, defined as the instantaneous recovery upon unloading, was calculated as:

$$\frac{End\ of\ Stress\ Relaxation - Beginning\ of\ Rest}{End\ of\ Stress\ Relaxation} \times 100\% \qquad (3.2)$$

The viscoelastic sliding recovery, defined as the time-dependent recovery at End of Rest after subtracting out the elastic sliding recovery, was calculated as:

$$\frac{Beginning\ of\ Rest - End\ of\ Rest}{End\ of\ Stress\ Relaxation} \times 100\% \qquad (3.3)$$

Finally, the non-recoverable sliding was defined as the percentage of permanent sliding that remained at End of Rest. It was calculated as the sliding value at End of Stress Relaxation minus the elastic and viscoelastic recovery. We also fit an exponential decay equation, $f(t) = D * exp(-t/\tau)$, where D is a constant, to the micro-scale sliding recovery response to quantify the time constant (τ_1) and to confirm that 60-minuate rest period was sufficient time to reach equilibrium.

3.2.6 Excluded Samples

Two fascicles from the 8% strain level, one each for No Rest and Rest groups, were removed for both tissue- and micro-scale analyses because these samples were twisted during loading and the Δ linear region moduli of the samples were more than two standard deviations from the population average. For the micro-scale analysis, one additional sample from the Rest group at the 8% strain level had diffused photobleached lines and was removed only for the micro-scale analysis. For the tissue-scale analysis, the final reported sample size was n=7, n=7, n=7, and n=6 for both No Rest and Rest groups at the 2, 4, 6, and 8% strain levels, respectively. For the micro-scale analysis, the final reported sample size was n=7, n=7, n=7, and n=5 for Rest group at the 2, 4, 6, and 8% strain levels, respectively.

3.2.7 Statistical Methods

All the statistical analyses were conducted using GraphPad Prism. To determine which tissue-scale parameters exhibit strain dependency, each of the parameters including Δ transition strain, Δ transition stress, Δ linear region modulus, Δ inflection point strain, and Δ inflection point stress was correlated with tissue strain by fitting a linear regression line. The extra-sum-of-squares F-test was performed to determine the effect of the 60-minute rest period on tissue-scale parameters by comparing the slopes of linear regression between the No Rest and Rest groups. In addition, each of the three decomposed sliding components (i.e., elastic, viscoelastic, and non-recoverable sliding) was correlated with applied strain by fitting a linear regression line to determine which component represents

strain-dependency at the micro-scale. Similarly, the non-recoverable sliding was correlated with Ramp to Failure linear region modulus, Ramp to Failure transition strain, and Ramp to Failure inflection point strain to relate the damage at the micro-scale to the changes of mechanical response at the tissue-scale. The significance was set at $p = 0.05$ and Pearson's correlation (r) is reported for all the comparisons.

3.3 Results

3.3.1 Tissue-scale Parameters

At the tissue-scale, tendon experienced a permanent change in mechanical parameters (i.e., tissue-scale observation of damage) that was strain-dependent (Figure 3.4, Table 3.1). For the Rest groups, the Δ transition strain increased (Figure 3.4a, $p<0.0001$) with applied tissue strain and the Δ linear region modulus decreased with applied tissue strain (Figure 3.4c). The Δ inflection point strain (Figure 3.4d, $p<0.0005$) and Δ inflection point stress (Figure 3.4e, $p<0.005$), and peak strain (Figure 3.5a, $p<0.01$) were also dependent on the applied strain. These results show that damage is strain-dependent. Some parameters including the Δ transition stress (Figure 3.4b) and peak stress (Figure 3.5b) did not exhibit strain dependency. In addition, the moduli reported in this study are similar to previous rat tail tendon results (Table 3.1) [38,100,101] and fascicles were loaded to the same magnitude of physiological stress [102]. The tissue-scale parameters that are strain-dependent, including the transition strain, linear region modulus, inflection point strain, and inflection point stress, may represent the effect of damage.

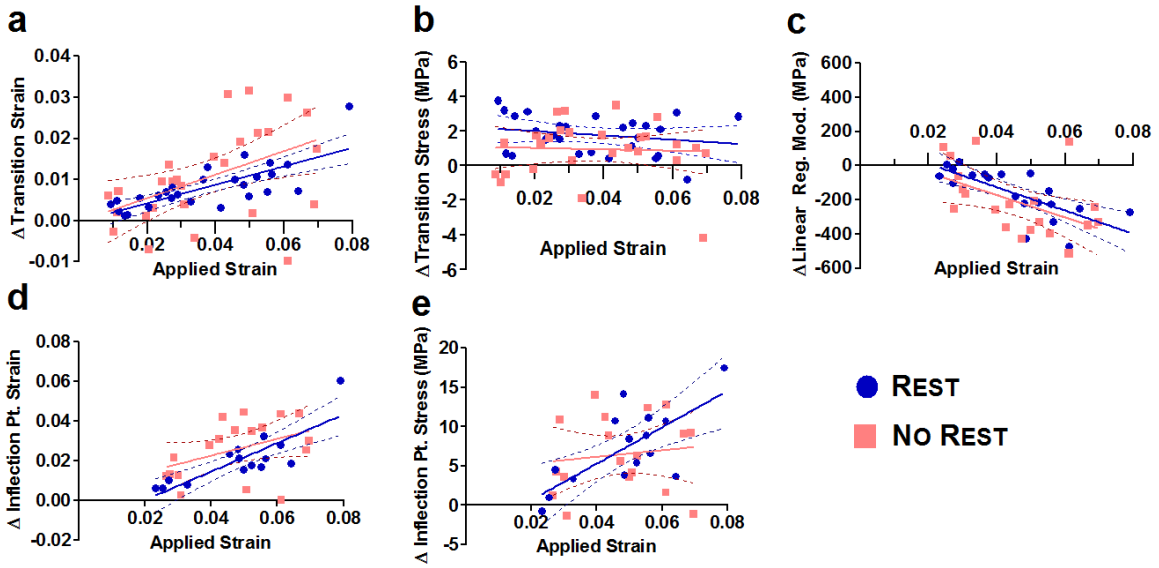

Figure 3.4: Tissue-scale tensile behavior. At the tissue-scale, tendon experienced a permanent change in mechanical parameters that was strain-dependent for (a) Δ transition strain, (c) Δ linear region modulus, (d) Δ inflection point strain, and (e) stress, but not for (b) Δ transition stress for the Rest group. For any of the parameters, there was no difference between the slopes of No Rest and Rest groups, suggesting the rest period does not alter the tissue-scale parameters and verifies that parameters measured are non-recoverable. The dashed lines represent the 95% confidence intervals.

Although only the Rest group is needed to separate recoverable viscoelastic effects from damage, we also included No Rest group to study the effect of viscoelastic recovery on mechanical parameters. Ultimately, there was no difference between the slopes of No Rest and Rest for any parameters (Figure 3.4, Table 3.1). For both No Rest and Rest groups, the Δ transition strain (Figure. 3.4a, $p<0.05$), Δ linear region modulus (Figure 3.4c, $p<0.0005$), and peak strain (Figure 3.5b, $p<0.05$) were significantly correlated with applied strain. However, a few parameters in No Rest had a different set of significant correlations

than seen in the Rest group. For example, the correlation of peak stress (Figure 3.5b, $p<0.05$) was significant only for No Rest group, Δ inflection point strain and stress did not show strain dependency for No Rest group. The different set of significant correlations between two groups might be attributed to a minor role of viscoelasticity and/or experimental variation since there was no statistical difference between the slopes of two groups. The summary of statistical analyses with Pearson's correlations and p-values are included in Table 3.2. No difference between the two groups suggests the 60-minute rest period does not alter the tissue-scale parameters and verifies that parameters measured are non-recoverable.

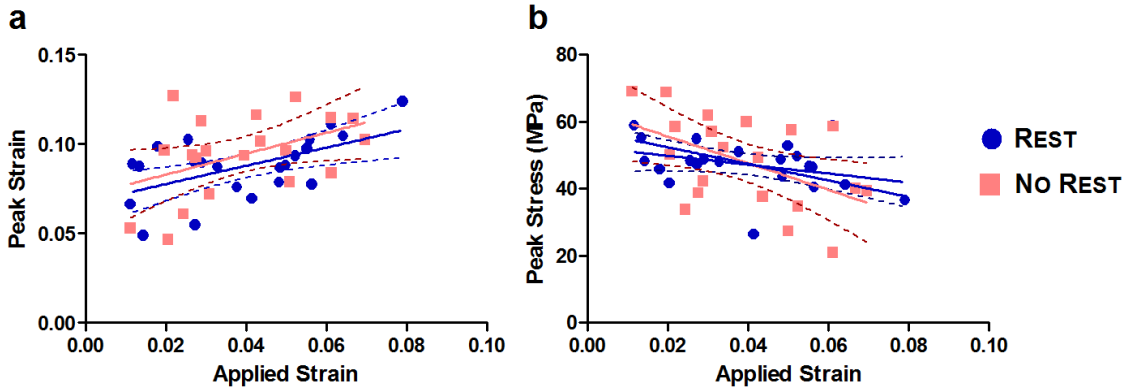

Figure 3.5: Peak strain and stress. (a) Peak strain increased with applied strain as expected for both groups, and (b) peak stress decreased with tissue strain only for No Rest group. However, there was no difference between the slopes of No Rest and Rest groups. The dashed lines represent the 95% confidence intervals.

Table 3.2: Summary of Pearson's correlation and p-value for No Rest and Rest. All parameters that have a p-value <0.05 are bolded and Pearson's correlations that have values greater than ± 0.70 are underlined.

	No Rest		**Rest**		**No Rest vs. Rest**
	p-value	*r*	*p-value*	*r*	*p-value*
Δ **Transition Strain**	**<0.05**	0.47	**<0.0001**	0.73	0.59
Δ **Transition Stress (MPa)**	0.82	0.42	0.28	-0.21	0.68
Δ **Linear Region Modulus (MPa)**	**<0.0005**	-0.66	**<0.0001**	-0.76	0.88
Δ **Inflection Pt. Strain**	0.083	0.42	**<0.0005**	0.83	0.30
Δ **Inflection Pt. Stress (MPa)**	0.61	0.12	**<0.005**	0.72	0.08
Peak Strain	**<0.05**	0.44	**<0.01**	0.53	0.81
Peak Stress (MPa)	**<0.05**	-0.50	0.12	-0.34	0.19

Table 3.3: Best-fit values and 95% confidence interval of the linear regression for Rest. Table includes slope and x-intercepts of all parameters (best-fit value ± SD).

	Best-fit		**95% Confidence Interval**	
	slope	*x-intercepts*	*slope*	*x-intercepts*
Δ **Transition Strain**	0.22 ± 0.04	0	0.146 to 0.304	-0.020 to 0.012
Δ **Transition Stress (MPa)**	-12.5 ± 11.4	0.179	-36.0 to 11.0	0.084 to ∞^+
Δ **Linear Region Modulus (MPa)**	-6830 ± 1530	0.021	-10030 to -3620	-0.001 to 0.031
Δ **Inflection Pt. Strain**	0.72 ± 0.13	0.020	-0.062 to 0.91	-0.002 to 0.029
Δ **Inflection Pt. Stress (MPa)**	232 ± 62	0.017	97.9 to 365.5	-0.028 to 0.031

Table 3.4: Inflection point in grip strain. Table includes Initial Ramp and Ramp to Failure values for inflection point in grip strain (average ± SD).

		Grip Strain			
		Inflection Point Strain		**Inflection Point Stress (MPa)**	
		Initial Ramp	*Ramp to Failure*	*Initial Ramp*	*Ramp to Failure*
2%	**No Rest**		0.031 ± 0.003		12.7 ± 3.31
	Rest		0.031 ± 0.002		12.9 ± 1.30
4%	**No Rest**		0.041 ± 0.001		15.3 ± 4.27
	Rest		0.041 ± 0.002		17.3 ± 3.42
6%	**No Rest**	0.032 ± 0.002	0.060 ± 0.003	14.3 ± 2.36	24.3 ± 4.86
	Rest	0.034 ± 0.004	0.057 ± 0.005	13.1 ± 3.33	22.1 ± 5.85
8%	**No Rest**	0.036 ± 0.002	0.074 ± 0.003	12.4 ± 2.04	21.5 ± 5.82
	Rest	0.036 ± 0.004	0.066 ± 0.006	14.1 ± 2.28	23.6 ± 2.76

Not only do the strain-dependent correlations suggested tendon damage, but also the x-intercept of these correlations suggest the damage threshold. The x-intercept of the Δ linear region modulus was 0.021 (Figure 3.4c), and the x-intercept of the Δ inflection point strain and stress (Figure 3.4d and 3.4e) was 0.017. Interestingly, these x-intercepts correspond to the averaged Initial Ramp inflection point of the 4, 6 and 8% strain level (Rest: 0.024 ± 0.005, Table 3.1), suggesting that the inflection point coincides with the damage threshold at the tissue-scale. In contrast, the x-intercept for the Δ transition strain was zero, such that this parameter increased instantaneously when loaded (Figure 3.4a), which implies that the transition strain behaves differently than the inflection point strain. We have also included inflection strain and stress measured in grip strain for future reference (Table 3.3).

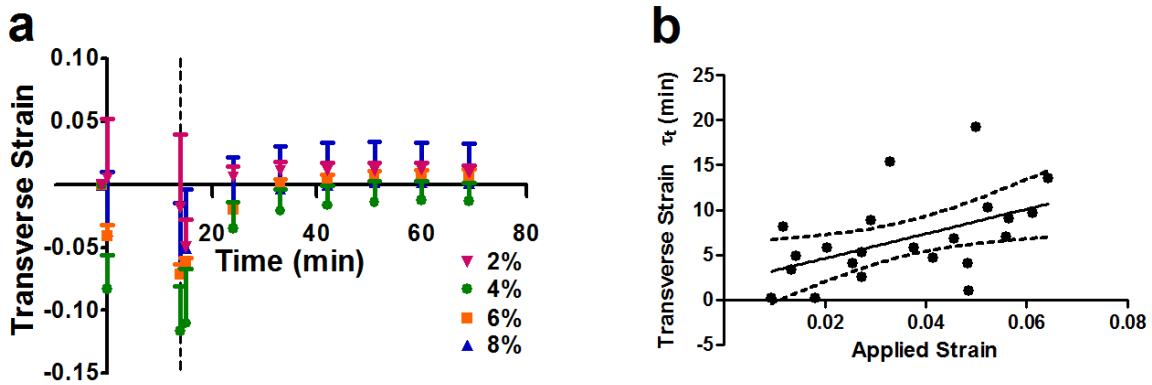

Figure 3.6: Transverse strain recovery. (a) Transverse strain fully recovered over time for all strain groups. The dashed line represents when samples were unloaded and error bars represent SEM. (b) The transverse τ_t was dependent on applied strain. The dashed lines represent the 95% confidence intervals.

Transverse strain fully recovered at all strain levels (Figure 3.5a) and the time-dependency of the transverse strain recovery was quantified using the exponential decay function. The time constant (τ_t) ranged from 0.13 minute at 2% strain to 19.3 minute at 8% strain and was strain-dependent (Figure 3.6b, n=22). Some samples recovered their transverse strain immediately upon unloading and were not included in the curve fit (n=5).

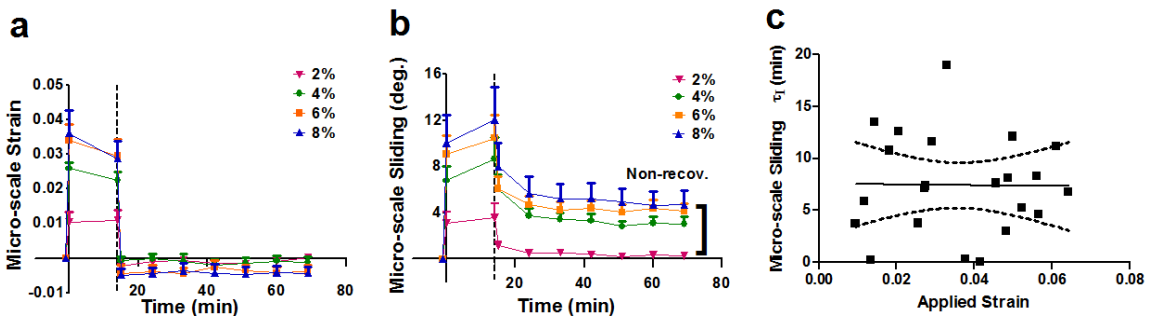

Figure 3.7: Micro-scale deformation of tendon fascicles. (a) Micro-scale strain fully recovered for all strain groups, suggesting that the collagen fibrils are undamaged. On the other hand, (b) micro-scale sliding only partially recovered. Dashed line represents when samples were unloaded and error bars represent SEM. (c) The micro-scale sliding was strain independent and averaged 7.43 min, suggesting that the rest period was long enough for a complete micro-scale sliding recovery. Dashed lines represent the 95% confidence intervals.

3.3.2 Micro-scale Parameters

At the micro-scale, the micro-scale strain fully recovered while the micro-scale sliding only partially recovered (Figure 3.7). The deformation demonstrated by the micro-scale fully recovered elastically (i.e., instantaneously) in all strain groups (Figure 3.7a), suggesting that the collagen fibrils are undamaged. On the other hand, the micro-scale sliding recovery was time-dependent and only partially recovered – up to 50% of the sliding was non-recoverable (Figure 3.7b). In addition, the time constant (τ_I) for micro-scale sliding recovery did not show any strain dependency, where the average τ_I was 7.43 minutes across all strain levels (Figure. 3.7c, *r= 0.01, p>0.95).* This is a further evidence

that the 60-minute rest period was sufficient for the viscoelastic response to reach equilibrium, leaving the remaining non-recoverable effects as damage.

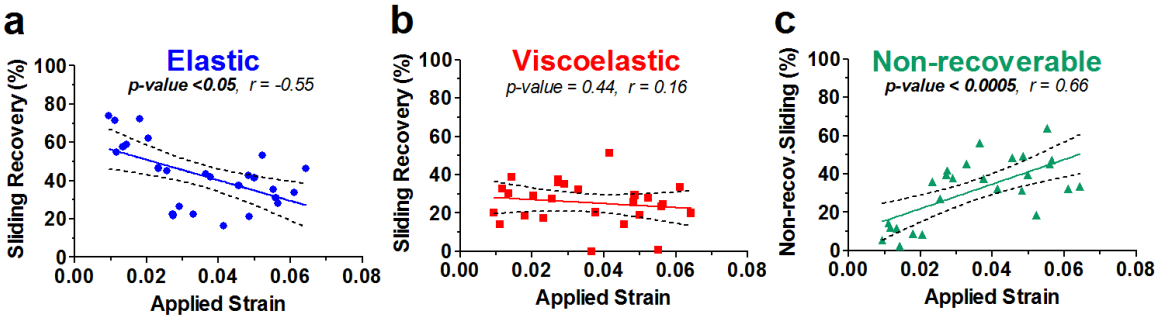

Figure 3.8: Decomposed micro-scale sliding recovery. The sliding recovery was decomposed to elastic, viscoelastic, and non-recoverable portions. (a) Elastic recovery decreased with tissue strain while (b) viscoelastic recovery showed no strain dependency. (c) Non-recoverable sliding increased with applied strain due to the decrease in elastic recovery. The dashed lines represent the 95% confidence intervals.

The micro-scale sliding recovery was decomposed and each component was plotted against tissue strain to quantify damage at the micro-scale (Figure 3.8). The elastic sliding recovery (Figure 3.8a, $r = -0.55$, $p<0.005$) and non-recoverable sliding (Figure 3.8c, $r=0.66$, $p<0.0005$) both correlated with applied strain. However, the viscoelastic sliding recovery was not correlated with applied strain (p=0.44) and averaged 27.5% ± 8.9% across all applied strain levels (Figure 3.8b).

3.3.3 Relationship between Tissue- and Micro-scale parameters

The non-recoverable sliding observed at the micro-scale was correlated with the Ramp to Failure tissue-scale parameters for the Rest group (Figure 3.9). The linear region modulus decreased with increasing non-recoverable sliding (Figure 3.9a, $r = -0.54$, $p < 0.005$), and the transition strain increased with increasing non-recoverable sliding (Figure 3.9b, $r = 0.63$, $p < 0.001$). The inflection point strain also increased with non-recoverable sliding (Figure 3.9c, $r = 0.64$, $p < 0.0005$). These correlations support the notion that the non-recoverable sliding at the micro-scale contributes to the mechanical behavior at the tissue-scale, consistent with the definition of tendon damage as an irreversible change in the microstructure that is related the macroscopic mechanical parameters. Refer to appendix for additional observations of transition and inflection point stress and Δ values (Figure A.1, 2)

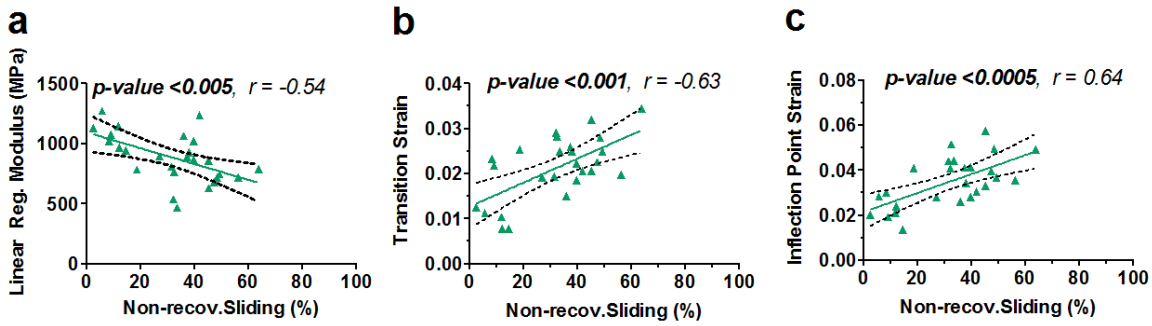

Figure 3.9: Relationship between tissue-scale mechanics and non-recoverable sliding. (a) Ramp to Failure linear region modulus, (b) transition strain, and (c) inflection point strain were all correlated with non-recoverable sliding. These correlations support the notion that the non-recoverable sliding at the micro-scale contributes to the mechanical behavior at the tissue-scale. The dashed lines represent the 95% confidence intervals.

3.4 Discussion

This study quantified tendon damage, an irreversible change in the microstructure that alters the macroscopic mechanical parameters, [66] by identifying the microstructural micro-scale changes that correlated with altered macroscopic mechanical parameters at the tissue-scale. Analysis of the micro-scale deformations demonstrated that the micro-scale strain fully recovered following loading and unloading (Figure 3.7a). However, the micro-scale sliding was only partially recoverable, suggesting tendon damage is localized to the structures that are responsible for sliding (Figure 3.7b, 3.7c). At the tissue-scale, irreversible mechanical parameter changes included a strain-dependent increase in transition strain (an elongated toe region, Figure 3.4a), decrease in linear modulus (Figure 3.4c), and increase in inflection point strain (Figure 3.4d). By relating tissue- and micro-scale parameters, we demonstrated that non-recoverable sliding is a mechanism for tendon damage that is responsible for the decreased linear modulus and elongated toe-region observed at the tissue-scale. In addition, we demonstrated that the inflection point of the stress-strain curve represents the damage threshold and, therefore, may be a useful parameter for future studies.

3.4.1 Microstructural Micro-scale Damage and Mechanisms

The microstructural observations, full elastic recovery of micro-scale strain and non-recoverable sliding, are consistent with previous findings in equine common digital extensor tendon, which bears relatively a low-stress. The equine tendon strain at the micro-scale showed 90% recovery after tensile loading, while the sliding showed only 50%

recovery. [80] The partial non-recoverable sliding (Figure 3.4), suggests that tendon damage was localized to the structure that is responsible for shear in tendon. This result directly supports the assumptions made in a previous mathematical shear lag model, where plastic deformation of the structure that allows micro-scale sliding was the only condition able to replicate experimental observations. [95]

This study provides strong evidence that tendon damage first occurs in a structure that is responsible for micro-scale sliding. Notably, the damage mechanisms identified in this study differs from other studies that observed damage in forms of collagen fibril kinking and discontinuities after fatigue loading. [51,52] The tendons in these studies, however, were subjected to higher applied strains [51,94,103] or a substantial amount of cyclic loading. [52] Thus, damage of the collagen fibrils may occur after non-recoverable sliding damage, when the non-recoverable sliding reaches its maximum capacity to transmit shear load. This is partially supported by a recent study, where damage in the collagen fibrils of rat tail tendon was detected at 7.5% grip strain by the use of collagen hybridizing peptide (CHP) that binds to denatured collagen. [104] The threshold is much higher than the threshold identified in this study (i.e., ~4% grip strain). A relatively low damage threshold in our study implies that damage initiates at the structure that allows micro-scale sliding and may precede the damage on collagen fibrils.

While this study identified non-recoverable sliding as mechanisms of tendon damage, the compositional structures responsible for micro-scale sliding elastic recovery (Figure 3.8a) and for loss of sliding recovery (Figure 3.8c) remain unknown. Although it is hard to draw any conclusion about the component of the structure that allows micro-

scale sliding with our optical observations (Figure 3.3c), small diameter collagen fibrils are a potential candidate. The bifurcation and fusion of the smaller diameter fibrils between larger fibril have been observed in many studies. [105–107] We recently used serial block-face scanning electron microscopy to demonstrate that a network of small diameter fibrils wrap around and fuse with larger collagen fibrils, suggesting that these smaller diameter fibrils may be the shear load transferring structures. [108] Moreover, digestion of all non-collagenous matrix with trypsin did not affect the micro-scale sliding in rat tail tendon, [108] consistent with glycosaminoglycan digestion studies that observed no changes in tissue-level mechanics. [109] Although we and others have previously used the terminology "matrix" to describe the material that provides micro-scale shear load transfer, we now suggest small diameter collagen fibrils and not "matrix" may be responsible for shear load transfer. Further investigation is needed to identify structural contributors to tendon damage, particularly at length scales at the nano-scale. [51,94,103,104]

3.4.2 Tissue-scale Changes Reflecting Tendon Damage

Damage was observed in several tissue-scale mechanical parameters including the transition strain, linear region modulus, and inflection point strain. Therefore, these three parameters can be used as metrics to quantify the effect of tendon damage. Although the inflection point stress was strongly dependent on applied strain, it did not correlate with the non-recoverable sliding like other parameters, suggesting inflection point stress may not be a good metric for measuring damage. These tissue-scale metrics are similar to those other studies have utilized, such as tissue lengthening or laxity (which was measured

indirectly by Δ transition strain in this study) and linear region modulus for tendon [17,76] and ligament. [86,90,91]

3.4.3 Damage Threshold

The study suggests that the damage threshold occurs at the inflection point of the stress-strain curve where strain softening begins (Figure 3.2). Evidence to support this as the damage threshold is that the strain value for the inflection point during Initial Ramp loading was similar to the independent calculations of x-intercepts for the strain-dependent tissue-scale parameters (Figure 3.4c-e). Furthermore, the inflection point strain strongly correlated with the non-recoverable sliding (Figure 3.7), suggesting that the inflection point marks the damage threshold at the micro-scale. Refer to appendix for an additional discussion of damage threshold (Figure A.3).

The study limitation is that damage was induced with a single type of loading protocol with one strain rate: a ramp at 1%/s to the applied strain level that was held static for a 15-minute stress relaxation. It is possible that different mechanisms of damage with other types of loading can occur, particularly with cyclic loading. In addition, it is unknown whether damage occurred during loading (i.e., as soon as tendon was stretched beyond a damage threshold) or damage occurred during the holding (stress-relaxation) period. Future studies will need to address the role of loading rate [110] and viscoelasticity. [104] Indeed, we performed cyclic preconditioning at 4% grip strain, which is presumably above the threshold of the static stress relaxation protocol we performed. However, our pilot data showed there was no difference in any of the tissue-scale parameters between 2% and 4%

preconditioning level (Figure 3.10). Thus, not only the strain magnitude but also the loading type (i.e., static vs. cyclic) and duration (i.e., 10 seconds vs. 15 minutes) of loading may have different contributions to damage. In addition, the rat tail tendon fascicle is a model system that can elucidate fundamental mechanics of tendon, yet the damage mechanism in other tendons, especially the ones that bear higher loads may be different. [80,82] Future studies need to address factors that can contribute to damage mechanism.

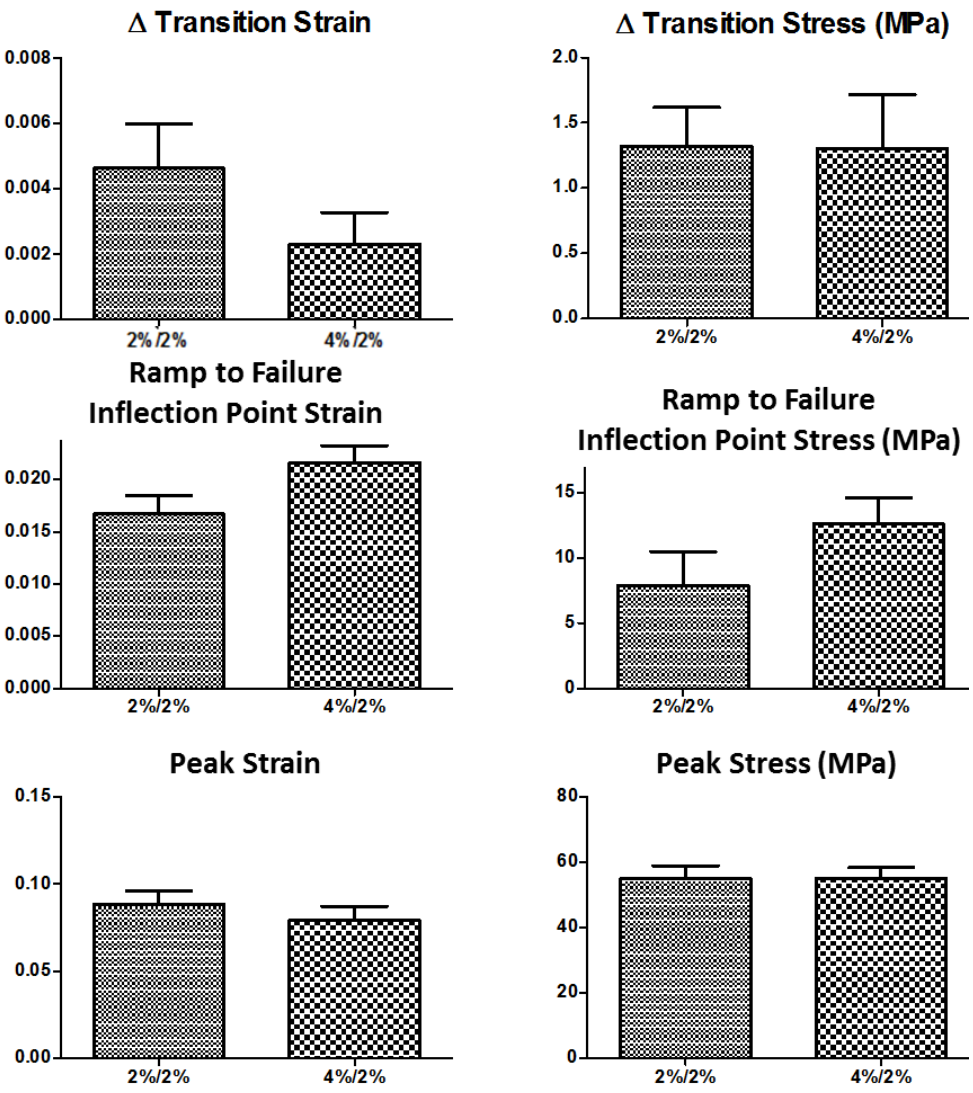

Figure 3.10: Tissue-scale mechanics comparison between two preconditioning groups. Both groups were loaded to 2% during Initial Ramp, but preconditioned at difference levels. 2% represents samples (n=4) preconditioned at 2% and 4% represents samples (n=14) preconditioned at 4%. There was no difference between two groups in all of the tissue-scale parameters ($p>0.10$). The error bars represents SEM.

3.4.4 Irreversible Damage Versus Viscoelastic Recoverable Effects

The experimental design that incorporated 60-minute rest was important to separate irreversible damage from viscoelastic effects. Two viscoelastic effects were measured: the transverse strain recovery (Figure 3.6) and the viscoelastic portion of the micro-scale sliding recovery (Figure 3.8b). It is likely that both of these viscoelastic responses were governed by fluid flow. [111,112] As predicted by biphasic theory, tensile stress-induced contraction in the transverse direction is governed by fluid exudation during loading [112,113] and the recovery of transverse strain should be caused by fluid influx back into the tissue. The transverse strain fully recovered for all strain groups without any non-recoverable portion (Figure 3.6a) and the time constant, while strain-dependent, was between 5-15 minutes. In addition, the viscoelastic sliding recovery was not strain-dependent (Figure 3.8b) and had a time constant of 7.4 min, similar in magnitude to the transverse strain recovery. Thus, this study design successfully separated irreversible damage for viscoelastic, likely fluid-flow based, effects.

3.5 Conclusion

This study used multi-scale mechanics to experimentally elucidate tendon damage mechanisms, where damage was defined as an irreversible change in the microstructure that is observable in macroscopic mechanical parameters. Key advances of this study were that damage was measured as a non-recoverable change in mechanical behavior (by allowing the tissue to recover after applying potentially damaging loading) and the threshold for damage initiation was determined. In contrast to the observed full recovery

of the micro-scale strain, the micro-scale sliding only partially recovered, indicating that the damage is localized to the structures that are responsible for sliding. We concluded that non-recoverable sliding is a mechanism for tendon damage and is responsible for the decreased linear modulus and elongated toe-region observed at the tissue-scale. These tissue-scale changes in transition strain (end of the toe region) and linear region modulus are therefore appropriate metrics of tendon damage. We also demonstrated that the inflection point of the stress-strain curve can successfully mark the threshold of damage in tendon.

Chapter 4

EFFECT OF FREEZING ON TENDON MECHANICS AND DAMAGE MECHANISMS AT MULTI-SCALE

Based on published work: Lee, AH.; Elliott, DM. "Freezing does not alter multi-scale tendon mechanics and damage mechanisms in tension,": Ann. N. Y. Acad. Sci, 2018 1409:85-94.

4.1 Introduction

It is common in biomechanics to use previously frozen tissue samples when studying tendon and other fibrous musculoskeletal tissues. Previously frozen tissue has the advantage of convenience for transport and exchange of tissue, when acquiring samples from commercial vendors or through collaborations. It is widely accepted to freeze tissue and store tissue samples for mechanical testing later. In addition, soft tissue allografts that are used for reconstructions are subjected to multiple freeze-thaw cycles before implantation to avoid biological degradation. [96,114] In all of these situations, it is assumed that the process of freezing and thawing does not cause mechanical and structural damage, or that potential changes are minimal and inconsequential. Several studies have addressed the effect of freezing, and most studies show no effect on mechanical properties between fresh and previously frozen tissue. [96,114–118] However, minor effects of freezing have been observed for modulus, [119,120] although other studies show no effect of freezing on modulus. [96,114–117] In addition, minor freezing effects on microstructure have been demonstrated as an increase in space between fibrils [121,122] and fibril

diameter. [121,123] It is unknown if these microstructural changes affect tendon micro-mechanics, and thus the effect of freezing on tendon mechanics needs to be investigated further to improve the design of future experiments and standard practice in biomechanics.

In our previous chapter, we demonstrated that the changes in tissue-scale mechanical parameters are closely associated with the micro-scale tendon damage, which was observed as the non-recoverable sliding, using a previously frozen tissue. In several other studies, minor freezing effects on microstructure have been observed such as an increase in space between fibrils [121,122] and fibril diameter. [121,123] Yet, it is unknown if these microstructural changes affect tendon micro-mechanics. Because damage is related to microstructural changes, and microstructural alterations have been shown to occur with freeze-thaw cycles, [121–123] it is unclear if freezing will alter tendon damage mechanisms. Therefore, the novelty of the study is to investigate the effect of freezing on tendon mechanics and damage mechanisms at multiple length scales. The objective of this study was to test the hypothesis that carefully controlled freezing does not alter tendon multi-scale mechanics and damage mechanisms and to confirm this qualitatively using scanning electron microscopy of rat tail fascicle. The effect of freezing on tendon mechanics can improve the design of future experiments and standard practice in biomechanics.

4.2 Materials and Methods

4.2.1 Sample Preparation

Rat tail tendon fascicles were harvested from six 4-7 month old Long Evans female rats. The study was conducted with two groups, Fresh and Frozen (n=10/group). The Fresh

group was dissected and mechanically tested within 7 hours of sacrifice. The entire tail was excised, and we further dissected an 8 cm long segment of the tail from the proximal end with its skin intact. Fascicles were pulled from the 8 cm long segment of the tail for mechanical testing. The proximal end of a rat tail (i.e., 8cm long with skin intact) was wrapped in a PBS soaked gauze and placed in a plastic bag to be frozen at -20°C for future studies.

The Frozen group (n=10) was prepared similarly to the Fresh except the tendon was previously frozen in situ within the tail with the skin intact. On the day of mechanical testing the 8 cm long tail segment, which was wrapped in a PBS soaked gauze and a plastic bag, was placed in warm water for 30 minutes to 1 hour to thaw. After thawing, fascicles were pulled from the tail for mechanical testing using forceps, as mentioned above. The average number of the freeze-thaw cycle for the Frozen group was two and the maximum number of the freeze-thaw cycle was limited to three. For the samples that underwent two or three freeze-thaw cycles, the exact same freezing and thawing procedure was conducted as above, that is, the intact tail segment was frozen while wrapped in a PBS soaked gauze and a plastic bag. The maximum storage time was limited to 6 months.

After isolating the fascicle for testing as described above, all procedures were identical for the Fresh and Frozen groups. First, 1 mm was cut from each end, removing any potential tissue that may have been altered due to handling during sample excision and preparation. We stained each sample with 10 μg/ml 5-DTAF (Life Technologies) in PBS for 45 minutes. This concentration is low enough to minimize the effect of DTAF on mechanics.[97] We tested the tendon fascicle on a custom-made uniaxial testing device

with a PBS bath mounted on the inverted confocal microscope (LSM 5 LIVE, objective Plan-Apochromat 10x/0.45) as previously described. [38] Each sample was soaked in PBS at room temperature for at least 3 hours before testing to allow the sample to reach equilibrium. In addition, all samples were kept at room temperature from the beginning of DTAF staining to the end of mechanical testing.

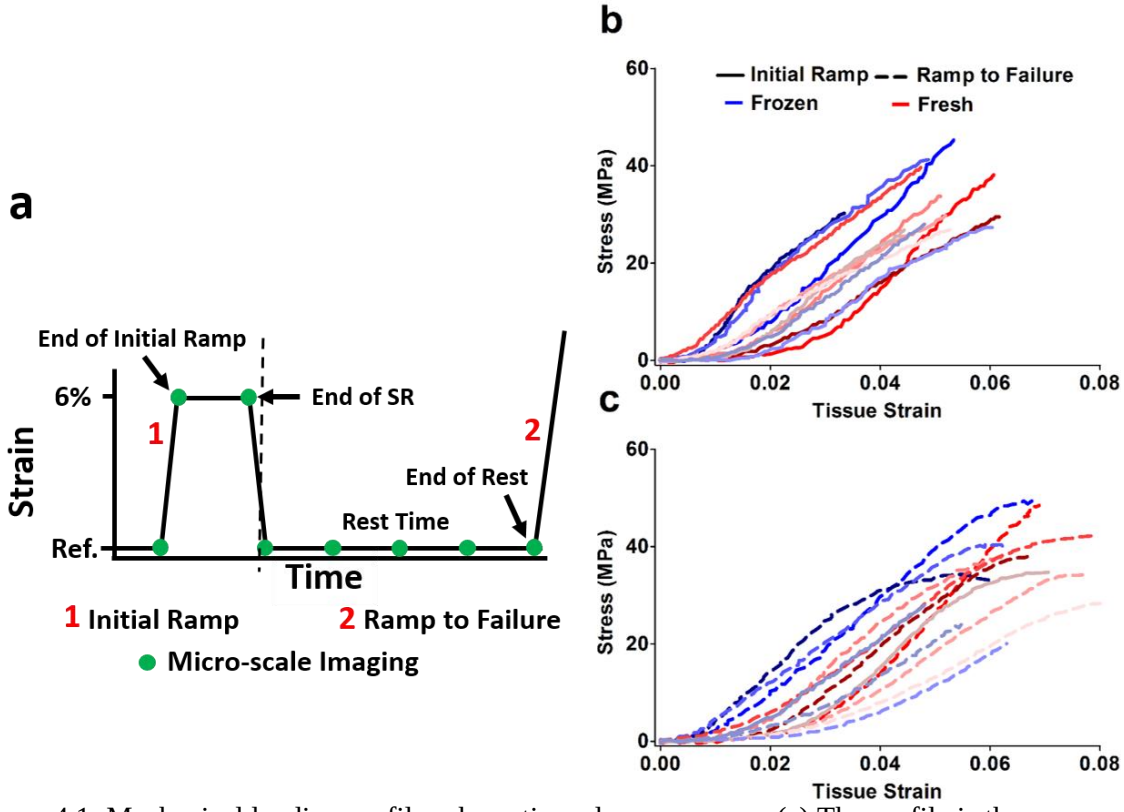

Figure 4.1: Mechanical loading profile schematic and σ-ε response. (a) The profile is the same as the previous chapter, except the rest time has been reduced to 40 minutes, and thus less micro-scale imaging points. Δ = Ramp to Failure = Initial Ramp. (b) σ-ε response of Initial Ramp and (c) Ramp to Failure of all the tendons are shown. The shades of blue and red from the Initial and Ramp graph and Ramp to Failure graph are matched to represent each sample.

4.2.2 Mechanical Testing Protocol

The mechanical testing protocol (Figure 4.1a) is similar to the previous chapter. [64] We preloaded each fascicle to 0.5g (~5mN) to define the reference length and preconditioned with 5 cycles of 2% grip strain. Then, we ramped the tendon to 6% and held at a constant stain level for 15 min of stress relaxation. We chose 6% strain to induce damage, based on our previous study. [64] The sample was unloaded to the reference length and held at its reference for 40 minutes and then loaded at a constant rate to failure. The strain rate for all loading and unloading was 1%/s. To observe the effect of damage, we quantified the tissue-scale parameters at 2 time points of the test protocol as demonstrated previously (Figure 4.1a). While the applied grip-to-grip strain was 6%, from optical imaging the tissue strain was 4.9 ± 0.9% and 4.8 $\pm$ 1.1% for Fresh and Frozen groups, respectively, with no significant difference between the groups.

4.2.3 Data Acquisition

The procedure was similar to the previous chapter. Briefly, we applied two ink markers directly on the tendon using a permanent marker and imaged with CCD camera to measure optical strain. In addition, we quantified the transverse strain and micro-scale parameters (i.e., micro-scale strain and sliding) using a confocal microscope. Throughout the test, we acquired confocal images at 8 time points, represented by green dots (Figure 4.1): reference image, at the beginning and end of the stress relaxation period, and every 10 minutes during the 40-minute rest period. The rest time was reduced from 60-minute to 40-minute, based on the previous observation of micro-scale sliding constant (Figure 3.7c)

4.2.4 Scanning Electron Microscopy (SEM)

For both Fresh and Frozen group, one sample per group was prepared for Scanning Electron Microscopy (SEM) to study fascicle ultrastructure. Each sample underwent the same dissection and storage procedure as above, and for the Frozen group, the sample underwent two freeze-thaw cycles. Each sample was incubated in PBS for at room temperature for at least 3 hours. Using insect pins, we pinned the sample in a straight line and fixed it for 48 hours in 4% SEM-grade paraformaldehyde. After fixation, the sample was incubated in 30% sucrose until it sank to the bottom, which took about 20 minutes with agitation. After a quick rinse in PBS, the sample was cut into smaller pieces, embedded in optimal cutting temperature compound and frozen using copper blocks cooled with liquid nitrogen to freeze the tissue without a direct contact with liquid nitrogen. Using a cryostat blade, the sample was cut longitudinally to observe interior ultrastructure. The sample was left in deionized water overnight to wash embedding medium. The next day we fixed the sample with 1% osmium tetroxide for 1 hour. The sample was then dehydrated in graded ethanol, critical point dried, mounted on SEM stubs using carbon tab with their cut-phase exposed surfaces, and coated using platinum. We examined the tendon at two different magnifications, 6,000x and 35,000x, using Hitachi S-4700 operating at 3 kV. The images were used to qualitatively assess the effect of freezing on the ultrastructure of tendon.

4.2.5 Data Analysis – Tissue-scale Parameters

The tissue-scale parameters were quantified the same way as the previous chapter (Figure 3.2, Figure 4.1a). The tissue-scale parameters including the transition strain, transition stress, linear region modulus, inflection point strain, and inflection point stress were calculated for Initial Ramp and Ramp to Failure (Figure 4.1a). Particularly, we were interested in transition strain, linear region modulus, and inflection point strain, which were previously established in the previous chapter as metrics to study damage[64]. To quantify the effect of damage, we calculated the change in each parameter (Δ), defined as Δ= Initial Ramp – Ramp to Failure. In case of no damage, the values of the parameters for the Initial Ramp and Ramp to Failure are the same and the Δ is zero. In contrast, the Δ is a non-zero value if there is an observable effect of damage. Again, the transverse strain (ε_T) was calculated by measuring the change in fascicle width (w) and we fitted an exponential decay function, $f(t) = C * exp(-t/\tau)$, where C is a constant, to quantify the transverse strain recovery response by quantifying the time constant (τ_T).

4.2.6 Data Analysis – Micro-scale Parameters

The micro-scale deformations were measured using the same method used for the previous chapter. Four lines, separated by 200 μm, were photobleached perpendicular to the fibril direction to measure deformations. The lines were tracked to calculate the micro-scale strain and sliding as previously described (Figure 3.3). [38,64,97,108,124] The micro-scale sliding was decomposed into three components: elastic, viscoelastic, and non-

recoverable. We also fit an exponential decay equation, $f(t) = D * exp(-t/\tau)$, where D is a constant, to the micro-scale sliding recovery response to quantify the time constant (τ_I).

4.2.7 Statistical Methods

Our first hypothesis was that tissue- and micro-scale mechanics are not different between Fresh and Frozen groups. To test if freezing tissue affects the tendon mechanics at the tissue-scale, each of the parameters including Δ transition strain, transition stress, linear region modulus, inflection point strain, and inflection point stress was compared using two-tailed t-tests. We also separated the Δ parameter into Initial Ramp and Ramp to Failure to test if there is a difference within each Initial Ramp and Ramp to Failure between Fresh and Frozen using two-tailed t-test. At the micro-scale, the comparisons between Fresh and Frozen parameters were made, including the transverse strain τ_T, micro-scale sliding τ_I, elastic recovery, viscoelastic recovery, and non-recoverable sliding. These comparisons were performed using a two-tailed t-test to test if freezing has any effect on tendon at the micro-scale.

Our second hypothesis was that the damage mechanisms are similar between Fresh and Frozen groups. To test this hypothesis at the tissue-scale, we used two paired tailed t-test to compare Initial Ramp and Ramp to Failure within Fresh and Frozen (Figure 3), specifically focusing on transition strain, linear region modulus, and inflection point strain. These parameters showed an effect of damage in our previous study of previously frozen tissue. [64] For all statistical tests, significance was set at p =0.05 and all the statistical analyses were conducted using GraphPad Prism.

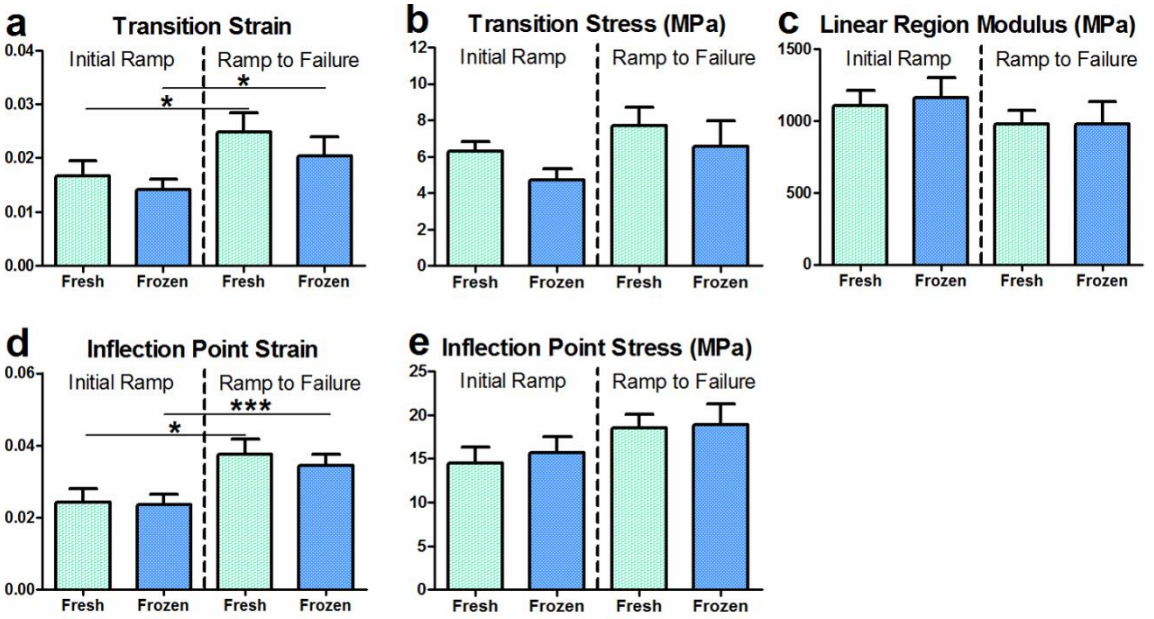

Figure 4.2: Tissue-scale mechanical parameters with Initial Ramp and Ramp to Failure. For any of the parameters, there was no difference between the Fresh and Frozen groups ($p>0.07$). Transition and inflection point strain both increased, consistent with our previous findings. These results suggest that freezing does not alter tissue-scale tendon mechanics and damage mechanisms. The error bars represent SEM.

4.3 Results

4.3.1 Tissue-scale Parameters

At the tissue-scale, the σ - ε responses showed that there was no qualitative difference between the Fresh and Frozen at Initial Ramp (i.e., pre-damage, Figure 4,1b) and Ramp to Failure (i.e., post-damage, Figure 4,1c). To quantitatively compare, we compared the Fresh to Frozen mechanical parameters individually at the Initial Ramp and Ramp to Failure and also compared the Fresh to Frozen using the Δ parameter, a representation of damage at the tissue-scale. There was no difference between Fresh and Frozen groups at either Initial Ramp or Ramp to Failure for any of the parameters including,

transition strain and stress, linear region modulus, or inflection strain and stress ($p>0.07$, Figure 4.2). In addition, there was no difference between Fresh and Frozen groups for the Δ parameters for all of these parameters ($p>0.6$, Figure 4.3).

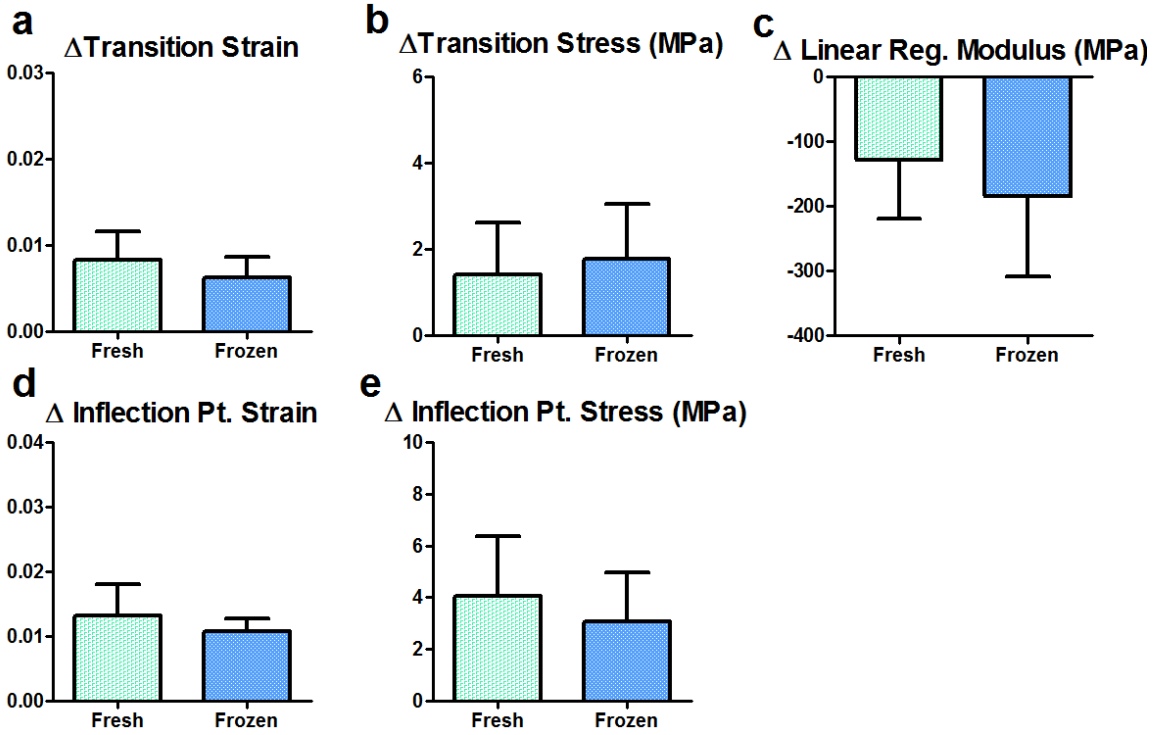

Figure 4.3: Tissue-scale mechanical parameters in Δ. Tendon experienced a permanent change in mechanical parameters $\Delta \neq 0$ for both groups. For any of the parameters, there was no difference between the Fresh and Frozen groups ($p>0.07$). The error bars represent SEM.

Damage was previously quantified at the tissue-scale in previously frozen tissue using the Δ parameter (Ramp to Failure- Initial Ramp), [64,93] and we used similar comparisons to test if these differences were maintained in the Fresh tendon. When we compared between Initial Ramp and Ramp to Failure within each group, the transition strain (Figure 4.2a) and inflection point stain (Figure 4.2d) significantly increased for both

Fresh ($p < 0.05$) and Frozen ($p < 0.0005$), consistent with our previous findings. [64] Additionally, the linear region modulus (Figure 4.2b) did not change from Initial Ramp to Ramp to Failure, as expected, for both groups ($p > 0.2$). The stress relaxation was 52.7 ± 6.9% and 57.1 ± 2.6% for the Fresh and Frozen groups, respectively, and was not different when comparing Initial Ramp and Ramp to Failure. We have provided the values for each parameter as an appendix (Table B.1).

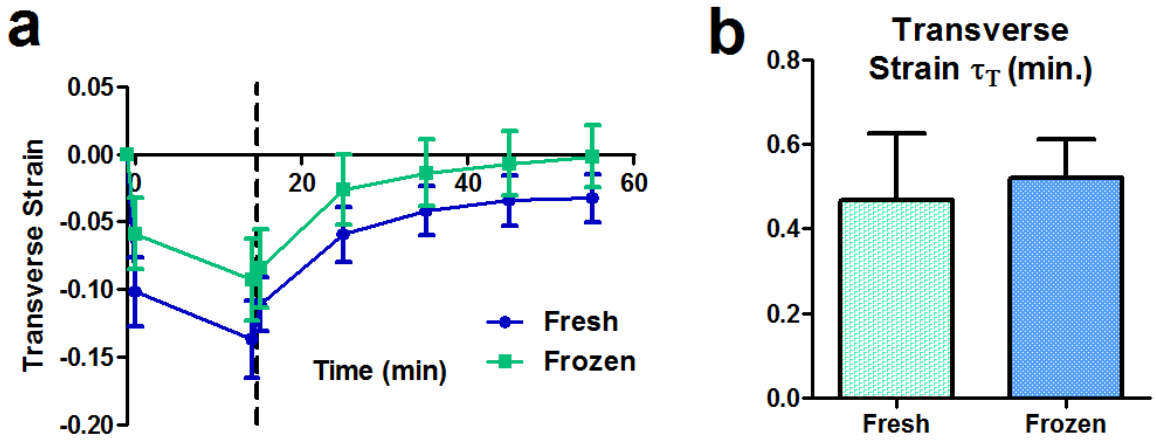

Figure 4.4: Transverse strain recovery. (a) Transverse strain fully recovered over time for both groups. The dashed line represents when samples were unloaded. (b) The transverse τ_T was not significantly different for both groups ($p > 0.80$). Similarly, the constant C averaged -0.11 ± 0.12 and -0.13 ± 0.04 for Fresh and Frozen, respectively, with no difference between the two groups ($p > 0.47$). The error bars represent SEM.

The transverse strain fully recovered for both groups (Figure 4.4a) and the time-dependency of the transverse strain recovery was quantified using an exponential decay function. The time constant averaged 0.47 ± 0.51 and 0.52 ± 0.24 minutes for Fresh and Frozen, respectively (Figure 4.4b), with no difference between the two groups. Similarly, the constant C averaged -0.11 ± 0.12 and -0.13 ± 0.04 for Fresh and Frozen, respectively,

with no difference between the two groups ($p>0.5$). Three samples from the Frozen group were not included in the exponential curve fit because these recovered their transverse strain immediately upon unloading with no time-dependent recovery. Although only Frozen group showed immediate recovery, this is likely due to an experimental variation since the acquisition of micro-scale confocal images was delayed in these samples. In summary, there was no difference between Fresh and Frozen tendons for any of the tissue-scale parameters.

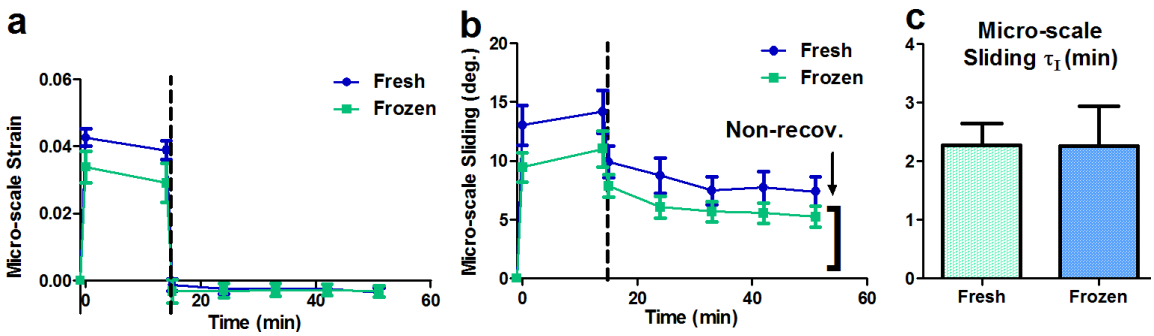

Figure 4.5: Micro-scale deformation of tendon fascicles. (a) Micro-scale strain fully recovered for both groups, suggesting that the collagen fibrils are undamaged. (b) On the other hand, the sliding only partially recovered, exhibiting damage at the micro-scale, suggesting tendon damage is observable by non-recoverable sliding and the mechanisms of tendon damage are the same in both Fresh and Frozen tendons. Dashed line represents when samples were unloaded. (c) The sliding τ_I was not significantly different for both groups ($p>0.98$). Similarly, the constant D averaged 9.60 ± 4.21 and 7.4 ± 2.94 for Fresh and Frozen, respectively, with no difference between the two groups ($p>0.19$). The error bars represent SEM.

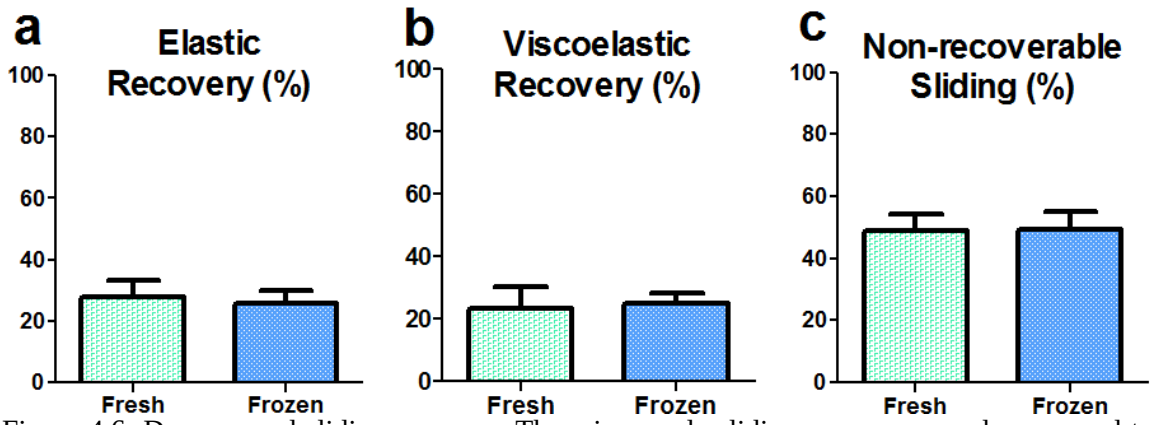

Figure 4.6: Decomposed sliding recovery. The micro-scale sliding recovery was decomposed to elastic, viscoelastic, and non-recoverable portions. For all three components, there was no significant difference between two groups ($p>0.78$). The error bars represent SEM.

4.3.2 Micro-scale Parameters

Because tendon microstructural changes have been observed at the micro-scale due to freezing the tendon, [121–123] we were particularly interested in evaluating the effect of freezing on micro-scale mechanics. The micro-scale strain fully recovered (Figure 4.5a) upon unloading and micro-scale sliding partially recovered (Figure 4.5b) for both the Fresh and Frozen groups. The micro-scale sliding time constant, which averaged 2.27 ± 1.19 minutes for Fresh and 2.25 ± 2.16 minutes for Frozen, was not different between the groups (Figure 4.5c). Similarly, the constant D averaged 9.60 ± 4.21 and 7.40 ± 2.94 for Fresh and Frozen, respectively, with no difference between the two groups ($p>0.19$). When the micro-scale sliding recovery was decomposed into elastic sliding recovery, viscoelastic sliding recovery, and non-recoverable sliding, there was still no significant difference between the two groups (Figure 4.6, $p>0.8$) in all recovery parameters. Notably, the non-recoverable sliding, which represents damage at the micro-scale, was very similar,

averaging 48.9 ± 17.4% and 49.4 ± 17.7% for Fresh and Frozen groups, respectively (Figure 4.6c). There was no difference between Fresh (0.043 ± 0.008 deg.) and Frozen (0.034 ± 0.015 deg.) for the sliding quantified at the End of Stress Relaxation (Figure 4.1).

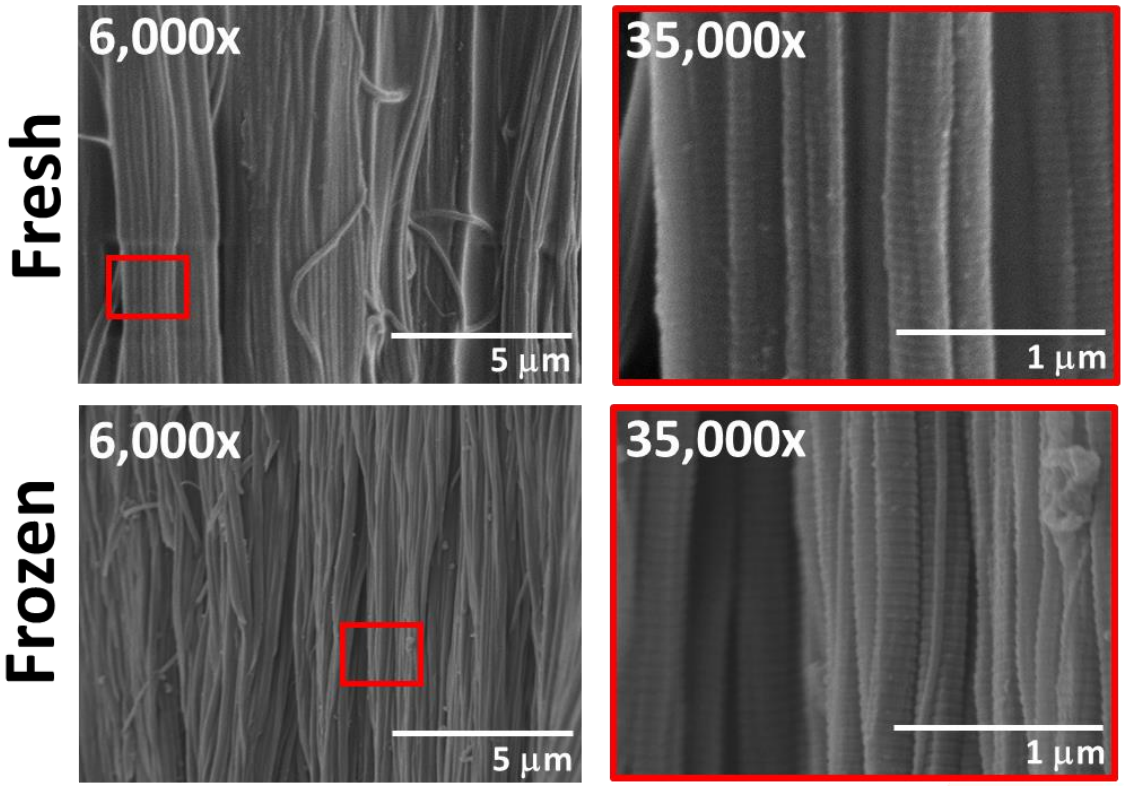

Figure 4.7: SEM images of collagen fibrils for the Fresh and Frozen groups. The qualitative observation of SEM images at that the fibril morphology and organization were similar at two different magnifications—6,000× and 35,000×— between the two groups. The red box at the low magnification represents the area imaged for the high magnification.

When studying the micro-scale damage mechanisms, the Fresh group showed the same damage mechanisms as we have previously established in previously frozen tissue.[64] The micro-scale strain fully recovered (Figure 4.5a), suggesting that there is no damage to collagen fibrils. In addition, the micro-scale sliding only partially recovered (Figure 4.5b) with 50% non-recoverable sliding, suggesting that damage is localized to the

structure that connects adjacent collagen fibrils together. The qualitative observation of tendon ultrastructure using SEM revealed that the fibril morphology and organizations are both similar in both Fresh and Frozen groups (Figure 4.7). In summary, at the micro-scale, there was no difference between the Fresh and Frozen groups and the damage mechanisms were also the same.

4.4 Discussion

This study investigated the effect of freezing on multi-scale tendon mechanics and novel damage mechanisms that was discussed in Chapter 3. There was no difference between Fresh and Frozen groups for any of the parameters measured at the tissue-scale, suggesting that there is no effect of freezing on tendon tissue-scale mechanics. We also showed that the micro-scale strain fully recovered (Figure 4.5a) and micro-scale sliding was only partially recoverable (Figure 4.5b), suggesting tendon damage is localized to the structure that connects adjacent fibrils together, and the mechanisms of tendon damage are the same in both Fresh and previously Frozen tendons. The novelty of the study is that we demonstrated that there is no effect of freezing by introducing novel tissue-scale parameters, quantifying micro-scale mechanics, and evaluating the effect of freezing on damage mechanisms, which have not been addressed in previous studies.

4.4.1 Effects of Freezing on Tendon Mechanics

This study demonstrated that there is no difference between Fresh and Frozen groups at both the tissue- and micro-scales. Our findings are consistent with other studies

using tendon and ligament that compared Fresh and Frozen group at the tissue-scale. [96,114–118] Notably, there was no difference at the micro-scale, despite the previously observed increase in interfibrillar space [121,122] and increase in fibril diameter [121,123] following freezing. While the formation of ice crystals may alter collagen integrity, this alteration has only been observed in engineered biomaterials. [125,126] This suggests that native tendon and ligament may be less affected by the ice crystals, especially when carefully frozen. We preserved fascicles by freezing the whole rat tail with its skin still intact, without freezing the isolated individual fascicles, and placing fascicles in plastic bags, wrapped in a PBS soaked gauge. This likely helped protect the tendon to maintain its micro-scale mechanics throughout the freeze-thaw process. In addition, we limited our freeze-thaw cycle to three to minimize the effect of freezing. [96] The method of storage and the number of freeze-thaw cycles may be important in preserving the mechanics of tendon and ligament, and the protocol used in this study was effective for this preservation.

4.4.2 Effects of Freezing on Damage Mechanisms

Freezing tendon had no effect on damage mechanisms at either length scale. At the tissue-scale, we used previously established mechanical parameters that reflect tendon damage. Similar to other studies, we observed elongation of toe-region (i.e., increase in transition strain) [17,90,127] and increase in inflection point strain, [64] which can mark a damage threshold. [64] Thus, this study suggests that the damage initiates at the same strain level for both Fresh and Frozen groups (i.e., Initial Ramp inflection point). Interestingly, there was no difference between Initial Ramp and Ramp to Failure linear region modulus,

as expected. [17,64,86,90,127,128] All of the tissue- and micro-scale parameters were within a standard deviation from our previous study, [64] and some of the variations may be due to the use of different rat strain, age, and gender.

At the microscale, we observed full recovery of micro-scale strain and partial recovery of micro-scale sliding, which is consistent with our previous study. [64] In both groups, the non-recoverable sliding averaged about 50%. Thus, the damage mechanisms investigated in previously frozen tendon can be applied to fresh tendons. In addition, the fibril morphology and organizations were similar for both groups, suggesting that freezing, using this protocol, does not have an effect on the ultrastructure of tendon. This supports the use of previously frozen tissue for future experiments with a careful consideration of the method of storage and number of freeze-thaw cycles.

The limitation of the study was that we combined samples that underwent from one to three freeze-thaw cycles into a single group. Although it is possible that there is a difference between samples that underwent one and three freeze-thaw cycles, a previous study in human flexor tendons also demonstrated that there is no difference in mechanics between samples that underwent one and three freeze-thaw cycles. [96] In addition, several studies have not observed a difference among samples that underwent multiple freeze-thaw cycles; there was no difference between human patellar tendon that underwent one and eight freeze-thaw cycles [114] and human Achilles tendon that was fresh and underwent five freeze-thaw cycles. [118] Thus, combining all freeze-thaw cycles groups into a single group was unlikely to cause any difference. In addition, while it is possible that the freezing can affect other types of tendons, due to a difference in their ultrastructure, this is unlikely

because the rat tail tendon is one of the smallest tendons used in research, and thus it is more likely than other tendons to be vulnerable to potential freezing effect.

4.5 Conclusion

This study used multi-scale mechanics to evaluate the effect of freezing on tendon mechanics and on damage mechanisms. Our study demonstrated that there was no difference between Fresh and Frozen tendon in any of the tissue- and micro-scales parameters up to three freeze-thaw cycles. In addition, we observed the full recovery of the micro-scale strain but partial recovery of micro-scale sliding, indicating that the damage mechanisms are the same for both Fresh and Frozen tendons. We support the use of previously frozen tissue for future experiments with a careful consideration of the method of storage and number of freeze-thaw cycles.

Chapter 5

COMPARATIVE MULTI-SCALE HIERARCHICAL STRUCTURE OF THE TAIL, PLANTARIS, AND ACHILLES TENDONS IN RAT

Based on accepted work: Lee, AH.; Elliott, DM. "Comparative Multi-scale Hierarchical Structure of the Tail, Plantaris, and Achilles Tendons in the Rat,": J. Anat. (in press)

5.1 Introduction

Rodent tendons are widely used to study human pathologies. Specifically, rat tail tendon is widely used because its structure is relatively simple, easy to isolate, and often available as waste tissue; however, rat tail tendon is highly specialized due to its relatively low load-bearing mechanical function. [129–132] Rat plantaris and Achilles tendons are also popular model systems, [5,133–137] and there is an increasing interest in plantaris tendon as it has recently been suggested to contribute to chronic Achilles tendinopathy. [138–140] However, the gross morphology and multi-scale hierarchical structure of these rat tendons are not fully understood.

Tendon hierarchical structure, spanning multiple length scales, is widely known, yet there remains disagreement about terminology and definitions, which hinders communication among scientists and interpretation of experimental results. For example, much of the literature uses the terms fiber and fiber bundle to arbitrarily refer structures made of collagen. This general usage of 'fiber' can cause a confusion when studies report fibrils [141] and fascicles [19] as fibers. It is widely accepted that fascicle is the largest

tendon subunit, [19,35,36] followed by smaller subunits called fibers, and each fiber is composed of fibrils. However, the definitions of fascicle and fiber are often dependent on their size and not their characteristic features. These definitions impair the ability to compare across species, where the sizes of a fiber and fascicle may change with animal sizes. [36,142] In support of this notion, fascicle size in larger animals [36] is about the same size as an entire rat tendon. *Fascicle* should be defined as a bundle of fibers with distinct interfascicular matrix boundaries at the tissue-scale that is populated with round cells. [143,144] We hypothesize that rat tendons do not have fascicles due to the small size, with the exception for the special case of rat tail tendon. [130,131] Precise definition and terminology of these hierarchical structures are crucial because tendon structures are directly related to physiology and mechanical function.

Another source of confusion is the existence, of a *fiber*. While some include fiber as a part of tendon hierarchical structure schematics [18,35,145], others exclude it,[19,95] and the terminology of fiber is used inconsistently. Moreover, when a fiber is defined, it is done by diameter size, which may be species-dependent. [36,142] This definition is problematic, and it is hard to distinguish between fiber from fascicle because they have been reported to have large and overlapping ranges of sizes. [18,145] An alternative way to define a fiber is to base on another structural component such as cells. Elongated tendon cells reside parallel to the direction of fibrils, and a group of cells is aligned and connected by gap junction.[143,146,147] These cells outline a bundle of collagen fibrils, and this bundle may be defined as a fiber. This definition is consistent with the developmental process of tendon, where multiple cells in contact deposit collagen between cell-cell

junctions during early development. [148] At later stages of development, cells surround a bundle of collagen fibrils and grow in size, [148] and thus this supports a hypothesis that cells may define the boundary of a fiber. In this study, we will test our hypothesis that fiber is defined by the surrounding cells.

Tendon hierarchical structures may also depend on the loading environment. For example, there are differences between non-load and load-bearing tendons for multi-scale mechanics [80–83] and composition [84] in equine and bovine tendons. These differences between tendons with different mechanical functions suggest that their hierarchical organizations may be different. [36] Thus, we selected the tail, plantaris, and Achilles tendons to represent tendons with different mechanical functions.

The objective of this study was to evaluate the hierarchical structure of rat tendons at multiple length scales to test our hypotheses that rat tendons, except for tail tendon, do not have fascicles due to the small size and cells may define the boundary of a fiber. Because the hierarchical structure is likely to depend on the species and loading environment, we chose a single species that is widely used for tendon research (rat) and tendons with varying mechanical functions (tail, plantaris, Achilles). This study was designed to investigate the gross morphology at the tissue-scale and hierarchical structures including fascicle and fiber at the micro-scale by using multiple imaging methods such as histology, SEM, and confocal imaging. In addition, we reconstructed a three-dimensional (3D) structure from confocal imaging stacks. Understanding and properly defining tendon hierarchical structures are critical in research to advance the design and interpretation of experiments and development of tissue engineered constructs.

5.2 Materials and Methods

5.2.1 Sample Preparation

All tendons were from 4-7-month-old female Long Evans rats and sacrificed on the day of the experiment. Rat tail (n=13), plantaris (n=13), and Achilles (n=13) tendons were divided into five experimental groups, where each group was a different imaging technique. Each tendon was processed for a longitudinal PicroSirus Red staining (n=3/tendon type), transverse H&E staining (n=3/tendon type), longitudinal scanning electron microscope (SEM) (n=3/tendon type), confocal imaging with second harmonic generation (SHG) signals and cells (n=3/tendon type), or 3D rendering of confocal image stack (n=1/tendon type).

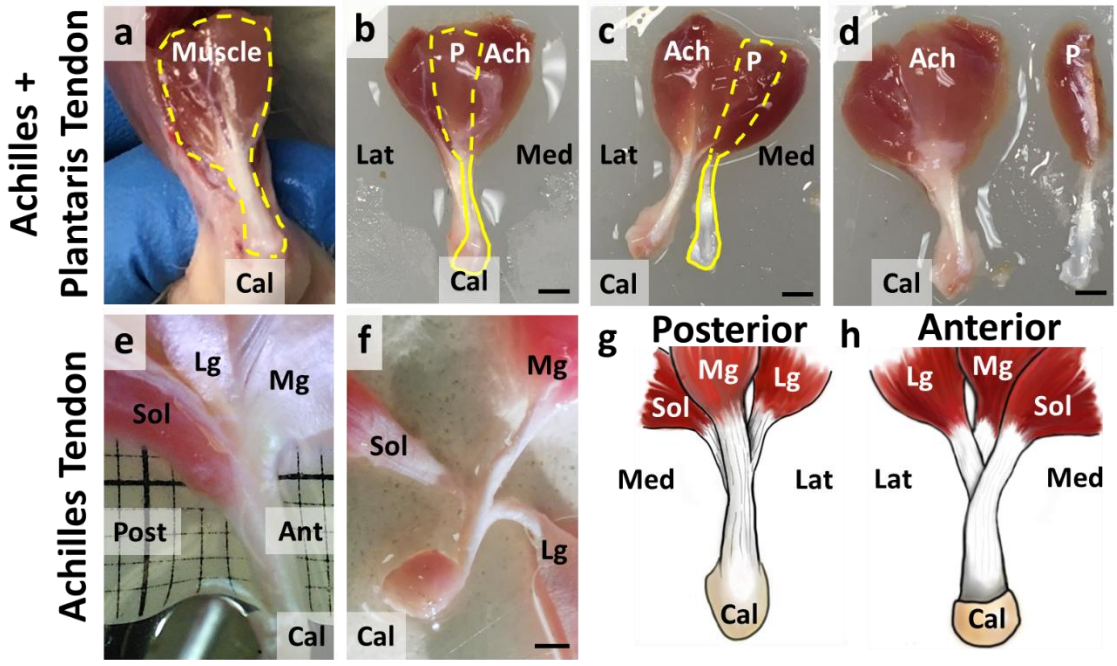

Figure 5.1: Gross morphology of plantaris and Achilles tendons. (a) Plantaris (P) and Achilles (Ach) tendons are bound together in situ (dashed yellow line). (b) Plantaris muscle is posterior to Achilles muscle complex (dashed yellow line), and plantaris tendon is visible above Achilles tendon (solid yellow line). (c) By cutting connective tissue binding plantaris and Achilles tendons from the insertion, these two tendons can be completely separated (d). (e) Achilles tendon was further dissected and is a fusion of three tendons originating from soleus (Sol), lateral gastrocnemius (Lg), and medial gastrocnemius (Mg) muscles. (f) Sub-tendons are tightly fused, and further separation of tendons is difficult without directly cutting the tendon. Scale bars: 2 mm. We created schematics of (g) posterior and (h) anterior views to show the complex structure of Achilles tendon.

5.2.2 Gross Morphology

Rat tail tendon fascicle was dissected following the same protocol from published studies.[64,149] Plantaris and Achilles tendons were dissected using bone cutting shears, scalpels, and forceps to dissect the Achilles and plantaris complex, about 4 cm in length

with the calcaneus attached (Figure 5.1a, b). We separated out plantaris and Achilles tendons from each other by removing excess surrounding soft tissue (Figure. 5.1c, d). Each tendon was randomly assigned to an imaging group after the dissection. An additional Achilles tendon was further dissected using a sharp dissection and microscope to study how Achilles tendon is fused. We separated each sub-tendon to verify that Achilles tendon is fused tightly. This sample was discarded after taking a reference picture (Figure 5.1e, f) and was not used further in the study.

5.2.3 Histology

Histological analyses were performed in longitudinal and transverse directions to observe the hierarchical structure of tendons in both directions. Each tendon was fixed in 4% paraformaldehyde at room temperature. For the longitudinal histology, all tendons were fixed overnight. For the transverse histology, the tail fascicle was fixed for 30 minutes, plantaris tendon was fixed for 2 hours, and Achilles tendon was fixed overnight. The fixed tendons were then incubated for 30 minutes in a 30% sucrose solution to avoid possible ice damage. To process as frozen sections, each tendon was mounted on a plastic mold with optimal cutting temperature compound (OCT) and was flash frozen with an indirect contact with liquid nitrogen. We used the CryoJane Tape Transfer System (Leica Biosystems) to cut 14 μm thickness sections for the longitudinal group and 12 μm thickness sections for the transverse group. We cut the mid-plane of the tendon, away from both anterior and superior planes. The longitudinal sections were stained with PicroSirus Red to visualize collagen alignment, and transverse sections were stained with H&E to visualize general

organization. The staining process followed a standard staining procedure for frozen sections, and the slides were mounted to be visualized under Axio Imager 2 Pol (Carl Zeiss Inc). Images were acquired at two different magnifications (20x and 40x).

5.2.4 Scanning Electron Microscopy (SEM)

We imaged tendon structure using SEM to visualize the ultrastructure and confirm histological observations. Tendons used for SEM were processed following the same procedure as histology until sectioning. Using the cryostat, each tendon was cut once in a longitudinal direction of the mid-plane to image the ultrastructure, and the sample was briefly placed in water to remove the remaining OCT. The section was processed for SEM using a standard processing technique consisting of fixation with 1% osmium tetroxide followed by a series of dehydration with ethanol. Each sample was dried using a critical point dryer, mounted on an SEM sample holder using carbon tabs, and coated with platinum (Leica Biosystems). The samples were visualized with a field emission SEM (Hitachi S-4700).

5.2.5 Confocal Imaging with Second Harmonic Generation (SHG) Signals and Cells

To test our hypothesis that cells outline fibers in tendon, we acquired SHG signals for the collagen alignment and fluorescence from cells. SHG microscopy is a nonlinear optical method that can visualize collagen without additional staining or processing. [52,150–152] Immediately after the sacrifice and dissection, the tendon was incubated in DMEM culture medium (Dulbecco's Modified Eagle Medium) supplemented with 25 mM

HEPES, 1% penicillin, and 1% streptomycin (Life Technologies) for 30 minutes at 37C. Each tendon was then stained with 10 μM CellTracker Green CMFDA dye (Life Technologies) for 45 minutes at 37C and washed in the medium for 30 min at 37C. Each sample was placed in a petri dish to image with a laser-scanning multi-photon microscope (LSM 780, objective Plan-Apochromat 20x/1.0, Carl Zeiss Inc). We used Chameleon Vision II Ti:S laser (Coherent Inc.) tuned to 810 nm and an external detector to collect SHG signals. The maximum penetration depth was ~ 100 μm. A cover glass was placed on top of the tendon to prevent it from floating. The confocal image stacks ($0.42 \times 0.42 \times 0.67$ μm pixel^{-1}) were taken at the mid-substance of each tendon. The SHG signals of the most superficial (closest to the skin) and deep layers (furthest from the skin) were separated from the rest of the stack to show the change of collagen alignment through the depth. To show the cell placement, an optical slice that showed the strongest cell staining in the deep plane was separated from the confocal stack.

5.2.6 Three-dimensional (3D) Rendering of Confocal Images

To observe collagen alignment and cell placement in 3D, a separate confocal image stack from above, spanning ~50 μm in the z-direction including the surface of tendons, was acquired with the same method as the previous section. The confocal image stacks were rendered by software AMIRA 6.3 (Thermo Fisher Scientific). The blood vessels and cells were selected using an automatic threshold method under segmentation editor. Additional structures that were not captured by the automatic segmentation were selected manually. The surface of vessels and cells were rendered, and the volume of the SHG signal of

collagen was rendered to show the 3D structure of tendon. The opacity of collagen was adjusted to show the 3D structure through the depth.

5.3 Results

5.3.1 Gross Morphology of Plantaris and Achilles Tendons

The gross morphology of the plantaris (P) and Achilles (Ach) tendon demonstrated its structural complexity. Plantaris and Achilles tendons are bound together in vivo (Figure 5.1a). The plantaris muscle originates on the anterior-lateral side of the Achilles muscle, passes over the calcaneus (Cal), and inserts into the bottom of the foot. Once the calcaneus is cut, the plantaris and Achilles tendons can be easily distinguished from each other. The plantaris muscle is posterior to the Achilles muscle complex (Figure 5.1b, dashed yellow line), and the plantaris tendon is visible anterior to the Achilles tendon (solid yellow line). We separated the two tendons by cutting connective tissue binding the plantaris and Achilles tendons together at the insertion (Figure 5.1c, d). Human plantaris tendon has been previously described as a vestigial tissue that is absent for a large portion of the population. [153–156] However, recent studies identified plantaris tendon in all or most cadavers with variable insertion sites. [138,157,158] We observed a single insertion site for all rat plantaris tendons, unlike human plantaris tendons. The Achilles tendon was further dissected to observe its gross morphology, and we verified that the Achilles tendon is a fusion of three sub-tendons originating from soleus (Sol), lateral gastrocnemius (Lg), and medial gastrocnemius (Mg) (Figure 5.1e) muscles, similar to human. [159,160] The sub-tendons from these muscles are tightly fused approximately at the half of the tendon length

and cannot be further separated without directly cutting the tendon (Figure 5.1f). Among the three muscle groups, the Sol tendon is the most anterior sub-tendon, and Mg tendon is the most posterior sub-tendon. Schematics of the posterior (Figure 5.1g) and anterior (Figure 5.1h) views show the complex 3D morphological structure of Achilles tendon.

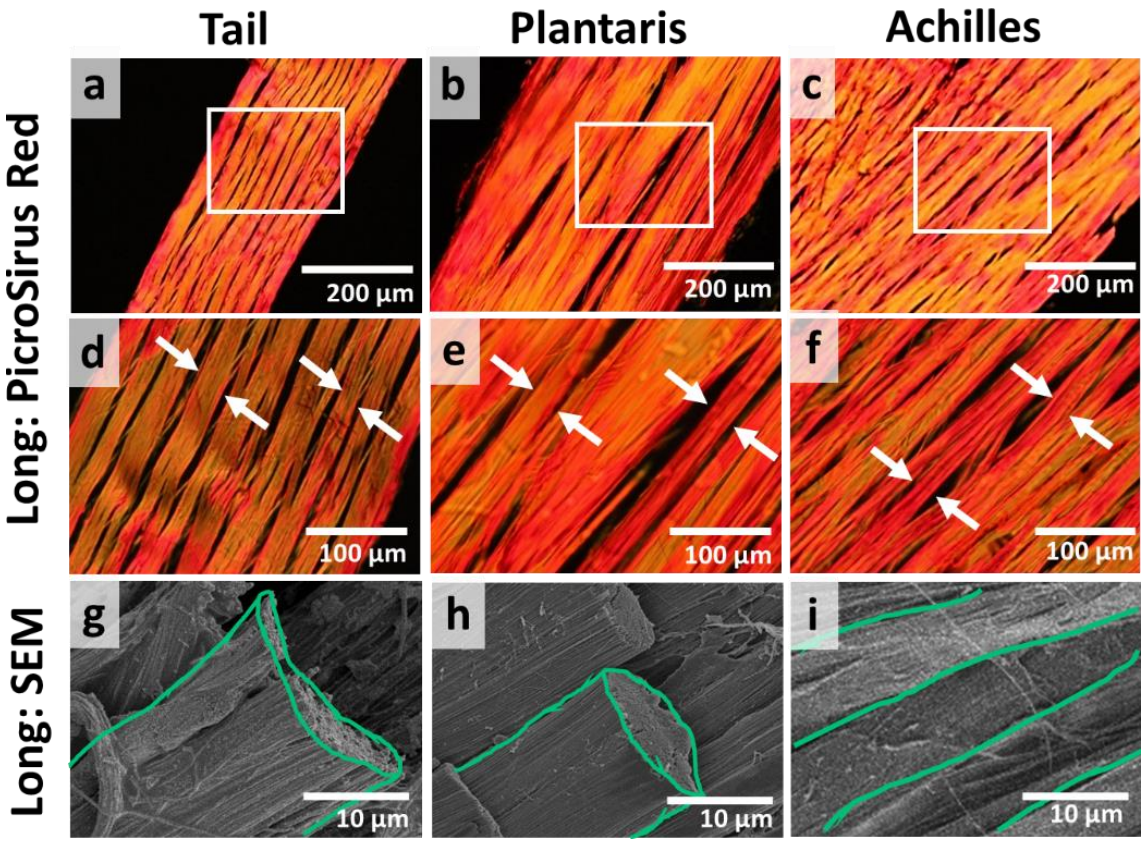

Figure 5.2: Evaluation of fiber structure in longitudinal direction. (a-c) Rat tail, plantaris, and Achilles tendons were cut in longitudinal (Long) direction, stained with PicroSirius Red, and viewed at low magnification. White boxes represent areas observed at (d-f) high magnifications, and fibers are highlighted (white arrows). (g-i) Longitudinal SEM shows fibers (green) with a similar diameter as observed in histology. No fascicle boundary was observed.

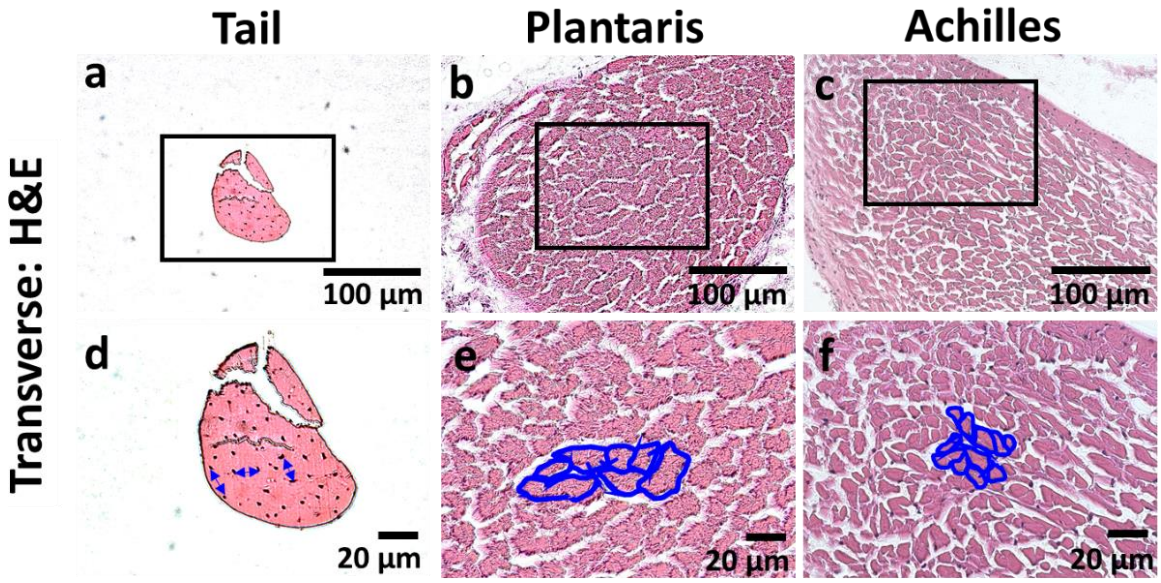

Figure 5.3: Evaluation of fiber structure in transverse direction. (a-c) Rat tail, plantaris, and Achilles tendons were cut in the transverse direction, stained with H&E, and viewed at low magnification. Black boxes represent areas observed at (d-f) high magnifications. The distance between cells are highlighted (blue arrow) for the rat tail tendon, and fibers in plantaris and Achilles tendons are outlined (blue). No fascicle boundary was observed.

5.3.2 Histological Evaluation of Tendon Micro-scale structure

To investigate the hierarchical structure and cell morphology in rat tendons, we conducted several analyses using multiple imaging methods. In longitudinal sections stained with PicroSirus Red, we observed a separation between structures with a diameter of 10-50 µm, at both low (Figure 5.2a-c) and high magnifications (Figure 5.2d-f) for all three tendons. The hierarchical structure defined by this unit of separation, highlighted in white arrows, is likely to be a fiber. Supporting this notion, we also observed structures with a similar diameter in a longitudinal view of SEM in all tendons, highlighted in green (Figure 5.2g-i). In addition, the transverse sections stained with H&E also had separations

with a similar diameter at low (Figure 5.3a-c) and high magnifications (Figure 5.3d-f), outlined in blue. Rat tail tendon fascicle did not have a similar pattern of separation between the subunits as seen in plantaris and Achilles tendons in the transverse direction, perhaps due to its small overall size. Nonetheless, the distance between cells of tail fascicle (blue arrows, Figure 5.3d) was similar to the separation observed in plantaris and Achilles tendons (blue outlines, Figure 5.3e, f). Interestingly, the microstructure of tendon may vary along the length based on our pilot study (Figure C.1). Note that the observed separation between fibers is likely due to loss of water and non-collagenous matrix during sample processing (Figure C.2).

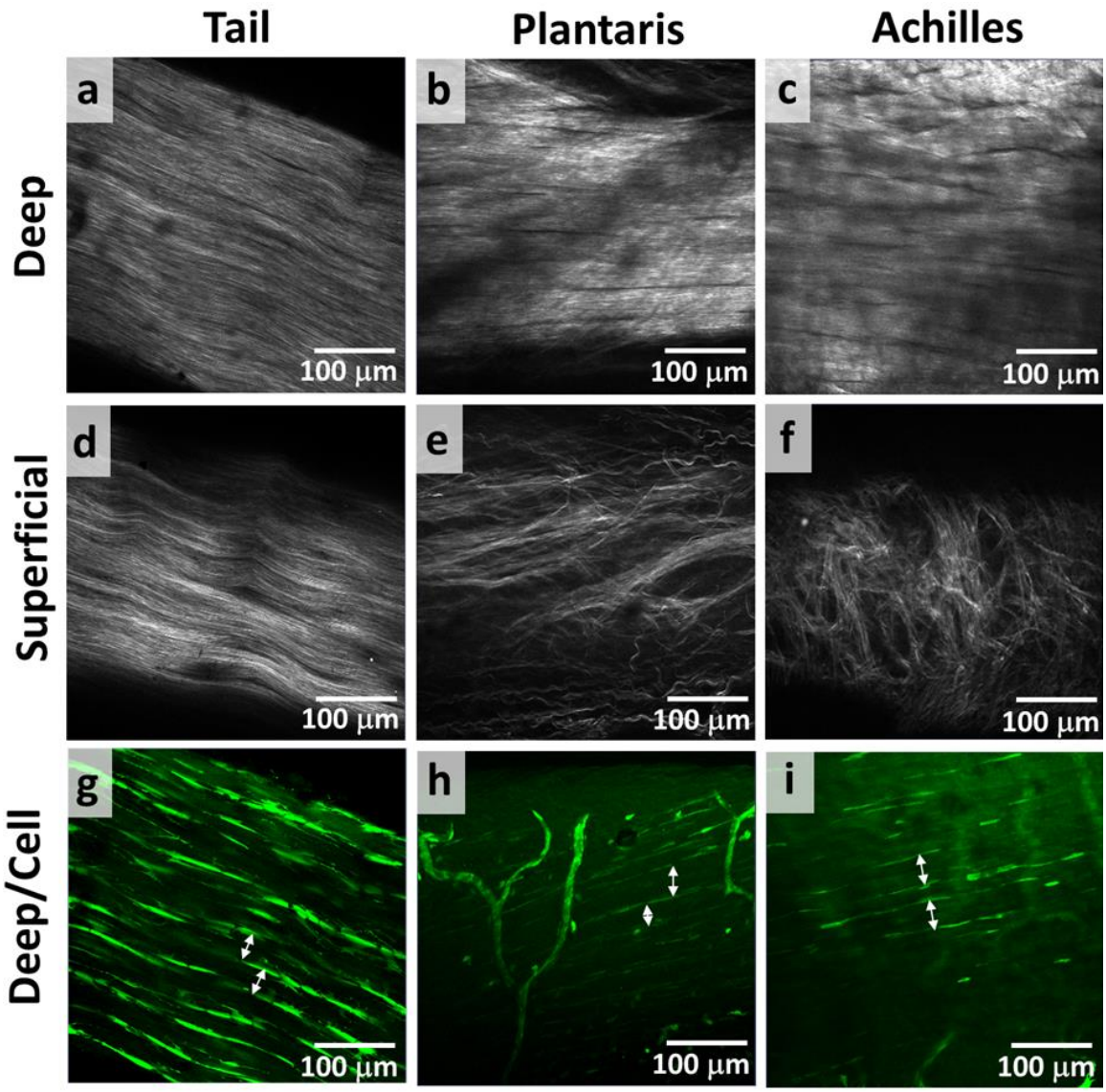

Figure 5.4: Collagen alignment and cell morphology. (a-c) Collagen alignment was viewed with SHG signals. Collagen was aligned at deep planes,away from the skin, for tail, plantaris, and Achilles tendons. (d-f) Whereas the collagen alignment was not different between the superficial, close to the skin, and deep planes for the tail tendon, plantaris and Achilles tendons had an additional layer of a complex meshwork of collagen or peritenon. (g,h) In deep planes, elongated cells outlined collagen bundle (white arrows), which matched the sizes of fiber observed with histology. Thus, we define fiber as a bundle of collagen with diameter 10–50 lm outlined by elongated cells. No fascicle boundary was observed.

5.3.3. SHG Evaluation of Fiber Structure and Cell Morphology

The collagen structure and cell morphology were visualized using the confocal microscope to confirm histological findings without the potential fixation and histological artifacts. At the deep plane (away from the surface of the tendon), all tendons had aligned collagen (Figure 5.4a-c). At the superficial plane (the surface of tendon), tail tendon fascicle had no change in collagen alignment from deep planes (Figure 5.4d), while both plantaris and Achilles tendons had an additional layer of peritenon, a complex meshwork of collagen that was about 20 μm thick (Figure 5.4e, f). In deep planes, the cells with elongated morphology aligned along collagen bundles (white arrows) that were the same diameter as observed histology (Figure 5.2, 5.3). Thus, rat tendons have a single hierarchical structure that is surrounded by the elongated cell, and this structure had consistent diameters between 10-50 μm: hereafter defined as fiber (Figure 5.4g-i).

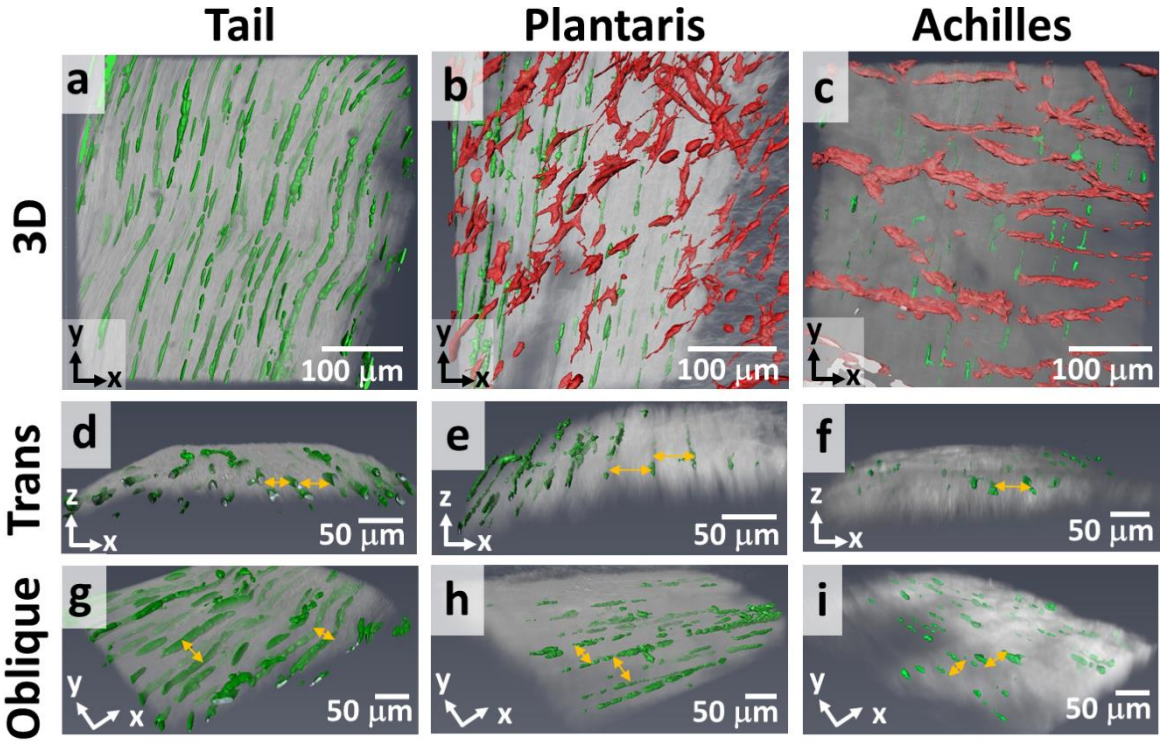

Figure 5.5: 3D structure of tendon. (a-c) 3D structure of tendon was rendered from a confocal imaging stack (50 lm deep in z-direction) to show the overall cell morphology and collagen alignment. All tendons show that cells in the deep region (green) outline collagen (gray). For plantaris and Achilles, blood vessels and cells on peritenon (red) were observed, unlike rat tail tendon. (d-f) Transverse view, x–z plane, without blood vessels further illustrates that elongated cells are between adjacent fibers (yellow arrows) with a consistent diameter. (g-i) Oblique view, x–y plane, shows a spacing between collagen (yellow arrows). The opacity of collagen was adjusted to show the 3D structure.

5.3.4 Three-dimensional Evaluation of Tendon

The confocal image stacks were reconstructed to view the 3D tendon structure (Figure 5.5). The 3D reconstruction confirms that cells, shaded in green, surround the collagen bundles (grey) that match the size of the fiber that was identified by histology (Figure 5.2, 5.3). For the tail tendon fascicle, we again observed no peritenon (Figure 5.5a),

but we observed peritenon for the plantaris and Achilles tendons. The peritenon was populated with blood vessels, characterized by high fluorescent density and web-like network that wraps the surface, and with localized cells having a different morphology than the elongated cells between fibers, shaded in red (Figure 5.5b, c). In the transverse direction, the 3D structure of tendon shows that cells surround the fiber, highlighted with yellow arrows (Figure 5.5d-f). Similarly, the cells surround the fiber in an oblique view, highlighted with yellow arrows (Figure 5.5g-i). Again, we observed no additional boundary. Thus, the 3D rendering of tendon confirms that the definition of a fiber is a bundle of collagen that is outlined by elongated cells, supported by both histologically processed and unprocessed samples. In all rat tendons studied, the fiber diameters were consistently 10-50 μm.

There were no additional boundaries that further divided any of the rat tendons. We confirmed that in rat tendons there are no fascicles and the fiber is the largest subunit. Whereas we call the sub-structure in rat tail tendon a fascicle, rat tail tendon is a specialized tendon. Fiber may be the largest subunit in rat tendons, and this diameter was consistent in transverse and longitudinal histology and SEM.

5.4 Discussion

In this study, we evaluated the hierarchical structure of rat tendons at multiple length scales for tendons with varying mechanical functions, including the tail, plantaris, and Achilles tendons and created tendon-specific schematics based on our observations (Figure 5.6). Using multiple imaging methods, we confirmed that rat tendons do not

contain fascicles, with the exception of the specialized rat tail tendon, and thus fiber is the largest tendon subunit in the rat. In addition, we provided a structurally based definition of a fiber as a bundle of collagen fibrils that is surrounded by elongated cells, and this definition was supported by both histologically processed and unprocessed samples. In all rat tendons studied, the fiber diameters were consistently 10-50 µm.

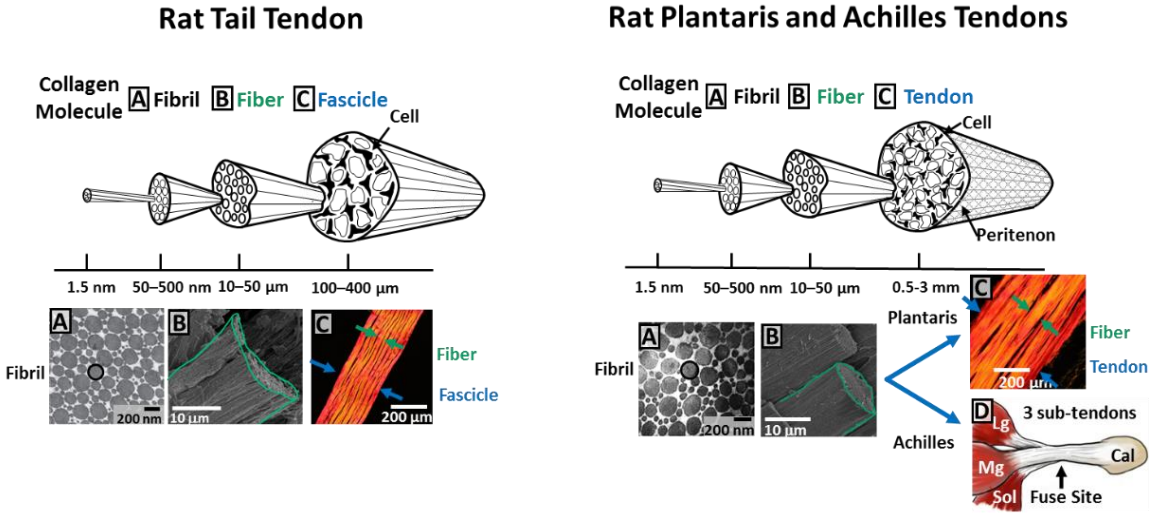

Figure 5.6: Schematic of hierarchical structure of rat tendons. Hierarchical structure of rat tail and plantaris and Achilles tendons were recreated based on the evidence from this study, and we recommend future studies consider these schematics when studying rat tendons. Data incorporated in the schematic were adapted from: [95,106,161]

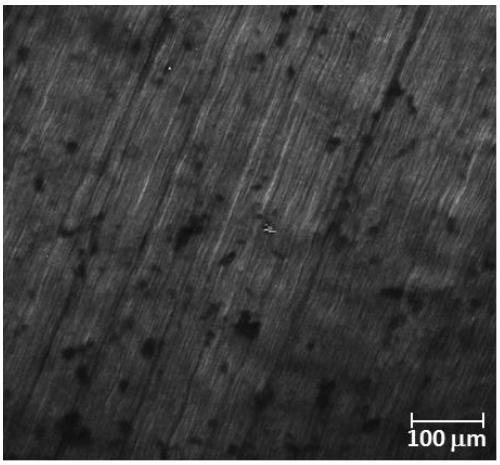

Figure 5.7: SHG of rat patellar tendon. Additional patellar tendon was harvested from 7-month old female Long Evans rat and examined under the confocal microscope. The SHG signal shows that there is no additional boundary in the patellar tendon that indicates the existence of a fascicle in rat. Thus, this data suggest that rats do not have a fascicle, with the exception of rat tail tendon.

5.4.1 Structure-based Definitions of the Fascicle and Fiber

This study provides hierarchical schematics of rat tendons that clarify structural-based definitions of fibers and fascicles (Figure 5.6). A fascicle is defined by the surrounding interfascicular matrix, which is populated with round cells [143,144] and is not simply a bundle of fibers. With the exception of the specialized rat tail tendon, we confirmed that there are no fascicles and the fiber is the largest subunit in rat tendons. In addition, a supplementary observation of SHG signals of rat patellar tendon in this study (Figure 5.7) and a previously published study [152] did not observe an additional boundary, verifying that rat tendons do not have fascicles. Considering the size of rat tendon, it is not surprising that the structural complexity is reduced with the scale of the animal.[36] In large animals, the fascicle and interfascicular matrix are easily identified and have

diameters that are larger than the entire rat tendons. [18,19,35,36,145] In the rat tendons studied here, the fiber diameter was 10-50 μm. Although this is not the first paper to identify the fiber in rat tendons,[130] this study provides evidence and a definition of a fiber that is based on characteristic features, confirmed by multiple imaging methods. Importantly, this definition is consistent with the developmental process of tendon. At later stages of development, as cells deposit more collagen, the tendon fiber is delineated as cells are pushed to the periphery.[148] To avoid confusion, the term fiber should be reserved to specifically identify this hierarchical structure of tendon, not to generally refer a bundle of collagen.

As a point of clarification, the visualizations of cell density in confocal images and 3D rendering can be misleading because they depend on a staining intensity. Because blood vessels and cells on the peritenon can also uptake the fluorophore, less fluorophore penetrated to the deeper planes of the plantaris and Achilles tendons. In addition, the diameters of plantaris and Achilles tendons are larger than that of the tail tendon fascicle, and thus it contributes to the lack of fluorophore penetration. While it may appear that cell density in the tail fascicle is higher than the plantaris and Achilles tendons, this is strictly due to the penetration of fluorophore, and this is the cause for a reduced number of cells visualized in these tendons.

5.4.2 Comparative Anatomy Across Species

We considered if the fiber and fascicle sizes may be conserved across species. Tendons from larger animals such as horse and human have a subunit that falls within the

fiber diameter and is outlined by cells, confirming these units as fibers. [37,143,162] For example, the equine tendon fiber diameter is 1-20 μm [36,81] and the human tendon primary fiber bundle diameter is 15 μm [18], which are similar to the fiber diameter 10-50 μm reported here. Thus, the definition of fiber appears to apply across species, and this supports the idea that the organization of rat tendon is not a simple scale-down of larger animals, but that the fiber size is *conserved* across species. It is likely that mouse tendon only has fibers, not fascicles, similar to rat tendon due to its small size. Tendon cell volumes [163] also appear to be consistent across species, which suggests that cells and fibers are the key units in growing aligned collagen region during the developmental process. It is unclear if the fascicle diameters are consistent across species, and it is possible that the number of fascicles or the size of fascicles may scale with the size of the animal.

The absence of fascicles in rat tendons should impact a researcher's animal model choice; studies that are focused on the structure and mechanics of the interfascicular matrix should exclude rat models. Interestingly, the age-related tendinopathy is mostly attributed to the degeneration of interfascicular matrix [164,165] and animals with the interfascicular matrix, such as horses and human, develop naturally occurring age-related tendinopathy, [166] while rats do not appear to do so. While this difference may be due to the animal's life-span and activity level, studies of age-related tendinopathy should be aware that rats lack fascicles, and thus rats lack interfascicular matrix. Nonetheless, the rat tendon is a useful model system when studying tendon structure and mechanics because rat tendon is a simpler model system, especially because the fiber structure and diameter is conserved across species.

5.4.3 Comparative Anatomy of Rat Tendons

We demonstrated that the anatomies of the rat tail, plantaris, and Achilles tendons have distinct features that are related to their mechanical functions, and each tendon can be used to answer specific research questions. The structure of tail fascicle is simple, and its mechanics are less variable, making it a suitable model to address fundamental research questions. However, the tail fascicle is limited in that it bears low-stresses and lacks peritenon, cells on peritenon, and blood vessels. Thus, it may not be a suitable model for studying research questions related to high-stress tendon or healing processes.

The plantaris tendon, on the other hand, bears a high-stress in vivo [167] and has a physiological structure including the muscle-tendon junction and blood vessels. In addition, synergist ablation, an established rat model applied to study overuse-induced muscle hypertrophy, [168–170] may be a useful model to study tendinopathy. For example, the synergistic ablation model, where the Achilles is removed to overload the synergist plantaris tendon, leads to increased matrix production and thickened plantaris tendon after 4 weeks. [133,134] This suggests that this model may represent tendinopathic changes.

The Achilles tendon also bears a high-stress, and we observed a similarity between the rat and human Achilles tendons. The major similarity is that both tendons are composed of three sub-tendons extending from medial and lateral gastrocnemius and soleus muscles with a complex arrangement. [159,160] Due to its complex structure, the Achilles tendon is difficult to study at multiple length scales. Because of the fusion of three tendons, there is likely an inter-tendon sliding [171] in addition to the micro-scale sliding. This likely

contributes to the inhomogeneous loading observed in vivo. [171–173] This structural complexity should be addressed when using the Achilles tendon as a model system.

While we and others have referred to the dissected substructure from a rat tail tendon as a *fascicle*, we want to stress that the rat tail fascicle is different from the fascicle in larger animal tendons. The tail tendon has a sheath that divides individual *fascicles* that is populated with round cells, [174] and fascicles in larger animal tendons have interfascicular matrix that is populated with round cells. [143,144] However, this sheath in the tail tendon and the interfascicular matrix of larger animals are distinctly different. In large animals, surrounding interfascicular matrix boundaries are easily visible at the tissue-scale, [83] yet the sheath around rat tail tendon is only observable at the micro-scale. [130,131] The fascicles of larger animals are tightly bound to each other and must be cut to be separated. [83] The interfascicular matrix in larger animals bears a small but measurable load and can resist deformation, [81] while the sheath in rat tail tendon can be easily peeled off with no resistance. Thus, the rat tail fascicle is a specialized tendon with a unique hierarchical structure and should not be directly compared to the fascicle in larger animals.

5.4.4 Multi-scale Tendon Structure-Function and Damage Mechanics

Tendon structure and mechanics are related at multiple scales, and the fiber-scale is likely to be an important contributor to tendon mechanics and damage. For example, the micro-scale structural damage in the tail tendon is related to the changes in tissue-scale mechanical parameters. [64] Micro-scale sliding, which represents shear between micro-

scale structures, is related to both loading [38] and damage [64] mechanisms. Because these studies used photobleached lines and optical microscopy, which cannot distinguish between fibrils and fibers, both substructures are captured in the term 'micro-scale'. [38,64] Other studies have shown damage that is localized within fibers. Rat tail tendon that is loaded and then labeled with collagen hybridizing peptide (CHP), which binds to denatured collagen, showed a localization of CHP staining in a structure that had the same diameter as fiber observed here. [104] A similar observation was made in rat flexor carpi ulnaris tendon after mechanical loading, where CHP was localized in a structure with the same diameter as fiber. [175] In addition, the 3D reconstruction of SHG signals showed that the space between fibers increased in loaded rat patellar tendon, suggesting that damage is related to structural changes in fiber. [152] Therefore, the fiber is likely to be a key substructure affected during tendon damage.

5.5 Conclusion

In conclusion, this study evaluated the hierarchical structure of the rat tail, plantaris, and Achilles tendons at multiple length scales. Structurally based definitions of fibers were established using multiple imaging methods. With the exception of the rat tail tendon, we confirmed that rat tendons do not contain fascicles, and the fiber is defined as a bundle of collagen fibrils that are surrounded by elongated cells. In all rat tendons studied, the fiber diameters were consistently between 10-50 μm, and this diameter range appears to be conserved across larger species. Specific recommendations were made highlighting the strengths and limitations of each rat tendon as a research model.

Chapter 6

MULTI-SCALE LOADING AND DAMAGE MECHANISMS OF RAT TAIL, PLANTARIS, AND ACHILLES TENDON

6.1 Introduction

Using rat tail tendon, we demonstrated that micro-scale sliding is the load transfer mechanism [38] and non-recoverable sliding is the damage mechanism in Chapter 3. [64] Yet, rat tail tendon has a specialized structure as demonstrated in Chapter 5 and is a relatively non-load bearing tendon. [176] Thus, the load transfer and damage mechanisms are still unknown for load-bearing rat tendons. Despite some differences between rat tail tendon and load-bearing tendons, we hypothesize that micro-scale sliding is a key component for both mechanisms since they both have similar fiber structures. [176] We chose rat plantaris and Achilles tendons to study these mechanisms. The plantaris tendon bears high-stress *in vivo* [167] and has a relatively simple structure. [176] The Achilles tendon also bears high-stress and is a highly specialized tendon with a complex structure as shown in Chapter 5 and other studies. [171,172,176–178]

The objective of this study was to investigate the multi-scale load transfer and damage mechanisms of load-bearing tendons, the plantaris and Achilles tendons, and to evaluate if the mechanisms are similar to the mechanisms demonstrated in the tail tendon. Recently published data from the tail tendon, which has the simplest structure, was reanalyzed and included for comparison. [64] We hypothesize that the micro-scale sliding

will increase with applied strain and only be partially recoverable when loaded to high strain in the plantaris and Achilles tendons.

6.2 Materials and Methods

6.2.1 Sample Preparation

Mechanical testing was performed on rat plantaris (n=33) and Achilles (n=6) tendons that were harvested from 4-7-month-old female Long Evans rats. Additionally, the mechanical testing data of rat tail tendon (n=28) from the Rest group in Chapter 3 were reanalyzed for this study. [64] All tendons had been frozen at -20°C, and the maximum number of the freeze-thaw cycle was limited to three to minimize the effect of freezing, following the protocol discussed in Chapter 4. [149] A total summary of sample number and dimensions, including cross-sectional-area and gauge length, are included in Table 6.1 and 6.2.

Table 6.1: Total sample count. This table includes the total sample used for the mechanical analysis of the three tendons and reasons for exclusion.

	Tail				***Plantaris***			***Achilles***
Strain Group (%)	**2**	**4**	**6**	**8**	**14**	**20**	**25**	**14**
Mechanical Tested	7	7	7	7	11	11	11	6
Macro-scale Analysis	7	7	7	6*	10%	11	11	6
Micro-scale Analysis	7	7	7	5[#]	8[#]	11	6[#]	6
Total	26				25			6

* Excluded because the tendon fascicle was twisted, and, as a result, the linear modulus was two standard deviations away from the population average. [%] Excluded because of a grip slippage during the initial ramp and, as a result, the macro-scale strain was two standard deviations away from the population average. [#] Excluded because photobleached lines were not clear enough to be recognized with an automatic registration.

Table 6.2: Sample gauge length and area of mechanically tested tendons. Mean ± standard deviations.

	Tail	***Plantaris***	***Achilles***
Gauge Length (mm)	29.7 ± 1.4	7.7 ± 0.8	6.6 ± 0.5
Area (mm^2)	0.13 ± 0.04	0.28 ± 0.06	1.40 ± 0.3

A plantaris and Achilles tendon complex was dissected from a calcaneus bone, and each tendon was separated as shown previously. [176] The rat tail tendon was harvested as previously described. [149] All tendons were placed in PBS at room temperature. We stained the rat plantaris and tail tendons with 10 μg/ml 5-DTAF and Achilles tendon with 20 μg/ml 5-DTAF for 20 minutes. [97] We mechanically tested tendons on a custom-made uniaxial testing device with a PBS bath mounted on an inverted confocal microscope (LSM 5 LIVE, objective Plan-Apochromat 10x/0.45) as previously described.[38]

6.2.2 Mechanical Analysis – Mechanical Testing Protocol

Plantaris tendons were randomly assigned to 3 strain groups with n=11 tendons per group, where each group was mechanically loaded to a grip strain of 14, 20, or 25%. Each Achilles tendon was loaded to a single grip strain of 14%, with n=6 tendons. After mechanically testing one strain group of Achilles tendon, we decided to discontinue testing other strain groups due to the complexity of the structure [176] and a related limitation in our testing setup (Figure 6.1). The details will be further elaborated in future sections.

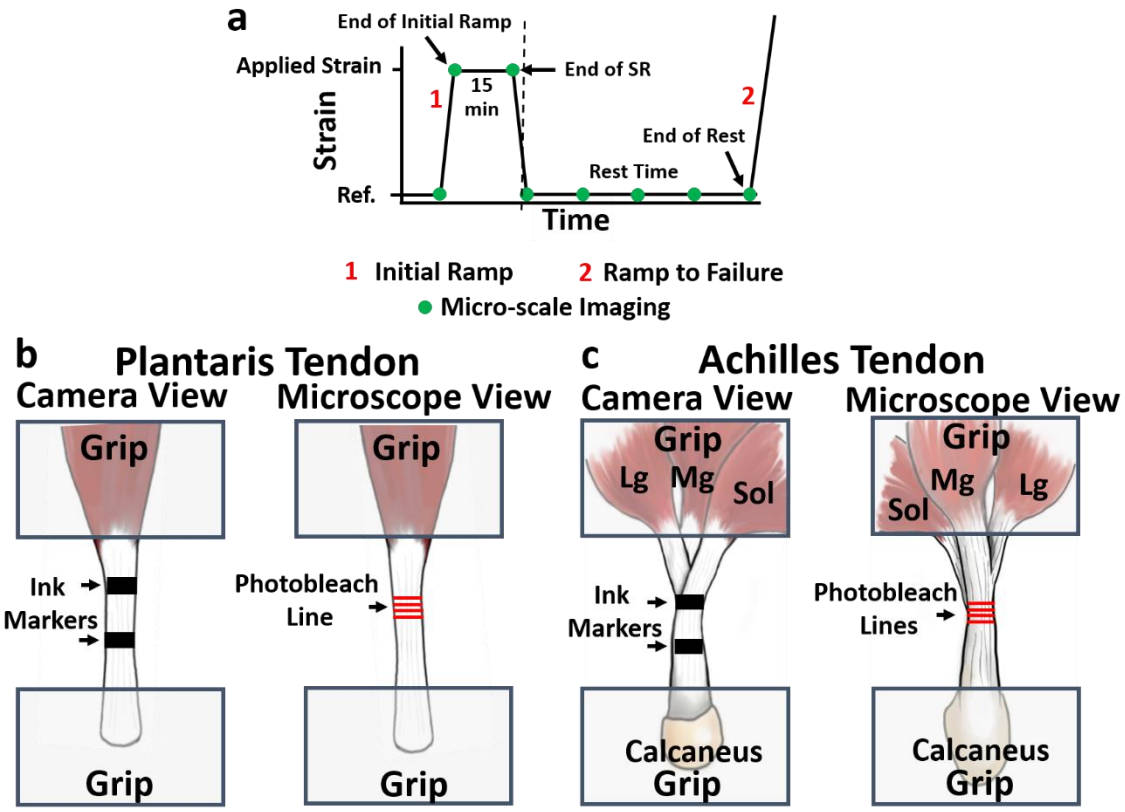

Figure 6.1: Schematic of experimental design and overall micro-scale deformation. (a) Mechanical testing profile was the same as previous chapters. Dashed line represents when tendon was unloaded to the reference length. (b) Ink markers were applied to plantaris tendon to optically measure the applied strain using a CCD camera. On the other side of the tendon, four photobleached lines were applied using a confocal microscope to measure the micro-scale deformations. Similarly, the ink markers and photobleached lines were applied for c) Achilles tendon. The photobleach lines are not to scale and enlarged for visualization.

We preloaded each tendon to 5mN to establish a reference length and preconditioned to 5 cycles of 3% grip strain. Each tendon was mechanically loaded to the assigned grip strain, and we held the strain constant for 15 minutes of stress relaxation followed by unloading to the reference length (Figure 6.1a). The dashed line represents

when tendon was unloaded. The tendon was held at the reference length for 40 minutes of rest period before ramping to failure. All loading and unloading strain rates were 1%/s. The detailed method of mechanical testing of tail tendon following is demonstrated in Chapter 3. [64] Briefly, the tail tendon was randomly assigned to 4 strain groups with n=7 tendons per group, where each group was mechanically loaded to a grip strain of 2, 4, 6, or 8%. The tail tendon was preconditioned to 5 cycles of 4% grip strain and held at the reference length for 60 minutes before ramping to failure.

6.2.3 Mechanical Analysis – Data Acquisition

To calculate the cross-sectional area, we used the confocal microscope and a scanning laser displacement sensor. [93] We collected confocal image stacks under preload and fitted with an ellipse to measure a cross-sectional area. For the plantaris and Achilles tendons, only a major axis was measured with the confocal microscope, and a scanning laser displacement sensor was used to measure a minor axis to calculate the area. For the tail tendon, both major and minor axes were measured with the confocal microscope.

To measure the tissue strain, we applied two ink markers directly on the tendon using a permanent marker (Figure 6.1b, c), imaged tendon with CCD camera to track displacement of markers, and quantified the strain using digital image correlation (Vic 2D, Correlated Solutions). We applied ink markers on the posterior side of the plantaris tendon and on the soleus (Sol) sub-tendon for the Achilles tendon (Figure 6.1c). For the tail tendon, we applied ink markers on the mid-substance of the tendon, away from the grips as shown in (Figure 3.1b).

We quantified the micro-scale parameters (i.e., micro-scale strain and sliding) using the confocal microscope as previously described. [38,64] We bleached lines on the anterior side of plantaris tendon and medial gastrocnemius (Mg) sub-tendon for the Achilles tendon (Figure 6.1c). We acquired confocal image stacks at 10 times points, represented by green dots (Figure 6.1a). The parameters measured at 3 time points, End of the Initial Ramp, End of Stress Relaxation (SR), and End of Rest, were primarily used for data analysis.

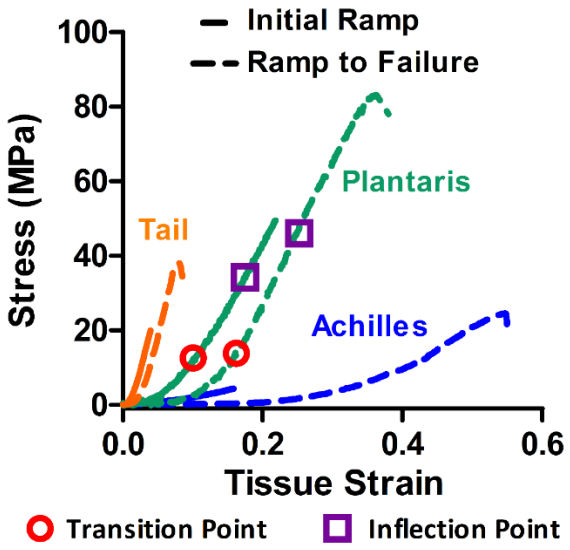

Figure 6.2: Tissue-scale parameter quantification. a) The representative σ-ε responses of plantaris, Achilles, and tail tendons are shown, where Initial Ramp is represented as a solid line and Ramp to Failure is represented as a dotted line. The stress relaxation and unloading are not shown in the graph. Transition point (red open circle), inflection point (purple open square), and linear region modulus (linear line between transition and inflection points) were quantified for both ramps. The representative sample for the plantaris tendon was loaded to 20%, Achilles tendon was loaded to 14%, and tail tendon was loaded to 6%.

6.2.4 Data Analysis – Tissue-scale Mechanical Parameters

The tissue-scale mechanical parameters were quantified at 2 time points: Initial Ramp and Ramp to Failure (Figure 6.1a). Representative stress-strain (σ-ε) responses of the three tendons are shown (Figure 6.2). The tissue-scale parameters were analyzed using the methods and procedure from our previously published paper. [64] Briefly, an inflection point, defined as a point where the σ-ε curve shifts from strain-stiffening to strain-softening, was determined (Figure 6.2). [64,93] The σ-ε response up to inflection point was used to determine the transition point and linear region modulus by fitting a nonlinear constitutive model. [64,99] The transition and inflection points calculated for this study are marked on the representative σ-ε of plantaris tendon (Figure 6.2). All the parameters quantified include transition strain and stress, linear region modulus, and inflection point strain and stress. The parameters were calculated for both Initial Ramp and Ramp to Failure. This chapter will focus on three tissue-scale parameters, Ramp to Failure transition strain, inflection point strain, and linear region modulus, because these parameters have been shown to represent damage. [64]

The peak stress and strain were also quantified for all the tendons (Figure 6.3). In addition, the normalized applied strain was quantified by taking a ratio between applied strain of each sample to averaged peak strain to visualize all tendons on the same x-axis. The peak strain was not statistically different among strain groups for the plantaris and tail tendons based on one-way ANOVA ($p > 0.2$, Table 6.3), and thus an averaged peak strain across all of the strain groups for each tendon was used. Many samples did not fail within

the load cell limit and some tendons had complex failures, where failure initiated near or inside the grips, and the data should be used with caution.

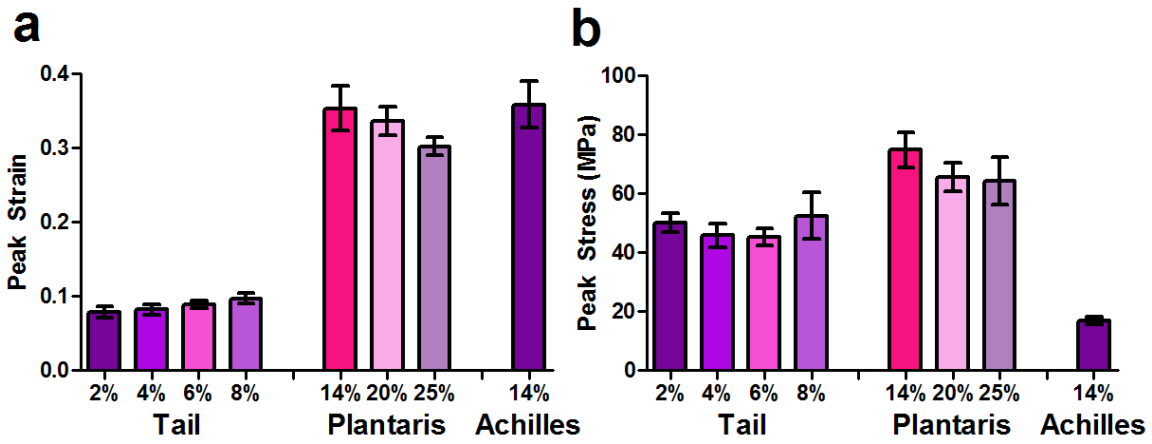

Figure 6.3: Peak strain and stress of rat tail, plantaris, and Achilles tendons. (a) The peak strain and stress among the strain groups within the same tendon were not significant. This bar graph demonstrates the unique σ-ε responses observed in Figure 6.2 for each tendon. Error bars are SEM.

Table 6.3: Mean, median, and standard deviation (SD) of peak strain and stress of three tendons. As the p-values show, there was no difference among strain groups so the mean value of peak strain was used to normalize macro-scale strain to calculate macro to peak strain ratio.

Peak Strain				
	Mean	**Median**	**SD**	**p-value ANOVA; strain groups**
Tail Tendon	0.087	0.088	0.017	0.23
Plantaris Tendon	0.331	0.333	0.073	0.26
Achilles Tendon	0.359	0.357	0.083	N/A
Peak Stress (MPa)				
	Mean (MPa)	**Median (MPa)**	**SD (MPa)**	**p-value ANOVA; strain groups**
Tail Tendon	48.2	48.1	12.8	0.71
Plantaris Tendon	68.1	67.8	21.4	0.47
Achilles Tendon	16.9	16.2	3.6	N/A

6.2.5 Data Analysis – Micro-scale Parameters

To measure the micro-scale deformation, we used the deformation of photobleached lines as discussed previously (Figure 3.3). [38] The micro-scale strain and sliding were quantified for every time point (green dots). In addition, the ratio of micro: tissue strain ratio was calculated at the End of Initial Ramp to measure a strain attenuation from the tissue-scale to micro-scale (Figure 6.1a). This was calculated by taking a ratio between micro-scale strain and applied strain. The non-recoverable sliding, which represents damage at the micro-scale, was calculated using the same method as Chapter 3. For visualization, only the first 40 minutes of the rest period was plotted for the rat tail micro-scale strain and sliding to match the rest period of plantaris and Achilles tendons, but the entire data from the rest period was used for the analyses. [64]

6.2.6 Excluded Samples

For the tissue-scale analyses, a total of two tendons were removed including one of the tail tendon fascicles excluded in Chapter 3. One of the plantaris tendons had a major grip slippage during the Initial Ramp, and as a result, applied strain were two standard deviations away from the population average. For the micro-scale analyses, a total of eight samples across all groups were removed because photobleach lines were not clear enough to be recognized with an automatic registration. The final sample count can be found in Table 6.1.

6.2.7 Statistical Methods

Pearson's correlations (r) with significance set at p=0.05 were conducted using GraphPad Prism. To determine which tissue-scale parameters show damage associated changes and depend on the applied strain, each of the Ramp to Failure tissue-scale parameters was linearly correlated with the applied strain. To study micro-scale deformation and determine the loading mechanism, micro-scale strain, micro: tissue strain ratio, and micro-scale sliding measured at End of Initial Ramp was linearly correlated with the applied strain. To measure the micro-scale damage and determine if it is dependent on the applied strain, we linearly correlated the micro-scale sliding with the applied strain. In addition, to determine the damage mechanisms, the micro-scale non-recoverable sliding was correlated with the applied and normalized target strains. To relate the damage at the micro-scale to the changes of mechanical response at the tissue-scale, the non-recoverable sliding was correlated with the Ramp to Failure properties.

6.3 Results

6.3.1 Tissue-scale Mechanical Parameters and Damage

The σ-ε curve of each tendon has unique characteristics, likely due to the structural differences among these tendons (Figure 6.2). [176] The tail tendon bears the lowest strain, the plantaris tendon bears the highest stress, and the Achilles tendon bears the lowest stress but the highest strains among three tendons. Notably, the maximum applied strain was 8% for the tail tendon, whereas the maximum applied strain was 25% for the plantaris tendon. These strains are about 80% of the peak failure strain (Figure 6.3), motivating the choices

in strain groups based on our pilot test. The grip strain was within the standard deviation of the optically measured applied strain for all tendons, confirming the σ-ε curve was not a result of a premature failure or grip slippage (Table 6.4).

Table 6.4: Initial Ramp data of plantaris and Achilles tendons. Initial Ramp for the rat tail tendon is shown in Table 3.1. Mean ± standard deviations.

	Plantaris			***Achilles***
Strain Group (%)	**14**	**20**	**25**	**14**
Transition Strain	0.095 ± 0.038	0.100 ± 0.032	0.095 ± 0.034	0.013 ± 0.022
Transition Stress (MPa)	8.9 ± 2.0	10.9 ± 3.3	12.6 ± 6.4	2.2 ± 0.5
Linear Reg. Modulus (MPa)	N/A	250 ± 66	334 ± 176	N/A
Inflection Pt. Strain	N/A	0.150 ± 0.042	0.162 ± 0.036	N/A
Inflection Pt. Stress (MPa)	N/A	33.4 ± 15.8	25.7 ± 10.3	N/A
Tissue Strain	0.147 ± 0.043	0.206 ± 0.021	0.237 ± 0.029	0.150 ± 0.030

The linear region and inflection point occur above the 14% grip strain, so the Initial Ramp 14% strain group data for the linear region modulus, inflection point strain, and inflection point stress are not reported.

Table 6.5: Ramp to Failure data of plantaris and Achilles tendons. Initial Ramp for the rat tail tendon is shown in Table 3.1. Mean ± standard deviations.

	Plantaris			***Achilles***
Strain Group (%)	**14**	**20**	**25**	**14**
Transition Strain	0.124 ± 0.033	0.144 ± 0.032	0.149 ± 0.027	0.160 ± 0.058
Transition Stress (MPa)	10.7 ± 5.6	11.4 ± 3.6	12.8 ± 4.47	4.53 ± 3.08
Linear Reg. Modulus (MPa)	316 ± 134	290 ± 67	355 ± 184	123 ± 35
Inflection Pt. Strain	0.198 ± 0.042	0.237 ± 0.052	0.21 ± 0.047	0.20 ± 0.043
Inflection Pt. Stress (MPa)	34.4 ± 17.1	39.7 ± 13.3	37.2 ± 16.7	7.83 ± 3.05

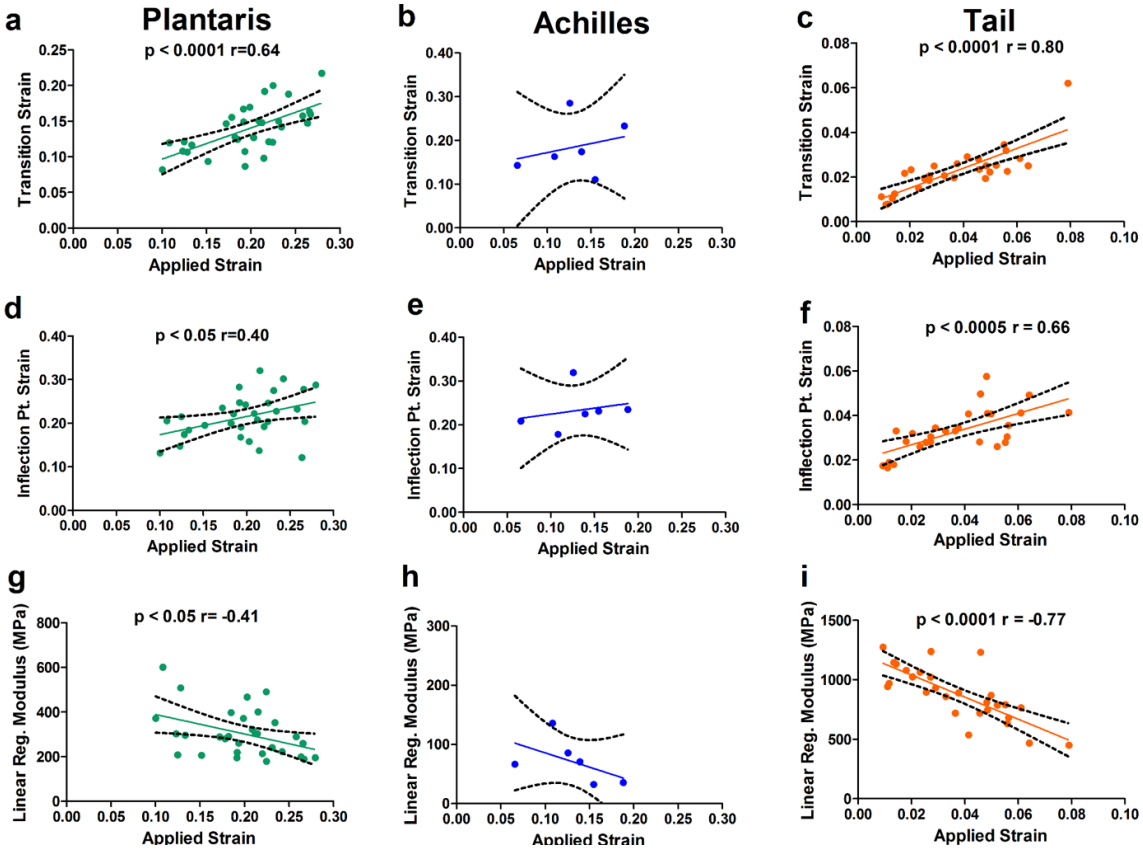

Figure 6.4: Tissue-scale mechanics of Ramp to Failure parameters. (a-c) The transition point strain, (d-f) inflection point strain, and (g-i) linear region modulus of plantaris, Achilles, and tail tendons were linearly correlated with the applied strain. The correlations of transition strain, inflection point strain, and linear region modulus of both plantaris and tail tendons were statistically significant, demonstrating that these parameters show damage and depend on the applied strain. None of the parameter of Achilles tendon correlated with the applied strain. Dashed lines represent 95% confidence intervals.

We quantified the Ramp to Failure mechanical properties (transition strain, inflection point strain, linear region modulus) from the σ-ε curves to investigate if damage was observed in the mechanical parameters and strain-dependent (Figure 6.4). The transition strain (Figure 6.4a, $p<0.0001$), inflection point strain (Figure 6.4d, $p<0.001$), and

linear region modulus (Figure 6.4g, $p<0.05$) significantly correlated with the applied strain for the plantaris tendons but not for the Achilles tendon (Figure 6.4b, e, h). The transition stress and inflection point stress did not correlate with the applied strain for the plantaris and Achilles tendons (Figure D.1). This demonstrates that these parameters show damage that is strain-dependent in the plantaris tendon, similar to our previous finding in the tail tendon (Figure 6.4c, f, i). [64]

None of the parameters for Achilles tendon correlated with the applied strain, and this is likely due to the complexity of the structure. [176] The tissue-scale parameters were quantified on the soleus sub-tendon, while the micro-scale parameters were quantified at medial gastrocnemius sub-tendon (Figure. 6.1d), and thus each tissue- and micro-scale parameter was measured at different sub-tendons. This mismatch of tissue- and micro-scale quantification is likely the cause of the observed inhomogeneity. Indeed, both human and rat Achilles tendons experience inhomogeneous strain. [171–173] Thus, we discontinued testing of Achilles tendon after the 6 samples that were loaded to 14% applied strain.

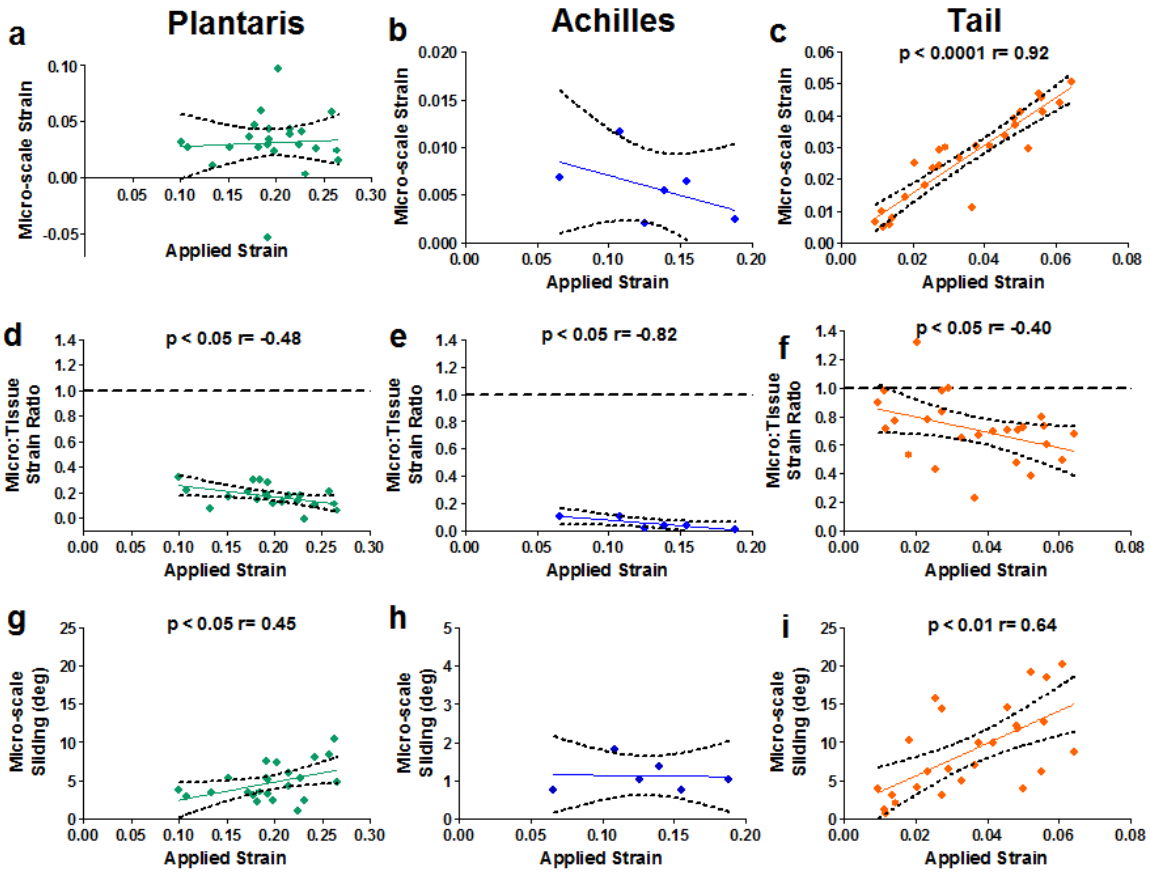

Figure 6.5: Loading mechanisms at multi-scale measured at the End of Initial Ramp. (a-c) The micro-scale strain, (d-f) micro: tissue strain ratio, and (g-i) micro-scale sliding of plantaris, Achilles, and tail tendons were linearly correlated with the applied strain. The micro-scale strain increased with the applied strain for the tail tendon, but not for the plantaris and Achilles tendons. The micro: tissue strain ratios were less than 1 for all tendons, demonstrating that strain is attenuated and the amount of strain attenuation is dependent on the applied strain. The micro-scale sliding increased with the applied strain for both plantaris and tail tendons, suggesting that load is transferred via relative shearing at the micro-scale. The micro-scale sliding did not correlate with the applied strain in Achilles tendon. Dashed lines represent 95% confidence intervals.

6.3.2 Multi-scale Tendon Loading Mechanisms

To study multi-scale deformation during loading, the micro-scale strain, micro: tissue strain ratio, and micro-scale sliding (quantified at the End of Initial Ramp) were correlated with the applied strain (Figure 6.5). The micro-scale strain did not correlate with the applied strain for the plantaris and Achilles tendons (Figure 6.5a,b), in contrast to the high correlation previously observed in the tail tendon (Figure 6.5c). [38] The micro: tissue strain ratios (micro-scale strain divided by applied strain) were less than 1 and decreased with increasing applied strain for all tendons as expected (Figure 6.5d-f, $p<0.05$), demonstrating that strain is attenuated and the amount of strain attenuation is dependent on the applied strain. Notably, this ratio was much lower in the plantaris and Achilles (~0.2) compared to the tail (~0.5-1.0). The micro-scale sliding of the plantaris and tail tendons increased with increasing applied strain (Figure 6.5g-i, $p <0.05$). The magnitude of the sliding of the Achilles tendon was low, and the sliding did not correlate with the applied strain. Despite the differences in applied strains and magnitudes of the responses, the directions of the correlations were the same and significant between the plantaris and tail tendons, whereas those of Achilles tendon were not significant.

6.3.3 Micro-scale Strains and Tendon Damage Mechanisms

All three tendons had a similar micro-scale strain and sliding response (Figure 6.6). The micro-scale strain fully recovered at the End of the Rest period (Figure 6.6a-c); however, the micro-scale sliding did not fully recover (Figure 6.6d-f, Figure 6.7). In addition, the non-recoverable sliding in percentage was strain-dependent for both plantaris

and tail tendons (Figure 6.6g, i, $p<0.005$), and not for the Achilles tendon. Interestingly, the overall magnitudes of micro-scale sliding in degrees were similar for the plantaris and Achilles tendons loaded to 14% strain (Figure 6.6d-e), and no statistical difference of non-recoverable sliding in degrees was observed between the plantaris and Achilles tendons (Figure 6.7, $p>0.9$). Note that this is the only place that we observed a similarity between the plantaris and Achilles tendons. Still, the non-recoverable sliding in percentage was much lower for the plantaris tendon because the micro-scale sliding at the End of SR was lower for the Achilles tendon (Figure 6.6h).

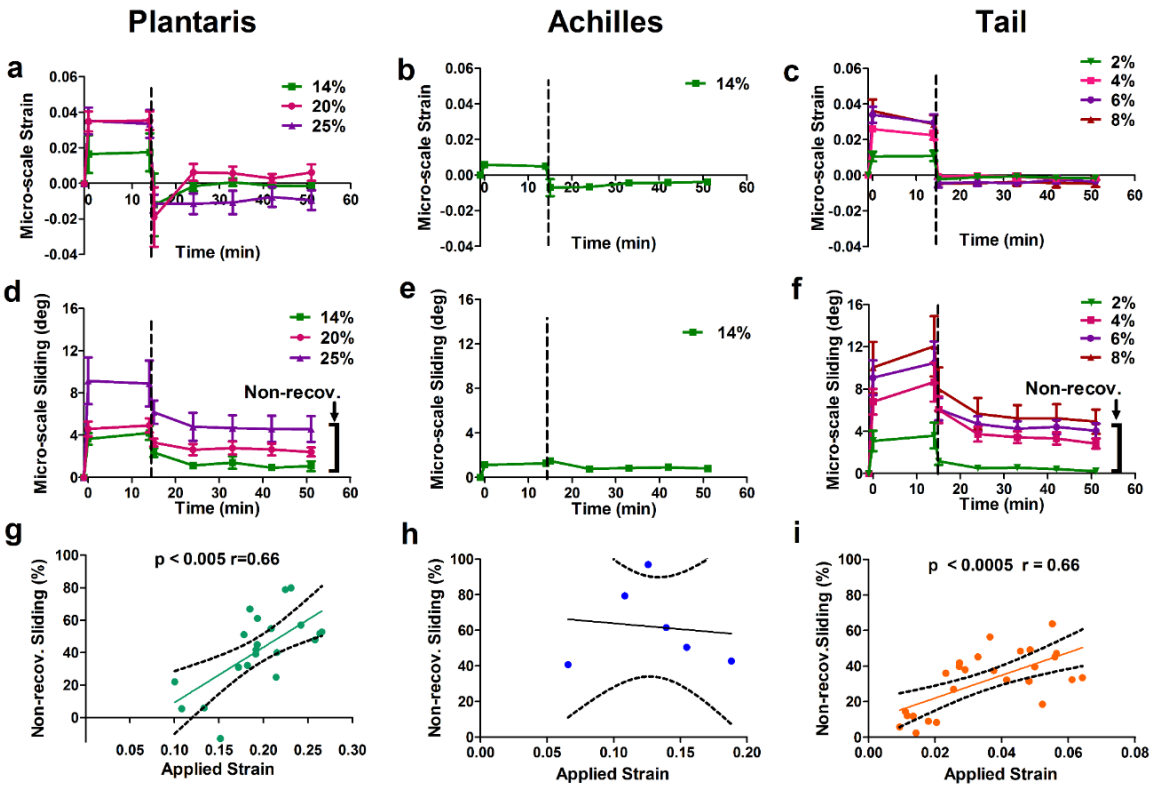

Figure 6.6: Overall micro-scale deformations. (a-c) For all three tendons, both the micro-scale strain and sliding had similar overall micro-scale deformation, where the micro-scale strain fully recovered at the End of the Rest Period. (d-f) On the other hand, the micro-scale sliding was not fully recoverable, suggesting the damage is observable by the micro-scale sliding. (g-i) The non-recoverable sliding was correlated with the applied strain for the plantaris and tail tendons but not for the Achilles tendon. Error bars are SEM and dashed lines represent 95% confidence intervals.

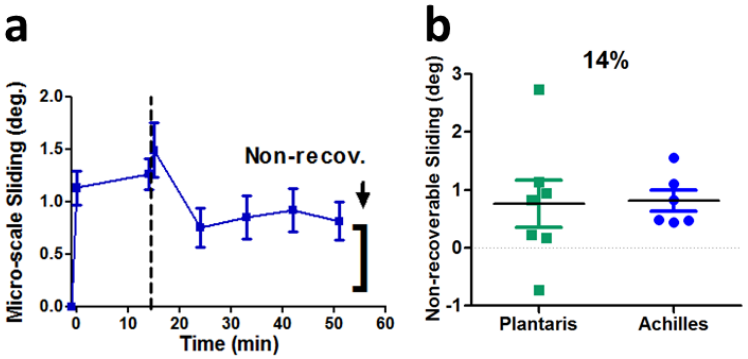

Figure 6.7: Achilles tendon micro-scale sliding. (a) Close up of micro-scale sliding response of Achilles tendon demonstrates that micro-scale sliding is non-recoverable. (b) The non-recoverable sliding (in degrees) of plantaris and Achilles tendons were not statistically significant for the 14% group ($p>0.9$).

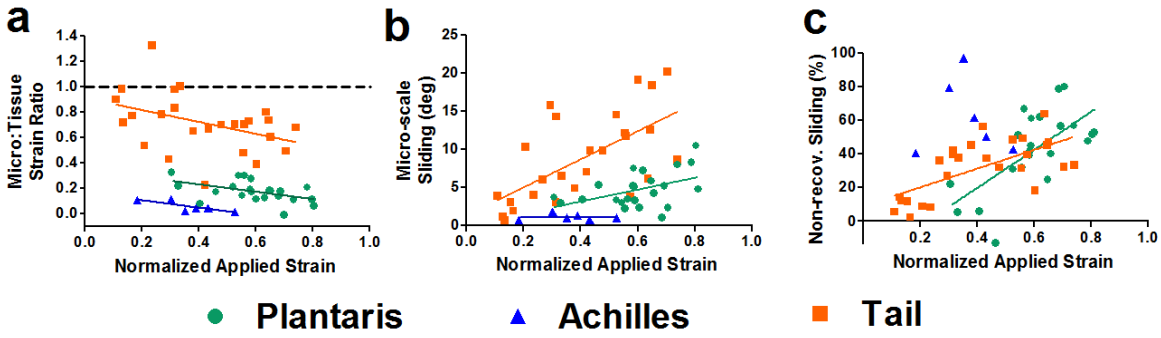

Figure 6.8: Normalized applied strain and key parameters. a) The applied strain was normalized to plot on the same x-axis, and the directions of correlation for the micro: tissue strain ratio were the same for three tendons. b) The directions of micro-scale sliding between the plantaris and tail tendons were also the same but not for the Achilles tendon. c) The non-recoverable sliding directions and magnitudes in percentage between plantaris and tail were notably comparable. Dashed lines represent 95% confidence intervals.

To compare across all three tendons, we evaluated the multi-scale mechanics with the normalized applied strain (Figure 6.8), calculated as the applied strain divided by the

average peak strain during Ramp to Failure (Figure 6.3). The directions of the correlations for the micro: tissue strain ratio (Figure 6.8a), micro-scale sliding during loading (Figure 6.8b), and non-recoverable sliding during recovery (Figure 6.8c) were the same for the plantaris and tail tendons. Indeed, the percentage of non-recoverable sliding overlapped between the plantaris and tail tendons (Figure 6.8c). The direction of correlation for the micro-scale deformation and non-recoverable sliding in percentage between plantaris and tail tendons suggest that their loading and damage mechanisms are similar.

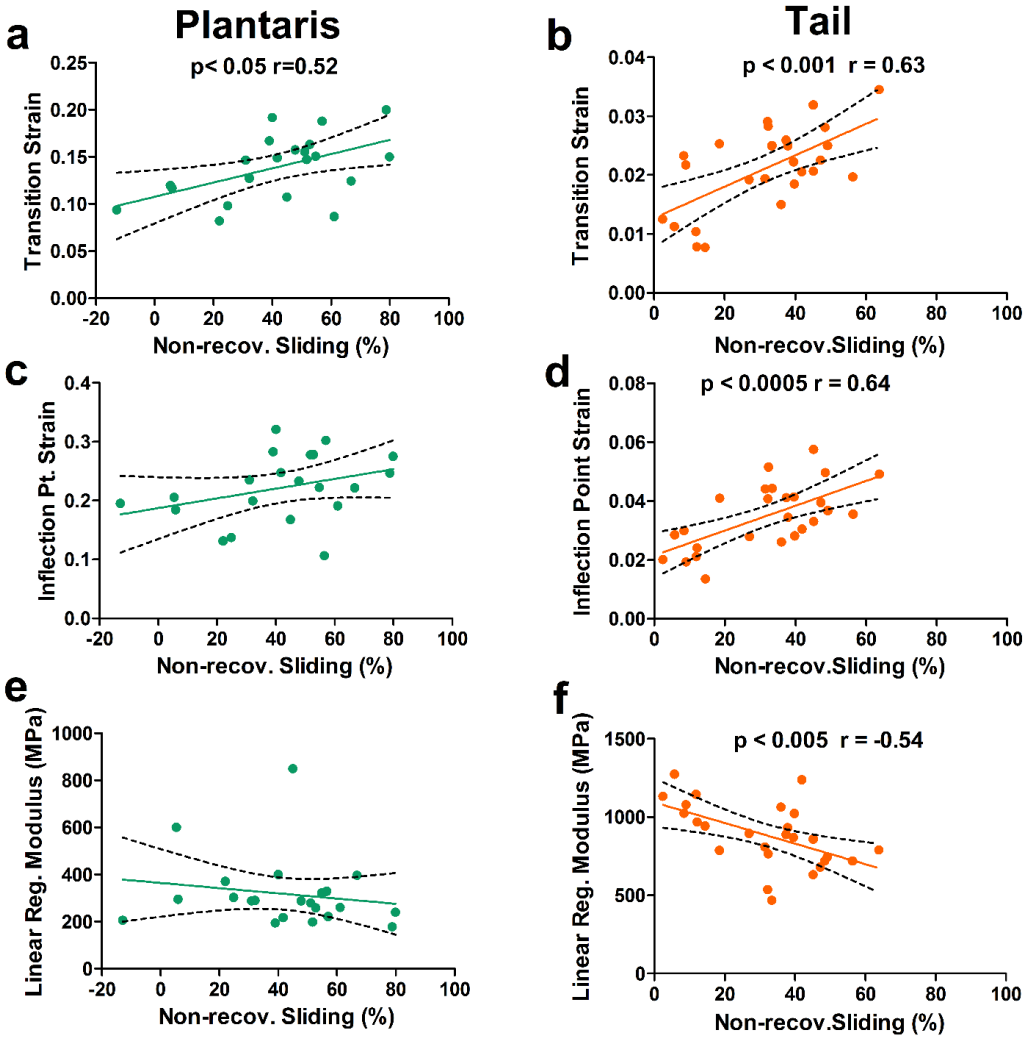

Figure 6.9: Relationship between tissue- and micro-scale parameters. (a-b) The transition strain was correlated with non-recoverable sliding. The transition strain is an indirect measurement of tissue elongation, and this suggests that an increase in tissue elongation is due to irreversible microstructure damage. (c-f) The inflection point strain and linear region modulus were only correlated for the tail tendon and not for the plantaris tendon. The correlation between micro- to tissue-scale parameter demonstrates that micro-scale sliding may be the damage mechanisms in both tendons. Dashed lines represent 95% confidence intervals.

6.3.4 Multi-scale Damage Mechanism Relationship between Tissue-scale and Micro-scale Parameters

Finally, we evaluated the relationship between the micro-scale damage (non-recoverable sliding) and tissue-scale mechanical properties. The transition strain was correlated with the non-recoverable sliding for both plantaris and tail tendons (Figure 6.9a-b). The transition strain is an indirect measurement of tissue elongation, and thus this suggests that an increase in tissue elongation is related to the irreversible microstructure damage. Although we observed correlations between non-recoverable sliding and tissue-scale inflection point strain and modulus in the tail tendon, these did not correlate in the plantaris tendon (Figure 6.9c-f).

6.4 Discussion

This study investigated the load transfer and damage mechanisms of load-bearing tendons, the plantaris and Achilles tendons, across multiple length scales and showed that the mechanisms in the plantaris tendon are similar to those in the tail tendon. Specifically, at the tissue-scale, damage was observed in the mechanical properties and was strain-dependent (Figure 6.4). At the micro-scale, the strain was highly attenuated in all tendons. The micro-scale sliding was correlated with the applied strain, demonstrating that load was transferred via micro-scale sliding (shear) in the plantaris and tail tendons (Figure 6.5). The micro-scale sliding was non-recoverable, strain-dependent (Figure 6.6), and correlated with tissue-scale properties (Figure 6.9), suggesting the non-recoverable sliding is an initial mechanism of tendon damage (Figure 6.6). In summary, micro-scale sliding is likely

responsible for both load transfer and damage mechanisms in load-bearing tendons, with the exception of Achilles tendon.

6.4.1 Damage Mechanisms of Functionally Distinct Tendons

While this study showed that micro-scale sliding is the mechanism of damage for both load-bearing rat tendons and non-load-bearing rat tail tendon, previous findings have suggested that functionally distinct tendons may not have the same damage mechanisms. This can be attributed to two main factors: 1) differences in structure and composition between larger and smaller animal tendons, and 2) differences in prescribed loading conditions. First, differences between low- and high- stress bearing tendons in equine and bovine tendons were observed in tendon mechanics, [81,82] fascicle and interfascicular mechanics, [80,81] interfascicular matrix composition, [84] cross-link density, [82] and fibril deformation. [82,85] These observations suggest that damage mechanisms may depend on the mechanical function of a tendon, contrasting our findings; however, the difference in mechanisms may be explained through the presence/absence of fascicle and interfascicular matrix. While larger animal tendons have fascicles and interfascicular matrix, rat tendons lack fascicles that are structurally and mechanically equivalent to those observed in larger animals. [176] To support this notion, prior studies observed a significant difference in fascicle and sliding deformation of interfascicular matrix between functionally distinct tendons [80,81], and thus fascicle and interfascicular matrix mechanics may dictate the damage mechanisms of functionally distinct tendons. The

absence of fascicular and interfascicular structures in rat tendons likely explains the observed common damage mechanisms between functionally distinct tendons in rat.

Second, while this study showed non-recoverable sliding is the mechanism for damage, other recent studies have demonstrated that fibrils rupture under high magnitude and/or cyclic loading. [51,82,85] Here, we observed a complete recovery of micro-scale strain, suggesting that fibrils did not rupture under the applied loading conditions. This challenges previous findings where the damage was observed in the form of collagen kinking, discontinuities, and denaturation. [51,82,104,175] This disagreement may be attributed to the notion that damage observed as micro-scale sliding may precede the damage observed as micro-scale strain and fibril rupture. [64,95,104,108] It is possible that micro-scale sliding damage precedes, regardless of the tendon type, and that damage related to fibril rupture takes place later, where this process may depend on the tendon type and loading protocol. It is likely that damage in the non-recoverable micro-scale strain will be observed in rat tendons after high magnitude and/or cyclic loading in forms of collagen kinking, discontinuities, and denaturation.

6.4.2 Unique Features of the Plantaris and Achilles Tendons

The plantaris and Achilles tendons have unique mechanical features that can be considered in the context of their tissue-scale structure.[176] The plantaris tendon has a single muscle-tendon junction and bone-tendon insertion, while the Achilles tendon has three muscle-tendon junctions and a single bone-tendon insertion. [176] This complex structure of Achilles tendon likely contributes to the observed mechanics. The observed σ-

ε response showed that the Achilles tendon bears high strain but low stress, and this is likely due to a combination of both micro-scale and inter-tendon slidings. [171] The inter-tendon sliding, a sliding between sub-tendons from each muscle in Achilles tendon, has been speculated to contribute to low strain transfer from tissue- to micro-scale and inhomogeneous deformation. [84,85] Notably, the tendon σ-ε response observed in rat plantaris (high stress) and Achilles (high strain and low stress) and inhomogeneous deformation have also been observed in human [140,171–173,179] and mouse. [180] In addition, the mechanical properties of rat Achilles tendons quantified in other studies were comparable to our mechanical properties. [135,137] The complex structure, σ-ε response, lower strain transfer, and inhomogeneous deformation observed in this study and previous findings suggest that Achilles tendon should be recognized as a specialized tendon, and the structural complexity of Achilles tendon should be carefully considered. Based on the structure and σ-ε response, we recommend selecting the rat plantaris tendon over the Achilles tendon as a small animal model system when studying load-bearing tendons.

6.4.3 Strain Attenuation and Micro-Scale Strain of Native Tissue

This study demonstrated that strain is highly attenuated in rat tendons, and since the micro-scale strain is a good indicative measure for cell strain [181], native cells in tendon will likely experience a small relative amount of strain, regardless of the applied strain. Mechanical stimulation is a crucial aspect of maintaining homeostasis of tendon cells, and thus strain transfer from the tissue- to micro-scale structure is important. [181] Interestingly, while the plantaris and Achilles tendons were loaded to an applied strain that

was about three times higher than the tail tendon, the magnitudes (in degree) of micro-scale strain were comparable, likely due to the load transfer mechanism of micro-scale sliding. [38] These observations are consistent with the magnitude of micro-scale strain measured in other aligned fibrous tissues such as meniscus and annulus fibrosus, [181] suggesting that mechanosensitive cells in the native environment may only require low strain to maintain homeostasis in a healthy state. This finding has important implications for mechanotransduction and the design of tissue engineered constructs.

6.5 Conclusion

This study determined the multi-scale load transfer and damage mechanisms in the rat plantaris, a load-bearing tendon, by demonstrating that the micro-scale sliding is a key component in both mechanisms. These mechanisms are similar to those previously quantified in the tail tendon. Namely, the micro-scale sliding correlated with the applied strain measured at the End of the Initial Ramp, suggesting that micro-scale sliding contributes to load transfer in tendon. In addition, while the micro-scale strain fully recovered, the micro-scale sliding was non-recoverable, strain-dependent, and correlated with a tissue-scale mechanical parameter. When the applied strain was normalized, the percentage magnitude of non-recoverable sliding was similar between the plantaris and tail tendons. Achilles tendon demonstrated some of the mechanical responses observed in plantaris and tail tendons, yet the results were inconclusive due to its complex structure. Thus, micro-scale sliding is responsible for both loading and damage mechanisms in load-bearing plantaris tendon.

Chapter 7

EFFECT OF AGING ON TENDON MULTI-SCALE MECHANICS: PILOT STUDY

7.1 Introduction

This part of the thesis contains a pilot study that was carried out during the dissertation, which investigated the effect of aging on tendon multi-scale mechanics. The incidence rate of tendinopathy increases with aging, and aging is identified as one of the factors that contribute to tendinopathy in clinical settings. [182,183] Yet, there is no consensus if aging has an effect on tendon mechanics. While some studies report no change in mechanical properties, [184–186] other studies report reduction of mechanical properties of the whole tendon with aging. [187–189] Interestingly, at the micro-scale, structure and mechanics of fascicles, interfascicular matrix, and collagen fibril diameter altered with aging, not to mention the decrease in cell density, migration and proliferation. [165,190–195] This pilot study was conducted to explore if aging has an effect on tendon multi-scale damage mechanism, and the study is briefly discussed to communicate the preliminary findings

7.2 Materials and Methods

Rat tail tendon fascicles were harvested from female F-344 rats. We selected 1-month, 12-month, and 24-month old rats to represent Young, Mature, and Old age groups,

respectively. These tails were previously frozen at -20C, where the maximum number of the freeze-thaw cycle was limited to three. [96] We stained each sample with 10 μg/ml 5-DTAF (Life Technologies) and tested using the same method as previously described. [38] Mechanical testing on a total of 3 groups with n=5 fascicles per group was performed. We preloaded each fascicle to 0.5g (~5mN) to define the reference length and preconditioned with 5 cycles of 2% grip strain. Then, we ramped the tendon to 6% and held at a constant stain level for 15 min of stress relaxation. The strain rate for all loading and unloading was 1%/s. To observe the effect of damage, we quantified the tissue-scale parameters at Initial Ramp and Ramp to Failure. We additionally quantified stress relaxation in percentage by taking a ratio between stress at End of Initial Ramp and equilibrium stress at the End of Stress Relaxation (Figure 3.3). All the tissue-scale and micro-scale parameters were quantified as described above.

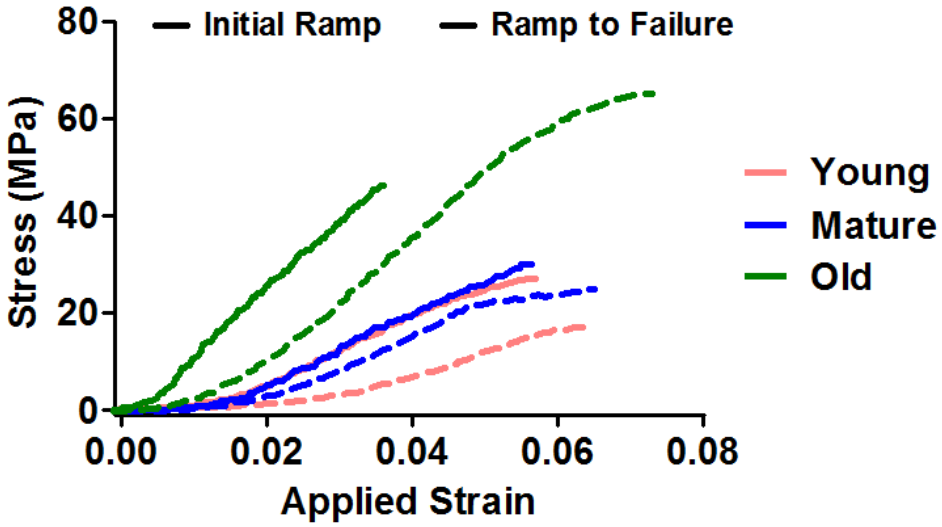

Figure 7.1: Representative σ-ε responses for both Initial Ramp and Ramp to Failure.

7.3 Results and Discussion

Representative stress-strain (σ-ε) responses of the three tendons are shown (Figure 7.1). A qualitative observation of the σ-ε response of the Old group showed that mechanics of Old group may be different compared to the Young and Mature groups. This difference seen in the σ-ε was captured in transition strain and linear region modulus (Figure 7.2). For the Young group, the transition strain increased from Initial Ramp to Ramp to Failure, whereas all the other groups showed no difference. This was surprising based on our previous results (Chapter 3, 4). We expected the transition strain to decrease after mechanical loading for all the groups, and this may be due to an experimental variation. We observed statistical significant differences for the linear region modulus. For both Young and Mature groups, we observed that the linear region modulus decreased from Initial Ramp and Ramp to Failure as demonstrated in Chapters 3 and 6, but not for the Old group. We observed differences in Initial Ramp linear region modulus between Mature and Old and in Ramp to Failure linear region modulus between Young and Mature. The stress relaxation percentage was different among all the groups, possibly related to the change in water content in tendons with aging. In addition, the tissue strain was not significant among the group ($p > 0.14$). Importantly, except for the Ramp to Failure transition strain, all the parameters showed a gradual trend from Young to Old group. Thus, the tissue-scale parameters suggest that aging may have an effect on tendon mechanics.

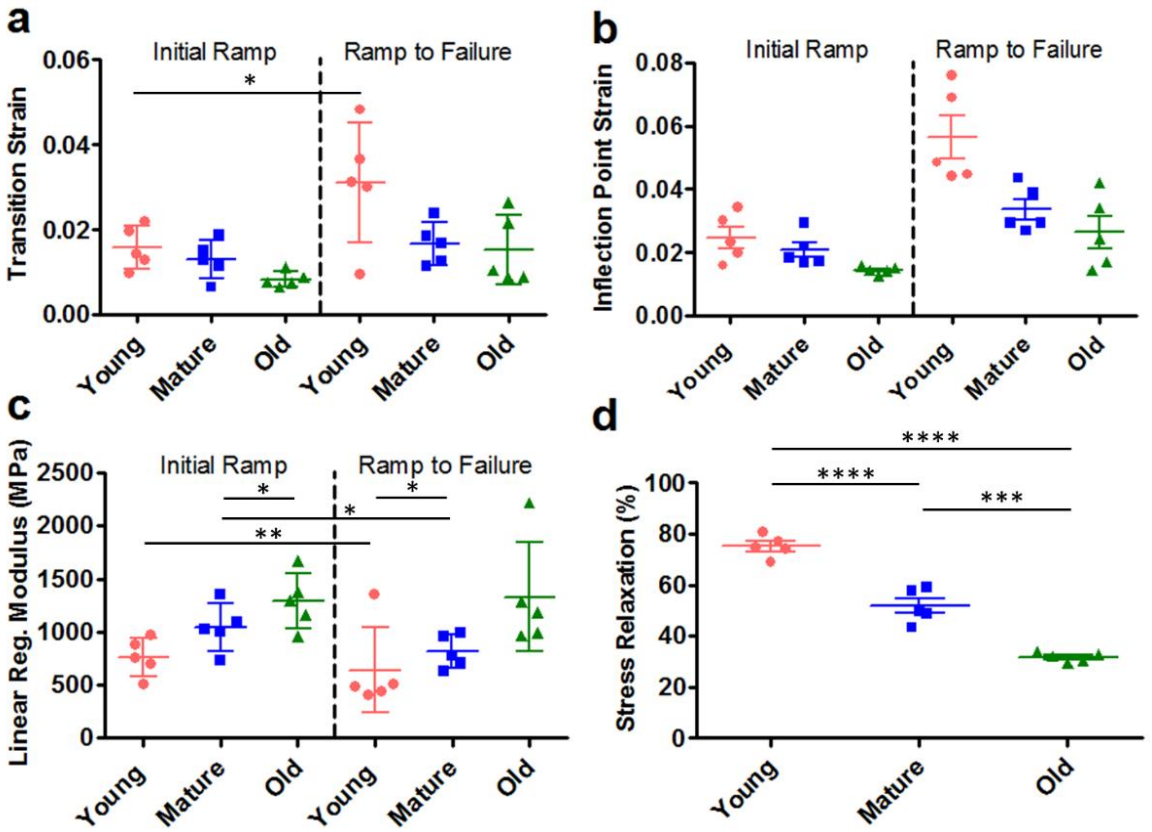

Figure 7.2: Tissue-scale parameters of Young, Mature, and Old. (a) Only the Young group showed a statistical difference from Initial Ramp to Ramp to Failure for the transition strain. (b) The inflection point showed no difference, (c) whereas the linear region modulus showed a statistical significance. For both the Young and Mature groups, we observed that the linear region modulus decreased from Initial Ramp and Ramp to Failure as expected, but not for the Old group. (d) Stress relaxations among all the groups were statistically significant.

At the micro-scale, we observed no qualitative and statistical difference in any of the parameter. Surprisingly, the overall micro-scale sliding was not different. We expected to observe a statistical difference in micro-scale sliding and non-recoverable sliding since we observed differences in tissue-scale parameters. In addition, we expected transverse strain to vary with age, based on the stress relaxation differences we observed. A power

analysis demonstrated that we need n=17/group to see the difference in Initial Ramp linear region modulus between the Mature and Old groups. We decided to discontinue the project because the age-related tendinopathy may be largely affected by the degeneration of interfascicular matrix [164,165], and thus rat tendons may not be an ideal animal system to study the effect of aging on tendon mechanics. Still, we observed differences in tissue-scale mechanics in our pilot study, and continuing this study may yield useful findings.

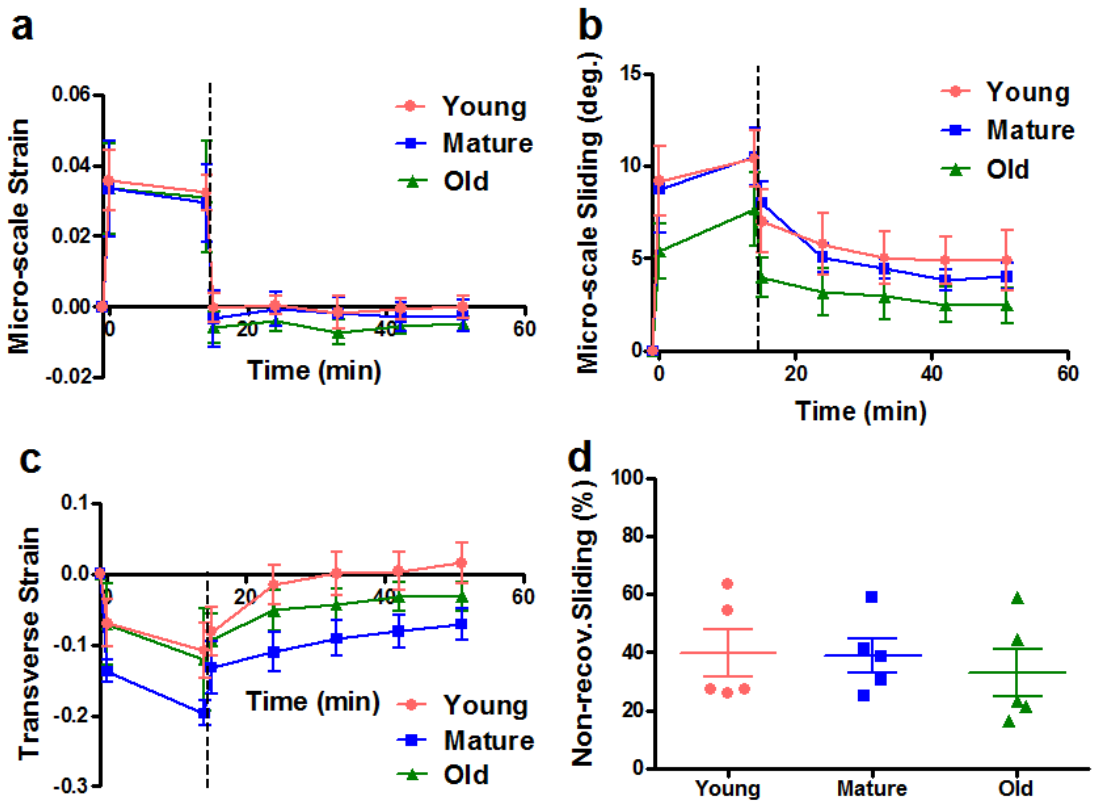

Figure 7.3: Micro-scale parameters. (a) Micro-scale strain, (b), micro-scale sliding, (c) transverse strain, and (d) non-recoverable sliding were not qualitatively and statistically different.

Chapter 8

SUMMARY AND FUTURE DIRECTIONS

8.1 Summary

Tendinopathy is becoming increasingly common in both sports and occupational settings, which leads to a significant loss in quality of life. Once tendinopathy is clinically diagnosed, current treatment and rehabilitation strategies are not sufficient to reverse the pathological changes. Thus, prevention of tendinopathy and studying the damage mechanisms of tendon are important. Many studies attribute the initiation of tendinopathy to damage initiated by mechanical loading, leading to microstructural changes. Yet, the link between mechanical loading and microstructural changes, resulting in macroscopic changes, has not fully elucidated.

The objectives of the dissertation were to investigate the damage mechanisms and hierarchical structure of non-load and load-bearing rat tendons, including the tail, plantaris, and Achilles tendons. Damage is defined as an irreversible change in micro-scale deformation that is observable in tissue-scale mechanical parameters. In Chapter 3, multi-scale mechanical testing was conducted to investigate the damage mechanisms of rat tail tendon, which has the simplest structure, by simultaneously quantifying tissue-scale mechanical and microstructural changes. This study quantified tendon damage by identifying the microstructural micro-scale changes that correlated with the altered macroscopic mechanical parameters at the tissue-scale. Analysis of the micro-scale deformations demonstrated that the micro-scale strain fully recovered following loading

and unloading, while the micro-scale sliding was only partially recoverable and non-recoverable sliding was dependent on the applied strain. At the tissue-scale, irreversible mechanical parameter alterations included increased transition strain (an elongated toe region), decreased linear modulus, and increased inflection point strain that were strain-dependent, and these parameters were correlated with the non-recoverable sliding. These findings suggesting that non-recoverable sliding is the damage mechanisms induced by mechanical loading.

In Chapter 4, the effect of freezing on tendon multi-scale mechanics and structure was evaluated to justify the use of previously frozen tendon to investigate the damage mechanisms. Using rat tail tendon and the experimental design developed as a part of the previous chapter, we verified that freezing does not alter multi-scale tendon mechanics and damage mechanisms under our study protocol. Specifically, the method of storage and the number of freeze-thaw cycles may be important factors in preserving the mechanics of tendon and ligament, and the protocol used in this study was effective for this preservation. The hierarchical structures of rat tendons at multiple length scales were studied to provide a definition of fiber based on the characteristic features in Chapter 5. We chose a single species (rat) and tendons with varying mechanical function (tail, plantaris, and Achilles tendons) to created tendon-specific schematics based on our observations. Using multiple imaging methods, we confirmed that rat tendons do not contain fascicles, with the exception of the specialized rat tail tendon, and thus fiber is the largest tendon subunit in the rat. In addition, we provided a structurally based definition of a fiber as a bundle of collagen fibrils that is surrounded by elongated cells, and this definition was supported by

both histologically processed and unprocessed samples. In all rat tendons studied, the fiber diameters were consistently 10-50 μm.

Based on the method and insight gained in previous chapters, we determined the multi-scale load transfer and damage mechanisms in the rat plantaris, a load-bearing tendon in Chapter 6. The study demonstrated that the micro-scale sliding is a key component in both mechanisms. These mechanisms are similar to those previously quantified in the tail tendon. Namely, the micro-scale sliding correlated with the applied strain, suggesting that the micro-scale sliding contributes to load transfer in the plantaris tendon. In addition, while the micro-scale strain fully recovered, the micro-scale sliding was non-recoverable, strain-dependent, and correlated with the inflection point at the tissue-scale. Thus, micro-scale sliding is a key component for both loading and damage mechanisms in the load-bearing plantaris tendon, similar to the findings in the non-load-bearing tail tendon.

The last chapter, Chapter 7, provides an important pilot data in evaluating the effect of aging on tendon mechanics at multiple length scales. We observed statistical differences between Young, Mature, and Old rat tail tendons in tissue-scale mechanics, but none in the micro-scale mechanics. Findings from this pilot study can suggest a future direction.

8.2 Future Directions

This thesis provides an important knowledge that serves as a foundation for future studies. Some natural questions that arise from the thesis is a translation of the findings from a small animal model (rat) to human or large animal model. As demonstrated in Chapter 5, rat tendons lack fascicles that are common in large animals and humans. Still,

rat can have an advantage when studying fiber structure and mechanics since the fiber structure may be conserved across species. To verify, the fiber structure and mechanics need to be compared between small and large animals; the existence and diameter of the fiber in large animals need to be examined, and the micro-scale deformation of fibers from large and small animals need to be compared directly. One way to study this is to photobleach lines and stain cells, [196] where the same method can be applied to measure micro-scale deformation based on the lines and cells can be used as markers to identify fiber boundaries based on the definition from Chapter 5. Thus, fiber deformation between animals can be directly compared, and this method can be applied to study human tendon. One of the most important differences between small and large animal tendons is that small animals lack interfascicular matrix. This structure has been extensively characterized by Dr. Hazel Screen's group, and they have suggested that interfascicular matrix is a key structure that contributes to age-related changes, [165,191] mechanical and structural differences between functionally distinct tendons, [76,80,81,144,197] and inflammation after fatigue loading [198] using equine tendons. Still, a micro-scale deformation of the interfascicular matrix has not been quantified in situ that can suggest damage mechanisms. The previous testing method used to quantify the deformation involves cutting each side of the fascicle to artificially induce shear to measure mechanical properties of the interfascicular matrix. [81] This is not a natural loading environment and simultaneous quantification of fiber and interfascicular matrix mechanics is impossible using this method. To simultaneously quantify fiber and interfascicular matrix mechanics, cells can be used to identify boundaries of fibers and interfascicular matrix, based on rounder nuclear aspect

ratio, and measure micro-scale deformation using cells as fiducial markers. [181] This method can isolate the micro-scale deformation at different regions (fiber, fascicle, and interfascicular matrix) in situ to suggest damage mechanisms of large animal tendons and human.

As mentioned in Chapter 2, tendinopathy leads to inferior structural and mechanical properties, where this can lead to changes in damage mechanisms. For example, healthy tendon's loading mechanism, strain transfer via micro-scale sliding, may be compromised due to inferior collagen alignment and increase in proteoglycan, which can overload fibers and fibrils, and non-recoverable sliding can be high. During stress relaxation, increased micro-scale strain and decreased sliding may be expected, and increased non-recoverable strain and non-recoverable sliding after rest can be expected in tendinopathic tendon. These altered micro-scale parameters can affect the tissue-scale mechanics, based on the findings of this dissertation. Small animal models, such as synergistic ablation or in vivo patellar tendon loading model, are recommended for future studies to study the effect of tendinopathy at multi-scale. [52,168–170]

One of the most surprising findings of the dissertation was the observed high magnitude of non-recoverable sliding and permanent elongation of tendon after loading to a relatively low strain. Currently, stretch exercises and yoga are recommended and have been shown to reduce pain and improve functions [199–201]by gradually loosening muscle and elongating connective tissues such as tendon. [202,203] In addition, there is a diurnal variation in tendon stiffness, [204,205] where human Achilles tendons were significantly stiffer in the evening than morning. Taken together, tendon elongation as a result of

mechanical loading that changes stiffness can occur in healthy tendon *in vivo*, and this suggests that damage observed in this study may a natural part of tendon life-cycle.

Yet, the elongation of tendon and change in stiffness must be recoverable over time to maintain tendon homeostasis *in vivo*. In this dissertation, we demonstrated that mechanical loading causes microstructural changes only using tendons that have undergone freeze-thaw cycles, where cells are no longer viable. Thus, it is possible that tendon cells can mechanically contribute to maintain homeostasis *in vivo*, and there is an increasing evidence that cells can sense changes in loading environment and mechanically respond in a short time frame (hours to days), apart from repair, healing, and remodeling. Previous studies have observed shortening of tendon length through actin-mediated contraction of cells [206] and cellular engineered construct experienced less deformation than the acellular counterpart. [207] This is likely due to mechanosensitive tendon cells, [206,208,209] and cells are known to sense the rigidity and/or alignment of surrounding matrix to adjust their adhesion, intracellular cytoskeleton organization, and morphology, which affects cell signaling, proliferation, and differentiation. [210–217] Thus, cells may be able to sense changes in surrounding microenvironment induced by mechanical loading and maintain homeostasis. On the other hand, a negligible difference in mechanics between cellular and acellular native tissue was reported in another paper. [218] Investigating short-term mechanical contribution of cells is a necessary step to address normal tendon function and damage *in vivo*.

It is important to note that this thesis focused on a single type of loading protocol with one strain rate to induce damage in tendons: a ramp at 1%/s to the applied strain that

was held statically for 15 minutes. Tendon is a viscoelastic material, where the mechanical response will be dependent on time and rate, and thus damage mechanisms may be affected by the strain rate. [110,219] In addition, it is possible that different mechanisms of damage with other types of loading can occur, particularly with cyclic loading and creep. [102,220] As mentioned in chapters of the thesis, collagen kinking, discontinuities, and denaturation were observed in tendons that underwent high magnitude and/or cyclic loading. [51,82,85,104,175] We argued throughout the thesis that the complete recovery of micro-scale strain suggest that fibrils do not rupture under the applied loading conditions, and damage observed as micro-scale sliding may precede the damage observed as micro-scale strain and fibril rupture. [64,95,108] To verify this notion, finding a relationship between CHP intensity and micro-scale sliding is an important next step. Some of the pilot studies are included as appendices (Figure E 1-4). Damage mechanisms may vary under different loading conditions and rate, and studying the effect of different loading rate and conditions on tendon damage can inform the mechanisms *in vivo*.

Even within a single loading protocol that was prescribed in this thesis, it is unknown whether damage is initiated as soon as damage threshold is surpassed or damage accumulates during stress-relaxation. As mentioned in Chapter 3, we performed cyclic preconditioning at 4% grip strain, which is presumably above the threshold for the rat tail tendon. We compared the tissue-scale parameters between 2% and 4% preconditioning level and observed no difference (Figure 3.10) Thus, not only the strain magnitude but also the loading type (i.e., static vs. cyclic) and duration (i.e., 10 seconds vs. 15 minutes) of loading may have different contributions to damage. Interestingly, when Ramp to Failure

inflection point strain and applied strain were plotted, the slope was 0.73 and the p-value was < 0.005. If we assume that the inflection point is equivalent to the damage threshold, then this correlation suggests that the damage threshold depends on the loading history (i.e., applied strain). This type of behavior is observed as flow plasticity in materials, [221] and this may suggest that the yield space increases once tendon is loaded beyond the threshold and stays constant without further perturbation. Identifying factors (i.e., strain magnitude, loading type, and duration) that initiate tendon damage can guide future prevention and rehabilitation strategies.

8.3 Final Conclusion

This dissertation investigated tendon structure, mechanical function, and damage mechanisms at multiple length scales in both non-load and load-bearing rat tendons, including the tail, plantaris, and Achilles tendons. The findings from the dissertation provide an important link between mechanical loading and microstructural changes, resulting in macroscopic changes, ultimately elucidating damage mechanisms. The outcome of the thesis can inform pathogenesis and progression of tendinopathy, which can improve prevention and rehabilitation strategies and guide therapies and design of engineered constructs.

REFERENCES

[1] N. Maffulli, K.M. Khan, G. Puddu, Overuse tendon conditions: time to change a confusing terminology., Arthroscopy. 14 (1998) 840–3. doi:10.1016/S0749-8063(98)70021-0.

[2] C. Tallon, B.D. Coleman, K.M. Khan, N. Maffulli, Outcome of surgery for chronic Achilles tendinopathy. A critical review., Am. J. Sports Med. 29 (2001) 315–20. doi:10.1177/03635465010290031101.

[3] P. Sharma, N. Maffulli, Tendon Injury and Tendinopathy: Healing and Repair, J. Bone Jt. Surg. 87 (2005). doi:10.2106/JBJS.D.01850.

[4] C.N. Maganaris, P. Chatzistergos, N.D. Reeves, M. V. Narici, Quantification of Internal Stress-Strain Fields in Human Tendon: Unraveling the Mechanisms that Underlie Regional Tendon Adaptations and Mal-Adaptations to Mechanical Loading and the Effectiveness of Therapeutic Eccentric Exercise, Front. Physiol. 8 (2017). doi:10.3389/fphys.2017.00091.

[5] N. Maffulli, D. Kader, Tendinopathy of Tendo Achillis, Bone Joint J. 84–B (2002). doi:10.1302/0301-620X.84B1.1279.

[6] J.P. de Jong, J.T. Nguyen, A.J.M. Sonnema, E.C. Nguyen, P.C. Amadio, S.L. Moran, The Incidence of Acute Traumatic Tendon Injuries in the Hand and Wrist: A 10-Year Population-based Study, Clin. Orthop. Surg. 6 (2014) 196. doi:10.4055/cios.2014.6.2.196.

[7] M. Hagberg, Occupational musculoskeletal stress and disorders of the neck and shoulder: a review of possible pathophysiology, Int. Arch. Occup. Environ. Health. 53 (1984) 269–278. doi:10.1007/BF00398820.

[8] K.G. Silbernagel, A. Brorsson, M. Lundberg, The Majority of Patients With Achilles Tendinopathy Recover Fully When Treated With Exercise Alone, Am. J. Sports Med. 39 (2011) 607–613. doi:10.1177/0363546510384789.

[9] N. Maffulli, Rupture of the Achilles tendon., J. Bone Joint Surg. Am. 81 (1999) 1019–36. http://www.ncbi.nlm.nih.gov/pubmed/10428136.

[10] U.M. Kujala, S. Sarna, J. Kaprio, Cumulative Incidence of Achilles Tendon Rupture and Tendinopathy in Male Former Elite Athletes, 2005.

[11] P. Malliaras, C.J. Barton, N.D. Reeves, H. Langberg, Achilles and Patellar Tendinopathy Loading Programmes, Sport. Med. 43 (2013) 267–286. doi:10.1007/s40279-013-0019-z.

[12] J.L. Cook, C.R. Purdam, Is tendon pathology a continuum? A pathology model to explain the clinical presentation of load-induced tendinopathy, Br. J. Sports Med. 43 (2009) 409–416. doi:10.1136/bjsm.2008.051193.

[13] P. Kannus, L. Józsa, Histopathological changes preceding spontaneous rupture of a tendon. A controlled study of 891 patients., J. Bone Joint Surg. Am. 73 (1991)

1507–25. doi:10.2106/00004623-199173100-00009.

[14] U. Fredberg, K. Stengaard-Pedersen, Chronic tendinopathy tissue pathology, pain mechanisms, and etiology with a special focus on inflammation., Scand. J. Med. Sci. Sports. 18 (2008) 3–15. doi:10.1111/j.1600-0838.2007.00746.x.

[15] M. Kvist, Achilles tendon injuries in athletes., Sports Med. 18 (1994) 173–201. doi:10.2165/00007256-199418030-00004.

[16] C. Couppé, R.B. Svensson, K.M. Heinemeier, E.W. Thomsen, M.L. Bayer, L. Christensen, M. Kjær, S.P. Magnusson, P. Schjerling, Quantification of cell density in rat Achilles tendon: development and application of a new method, Histochem. Cell Biol. 147 (2017) 97–102. doi:10.1007/s00418-016-1482-z.

[17] B.R. Freedman, A. Zuskov, J.J. Sarver, M.R. Buckley, L.J. Soslowsky, Evaluating changes in tendon crimp with fatigue loading as an ex vivo structural assessment of tendon damage., J. Orthop. Res. 33 (2015) 904–10. doi:10.1002/jor.22875.

[18] P. Kannus, Structure of the tendon connective tissue., Scand. J. Med. Sci. Sports. 10 (2000) 312–20. doi:https://doi.org/10.1034/j.1600-0838.2000.010006312.x.

[19] J. Kastelic, A. Galeski, E. Baer, The multicomposite structure of tendon., Connect. Tissue Res. 6 (1978) 11–23. doi:10.3109/03008207809152283.

[20] D.A. Parry, G.R. Barnes, A.S. Craig, A comparison of the size distribution of collagen fibrils in connective tissues as a function of age and a possible relation between fibril size distribution and mechanical properties., Proc. R. Soc. London. Ser. B, Biol. Sci. 203 (1978) 305–21. doi:10.1098/RSPB.1978.0107.

[21] D.A.D. Parry, A.S. Craig, Collagen fibrils and elastic fibers in rat-tail tendon: An electron microscopic investigation, Biopolymers. 17 (1978) 843–855. doi:10.1002/bip.1978.360170404.

[22] D.R. Eyre, M.A. Paz, P.M. Gallop, Cross-Linking in Collagen and Elastin, Annu. Rev. Biochem. 53 (1984) 717–748. doi:10.1146/annurev.bi.53.070184.003441.

[23] K.G. Vogel, D. Heinegård, Characterization of proteoglycans from adult bovine tendon, J. Biol. Chem. 260 (1985) 9298–9306. doi:260, 9298-9306.

[24] A. Aparecida de Aro, B. de Campos Vidal, E.R. Pimentel, Biochemical and anisotropical properties of tendons, Micron. 43 (2012) 205–214. doi:10.1016/j.micron.2011.07.015.

[25] K. von der Mark, Localization of Collagen Types in Tissues, Int. Rev. Connect. Tissue Res. 9 (1981) 265–324. doi:10.1016/B978-0-12-363709-3.50012-7.

[26] G.P. Riley, R.L. Harrall, C.R. Constant, M.D. Chard, T.E. Cawston, B.L. Hazleman, Tendon degeneration and chronic shoulder pain: changes in the collagen composition of the human rotator cuff tendons in rotator cuff tendinitis., Ann. Rheum. Dis. 53 (1994) 359–66.

[27] T.J. Wess, Collagen Fibrillar Structure and Hierarchies, in: Collagen, Springer US, Boston, MA, 2008: pp. 49–80. doi:10.1007/978-0-387-73906-9_3.

[28] K.A. Piez, A.H. Reddi, Extracellular matrix biochemistry, Elsevier, New York, 1984.

[29] A. Bhattacharjee, M. Bansal, Collagen Structure: The Madras Triple Helix and the Current Scenario, IUBMB Life (International Union Biochem. Mol. Biol. Life). 57 (2005) 161–172. doi:10.1080/15216540500090710.

[30] R. Berisio, L. Vitagliano, L. Mazzarella, A. Zagari, Crystal structure of the collagen triple helix model [(Pro-Pro-Gly)10]3, Protein Sci. 11 (2009) 262–270. doi:10.1110/ps.32602.

[31] A.S. Parmar, A.M. Nunes, J. Baum, B. Brodsky, A peptide study of the relationship between the collagen triple-helix and amyloid, Biopolymers. 97 (2012) 795–806. doi:10.1002/bip.22070.

[32] R. Harwood, M.E. Grant, D.S. Jackson, Studies on the glycosylation of hydroxylysine residues during collagen biosynthesis and the subcellular localization of collagen galactosyltransferase and collagen glucosyltransferase in tendon and cartilage cells., Biochem. J. 152 (1975) 291–302. doi:10.1042/bj1520291.

[33] D.J.S. Hulmes, Building Collagen Molecules, Fibrils, and Suprafibrillar Structures, J. Struct. Biol. 137 (2002) 2–10. doi:10.1006/jsbi.2002.4450.

[34] D.J. Hulmes, The collagen superfamily--diverse structures and assemblies., Essays Biochem. 27 (1992) 49–67.

[35] M. O'Brien, Structure and metabolism of tendons., Scand. J. Med. Sci. Sports. 7 (1997) 55–61. doi:10.1111/j.1600-0838.1997.tb00119.x.

[36] G.G. Handsfield, L.C. Slane, H.R.C. Screen, Nomenclature of the Tendon Hierarchy: An Overview of Inconsistent Terminology and a Proposed Size-Based Naming Scheme with Terminology for Multi-Muscle Tendons, J. Biomech. 49 (2016) 3122–3124. doi:10.1016/j.jbiomech.2016.06.028.

[37] O. Ali, E. Comerford, P. Clegg, E. Canty-Laird, Variations during ageing in the three-dimensional anatomical arrangement of fascicles within the equine superficial digital flexor tendon, Eur. Cells Mater. 35 (2018) 87–102. doi:10.22203/eCM.v035a07.

[38] S.E. Szczesny, D.M. Elliott, Interfibrillar shear stress is the loading mechanism of collagen fibrils in tendon., Acta Biomater. 10 (2014) 2582–90. doi:10.1016/j.actbio.2014.01.032.

[39] D.L. Butler, E.S. Grood, F.R. Noyes, R.F. Zernicke, Biomechanics of ligaments and tendons., Exerc. Sport Sci. Rev. 6 (1978) 125–81.

[40] S.P. Lake, K.S. Miller, D.M. Elliott, L.J. Soslowsky, Effect of fiber distribution and realignment on the nonlinear and inhomogeneous mechanical properties of human supraspinatus tendon under longitudinal tensile loading., J. Orthop. Res. 27 (2009) 1596–602. doi:10.1002/jor.20938.

[41] D.M. Elliott, L.A. Setton, Anisotropic and Inhomogeneous Tensile Behavior of the Human Anulus Fibrosus: Experimental Measurement and Material Model Predictions, J. Biomech. Eng. 123 (2001) 256. doi:10.1115/1.1374202.

[42] S.P. Lake, D.H. Cortes, J.A. Kadlowec, L.J. Soslowsky, D.M. Elliott, Evaluation of affine fiber kinematics in human supraspinatus tendon using quantitative projection plot analysis., Biomech. Model. Mechanobiol. 11 (2012) 197–205. doi:10.1007/s10237-011-0303-5.

[43] S.L. Curwin, Rehabilitation After Tendon Injuries, in: Tendon Inj., Springer-Verlag, London, 2005: pp. 242–266. doi:10.1007/1-84628-050-8_24.

[44] M. Aström, A. Rausing, Chronic Achilles tendinopathy. A survey of surgical and histopathologic findings., Clin. Orthop. Relat. Res. (1995) 151–64.

[45] R.A. Bank, J.M. TeKoppele, G. Oostingh, B.L. Hazleman, G.P. Riley, Lysylhydroxylation and non-reducible crosslinking of human supraspinatus tendon collagen: changes with age and in chronic rotator cuff tendinitis., Ann. Rheum. Dis. 58 (1999) 35–41.

[46] S. Arya, K. Kulig, Tendinopathy alters mechanical and material properties of the Achilles tendon, J. Appl. Physiol. 108 (2010). doi:10.1152/japplphysiol.00259.2009.

[47] R.L. Chimenti, A.S. Flemister, J. Tome, J.M. McMahon, M.A. Flannery, Y. Xue, J.R. Houck, Altered Tendon Characteristics and Mechanical Properties Associated With Insertional Achilles Tendinopathy, J. Orthop. Sport. Phys. Ther. 44 (2014) 680–689. doi:10.2519/jospt.2014.5369.

[48] Y. Nabeshima, E.S. Grood, A. Sakurai, J.H. Herman, Uniaxial tension inhibits tendon collagen degradation by collagenasein vitro, J. Orthop. Res. 14 (1996) 123–130. doi:10.1002/jor.1100140120.

[49] J. Zhang, J.H.-C. Wang, S. Lake, A. Hill, D. Glaser, The Effects of Mechanical Loading on Tendons - An In Vivo and In Vitro Model Study, PLoS One. 8 (2013) e71740. doi:10.1371/journal.pone.0071740.

[50] J.L. Cook, E. Rio, C.R. Purdam, S.I. Docking, Revisiting the continuum model of tendon pathology: what is its merit in clinical practice and research?, Br. J. Sports Med. 50 (2016) 1187–1191. doi:10.1136/bjsports-2015-095422.

[51] S.P. Veres, J.M. Harrison, J.M. Lee, Repeated subrupture overload causes progression of nanoscaled discrete plasticity damage in tendon collagen fibrils., J. Orthop. Res. 31 (2013) 731–7. doi:10.1002/jor.22292.

[52] D.T. Fung, V.M. Wang, N. Andarawis-Puri, J. Basta-Pljakic, Y. Li, D.M. Laudier, H.B. Sun, K.J. Jepsen, M.B. Schaffler, E. Flatow, Early response to tendon fatigue damage accumulation in a novel in vivo model., J. Biomech. 43 (2010) 274–9. doi:10.1016/j.jbiomech.2009.08.039.

[53] H.R.C. Screen, J.C. Shelton, D.L. Bader, D.A. Lee, Cyclic tensile strain upregulates collagen synthesis in isolated tendon fascicles, Biochem. Biophys.

Res. Commun. 336 (2005) 424–429. doi:10.1016/j.bbrc.2005.08.102.

[54] A.J. Banes, M. Tsuzaki, J. Yamamoto, T. Fischer, B. Brigman, T. Brown, L. Miller, Mechanoreception at the cellular level: the detection, interpretation, and diversity of responses to mechanical signals., Biochem Cell Biol. 73 (1995) 349–65. doi:10.1139/o95-043.

[55] M. Lavagnino, M.E. Wall, D. Little, A.J. Banes, F. Guilak, S.P. Arnoczky, Tendon mechanobiology: Current knowledge and future research opportunities., J. Orthop. Res. 33 (2015) 813–22. doi:10.1002/jor.22871.

[56] A.S. Lacroix, S.E. Duenwald-Kuehl, S. Brickson, T.L. Akins, G. Diffee, J. Aiken, R. Vanderby, R.S. Lakes, Effect of age and exercise on the viscoelastic properties of rat tail Tendon, Ann. Biomed. Eng. 41 (2013) 1120–1128. doi:10.1007/s10439-013-0796-4.

[57] S.L.-Y. Woo, M.A. Ritter, D. Amiel, T.M. Sanders, M.A. Gomez, S.C. Kuei, S.R. Garfin, W.H. Akeson, The Biomechanical and Biochemical Properties of Swine Tendons — Long Term Effects of Exercise on the Digital Extensors, Connect. Tissue Res. 7 (1980) 177–183. doi:10.3109/03008208009152109.

[58] S.L. Woo, M.A. Gomez, D. Amiel, M.A. Ritter, R.H. Gelberman, W.H. Akeson, The effects of exercise on the biomechanical and biochemical properties of swine digital flexor tendons., J. Biomech. Eng. 103 (1981) 51–6. doi:10.1115/1.3138246.

[59] H.B. Sun, N. Andarawis-Puri, Y. Li, D.T. Fung, J.Y. Lee, V.M. Wang, J. Basta-Pljakic, D.J. Leong, J.B. Sereysky, S.J. Ros, R.A. Klug, J. Braman, M.B. Schaffler, K.J. Jepsen, E. Flatow, Cycle-dependent matrix remodeling gene expression response in fatigue-loaded rat patellar tendons, J. Orthop. Res. 28 (2010) 1380–1386. doi:10.1002/jor.21132.

[60] J.M. Archambault, D.A. Hart, W. Herzog, Response of Rabbit Achilles Tendon to Chronic Repetitive Loading, Connect. Tissue Res. 42 (2001) 13–23. doi:10.3109/03008200109014245.

[61] Z.J. Zhang, G.Y. Ng, W.C. Lee, S.N. Fu, J. Bojsen-Moller, Changes in Morphological and Elastic Properties of Patellar Tendon in Athletes with Unilateral Patellar Tendinopathy and Their Relationships with Pain and Functional Disability, PLoS One. 9 (2014) e108337. doi:10.1371/journal.pone.0108337.

[62] G. Parent, N. Huppé, E. Langelier, Low stress tendon fatigue is a relatively rapid process in the context of overuse injuries., Ann. Biomed. Eng. 39 (2011) 1535–45. doi:10.1007/s10439-011-0254-0.

[63] J. Kondratko-Mittnacht, R. Lakes, R. Vanderby, Shear loads induce cellular damage in tendon fascicles., J. Biomech. 48 (2015) 3299–305. doi:10.1016/j.jbiomech.2015.06.006.

[64] A.H. Lee, S.E. Szczesny, M.H. Santare, D.M. Elliott, Investigating mechanisms of tendon damage by measuring multi-scale recovery following tensile loading, Acta Biomater. 57 (2017) 363–372. doi:10.1016/j.actbio.2017.04.011.

[65] S.P. Veres, E.P. Brennan-Pierce, J.M. Lee, Macrophage-like U937 cells recognize collagen fibrils with strain-induced discrete plasticity damage., J. Biomed. Mater. Res. A. 103 (2015) 397–408. doi:10.1002/jbm.a.35156.

[66] D. Krajcinovic, Continuous Damage Mechanics Revisited: Basic Concepts and Definitions, J. Appl. Mech. 52 (1985) 829. doi:10.1115/1.3169154.

[67] L. Kachanov, Rupture Time Under Creep Conditions, Int. J. Fract. 97 (1999) 11–18. doi:10.1023/A:1018671022008.

[68] J. Lemaitre, A Continuous Damage Mechanics Model for Ductile Fracture, J. Eng. Mater. Technol. 107 (1985) 83. doi:10.1115/1.3225775.

[69] J.L. Chaboche, Continuum Damage Mechanics: Part I—General Concepts, J. Appl. Mech. 55 (1988) 59. doi:10.1115/1.3173661.

[70] Z. Bartczak, A. Galeski, Plasticity of Semicrystalline Polymers, Macromol. Symp. 294 (2010) 67–90. doi:10.1002/masy.201050807.

[71] P.E. Bretz, R.W. Hertzberg, J.A. Manson, Mechanisms of fatigue damage and fracture in semi-crystalline polymers, Polymer (Guildf). 22 (1981) 1272–1278. doi:10.1016/0032-3861(81)90145-2.

[72] P. Ladeveze, E. LeDantec, Damage modelling of the elementary ply for laminated composites, Compos. Sci. Technol. 43 (1992) 257–267. doi:10.1016/0266-3538(92)90097-M.

[73] A. Charewicz, I. Daniel, Damage Mechanisms and Accumulation in Graphite/Epoxy Laminates, in: Compos. Mater. Fatigue Fract., ASTM International, 100 Barr Harbor Drive, PO Box C700, West Conshohocken, PA 19428-2959, 1986: pp. 274-274–24. doi:10.1520/STP19991S.

[74] L. Ewart, S. Suresh, Crack propagation in ceramics under cyclic loads, J. Mater. Sci. 22 (1987) 1173–1192. doi:10.1007/BF01233107.

[75] D.T. Fung, V.M. Wang, D.M. Laudier, J.H. Shine, J. Basta-Pljakic, K.J. Jepsen, M.B. Schaffler, E. Flatow, Subrupture tendon fatigue damage, J. Orthop. Res. 27 (2009) 264–273. doi:10.1002/jor.20722.

[76] C.T. Thorpe, G.P. Riley, H.L. Birch, P.D. Clegg, H.R.C. Screen, Effect of fatigue loading on structure and functional behaviour of fascicles from energy-storing tendons., Acta Biomater. 10 (2014) 3217–24. doi:10.1016/j.actbio.2014.04.008.

[77] T.A.L. Wren, D.P. Lindsey, G.S. Beaupré, D.R. Carter, Effects of Creep and Cyclic Loading on the Mechanical Properties and Failure of Human Achilles Tendons, Ann. Biomed. Eng. 31 (2003) 710–717. doi:10.1114/1.1569267.

[78] S. Torp, A. RG, A. CD, B. E, Structure-property relationships in tendon as a function of age., Struct. Fibrous Biopolym. 26 (1975) 197–221.

[79] F. Fang, S.P. Lake, Multiscale strain analysis of tendon subjected to shear and compression demonstrates strain attenuation, fiber sliding, and reorganization., J. Orthop. Res. 33 (2015) 1704–12. doi:10.1002/jor.22955.

[80] C.T. Thorpe, C. Klemt, G.P. Riley, H.L. Birch, P.D. Clegg, H.R.C. Screen, Helical sub-structures in energy-storing tendons provide a possible mechanism for efficient energy storage and return., Acta Biomater. 9 (2013) 7948–56. doi:10.1016/j.actbio.2013.05.004.

[81] C.T. Thorpe, C.P. Udeze, H.L. Birch, P.D. Clegg, H.R.C. Screen, Specialization of tendon mechanical properties results from interfascicular differences., J. R. Soc. Interface. 9 (2012) 3108–17. doi:10.1098/rsif.2012.0362.

[82] T.W. Herod, N.C. Chambers, S.P. Veres, Collagen fibrils in functionally distinct tendons have differing structural responses to tendon rupture and fatigue loading, Acta Biomater. 42 (2016). doi:10.1016/j.actbio.2016.06.017.

[83] C.T. Thorpe, M.S.C. Godinho, G.P. Riley, H.L. Birch, P.D. Clegg, H.R.C. Screen, The interfascicular matrix enables fascicle sliding and recovery in tendon, and behaves more elastically in energy storing tendons., J. Mech. Behav. Biomed. Mater. 52 (2015) 85–94. doi:10.1016/j.jmbbm.2015.04.009.

[84] C.T. Thorpe, K.J. Karunaseelan, J. Ng Chieng Hin, G.P. Riley, H.L. Birch, P.D. Clegg, H.R.C. Screen, Distribution of proteins within different compartments of tendon varies according to tendon type, J. Anat. 229 (2016) 450–458. doi:10.1111/joa.12485.

[85] A.S. Quigley, S. Bancelin, D. Deska-Gauthier, F. Légaré, L. Kreplak, S.P. Veres, In tendons, differing physiological requirements lead to functionally distinct nanostructures, Sci. Rep. 8 (2018) 4409. doi:10.1038/s41598-018-22741-8.

[86] S. Duenwald-Kuehl, J. Kondratko, R.S. Lakes, R. Vanderby, Damage mechanics of porcine flexor tendon: mechanical evaluation and modeling., Ann. Biomed. Eng. 40 (2012) 1692–707. doi:10.1007/s10439-012-0538-z.

[87] R.K.. Smith, H.. Birch, S. Goodman, D. Heinegård, A.. Goodship, The influence of ageing and exercise on tendon growth and degeneration—hypotheses for the initiation and prevention of strain-induced tendinopathies, Comp. Biochem. Physiol. Part A Mol. Integr. Physiol. 133 (2002) 1039–1050. doi:10.1016/S1095-6433(02)00148-4.

[88] A.N. Natali, P.G. Pavan, E.L. Carniel, M.E. Lucisano, G. Taglialavoro, Anisotropic elasto-damage constitutive model for the biomechanical analysis of tendons., Med. Eng. Phys. 27 (2005) 209–14. doi:10.1016/j.medengphy.2004.10.011.

[89] A.M. Reyes, H. Jahr, H.T.M. van Schie, H. Weinans, A.A. Zadpoor, Prediction of the elastic strain limit of tendons, J. Mech. Behav. Biomed. Mater. 30 (2014) 324–338. doi:10.1016/j.jmbbm.2013.11.020.

[90] P. Provenzano, D. Heisey, K. Hayashi, R. Lakes, J. Vanderby, Ray, Subfailure damage in ligament: a structural and cellular evaluation, J Appl Physiol. 92 (2002) 362–371. doi:10.1152/jappl.2002.92.1.362.

[91] Z. Guo, J.W. Freeman, J.G. Barrett, R. De Vita, Quantification of strain induced

damage in medial collateral ligaments., J. Biomech. Eng. 137 (2015). doi:10.1115/1.4030532.

[92] A. Viinikainen, H. Göransson, K. Huovinen, M. Kellomäki, P. Törmälä, P. Rokkanen, The Strength of the 6-Strand Modified Kessler Repair Performed With Triple-Stranded or Triple-Stranded Bound Suture in a Porcine Extensor Tendon Model: An Ex Vivo Study, J. Hand Surg. Am. 32 (2007) 510–517. doi:10.1016/j.jhsa.2007.01.010.

[93] J.M. Peloquin, M.H. Santare, D.M. Elliott, Advances in quantification of meniscus tensile mechanics including nonlinearity, yield, and failure., J. Biomech. Eng. 138 (2015) 021002. doi:10.1115/1.4032354.

[94] P. Fratzl, K. Misof, I. Zizak, G. Rapp, H. Amenitsch, S. Bernstorff, Fibrillar Structure and Mechanical Properties of Collagen, J. Struct. Biol. 122 (1998) 119–122. doi:10.1006/jsbi.1998.3966.

[95] S.E. Szczesny, D.M. Elliott, Incorporating plasticity of the interfibrillar matrix in shear lag models is necessary to replicate the multiscale mechanics of tendon fascicles., J. Mech. Behav. Biomed. Mater. 40 (2014) 325–38. doi:10.1016/j.jmbbm.2014.09.005.

[96] H. Huang, J. Zhang, K. Sun, X. Zhang, S. Tian, Effects of repetitive multiple freeze–thaw cycles on the biomechanical properties of human flexor digitorum superficialis and flexor pollicis longus tendons, Clin. Biomech. 26 (2011) 419–423. doi:10.1016/j.clinbiomech.2010.12.006.

[97] S.E. Szczesny, R.S. Edelstein, D.M. Elliott, DTAF dye concentrations commonly used to measure microscale deformations in biological tissues alter tissue mechanics, PLoS One. 9 (2014) e99588. doi:10.1371/journal.pone.0099588.

[98] B.N. Safa, K.D. Meadows, S.E. Szczesny, D.M. Elliott, Exposure to buffer solution alters tendon hydration and mechanics, J. Biomech. (2017). doi:10.1016/j.jbiomech.2017.06.045.

[99] M.L. Tanaka, C.A. Weisenbach, M. Carl Miller, L. Kuxhaus, A continuous method to compute model parameters for soft biological materials., J. Biomech. Eng. 133 (2011) 074502. doi:10.1115/1.4004412.

[100] B.J. Rigby, N. Hirai, J.D. Spikes, H. Eyring, The Mechanical Properties of Rat Tail Tendon., J. Gen. Physiol. 43 (1959) 265–83. doi:10.1085/jgp.43.2.265.

[101] K. Legerlotz, G.P. Riley, H.R.C. Screen, Specimen dimensions influence the measurement of material properties in tendon fascicles., J. Biomech. 43 (2010) 2274–80. doi:10.1016/j.jbiomech.2010.04.040.

[102] X.T. Wang, R.F. Ker, R.M. Alexander, Fatigue rupture of wallaby tail tendons., J. Exp. Biol. 198 (1995) 847–52.

[103] F. Bianchi, F. Hofmann, A.J. Smith, M.S. Thompson, Probing multi-scale mechanical damage in connective tissues using X-ray diffraction, Acta Biomater. 45 (2016) 321–327. doi:10.1016/j.actbio.2016.08.027.

[104] J.L. Zitnay, Y. Li, Z. Qin, B.H. San, B. Depalle, S.P. Reese, M.J. Buehler, S.M. Yu, J.A. Weiss, Molecular level detection and localization of mechanical damage in collagen enabled by collagen hybridizing peptides, Nat. Commun. 8 (2017) 14913. doi:10.1038/ncomms14913.

[105] P. Provenzano, R. Vanderby, Collagen fibril morphology and organization: implications for force transmission in ligament and tendon., Matrix Biol. 25 (2006) 71–84. doi:10.1016/j.matbio.2005.09.005.

[106] T. Starborg, Y. Lu, A. Huffman, D.F. Holmes, K.E. Kadler, Electron microscope 3D reconstruction of branched collagen fibrils in vivo., Scand. J. Med. Sci. Sports. 19 (2009) 547–52. doi:10.1111/j.1600-0838.2009.00907.x.

[107] T. Watanabe, Y. Imamura, Y. Hosaka, H. Ueda, K. Takehana, Graded Arrangement of Collagen Fibrils in the Equine Superficial Digital Flexor Tendon, Connect. Tissue Res. 48 (2007) 332–337. doi:10.1080/03008200701692800.

[108] S.E. Szczesny, K.L. Fetchko, G.R. Dodge, D.M. Elliott, Evidence that interfibrillar load transfer in tendon is supported by small diameter fibrils and not extrafibrillar tissue components, J. Orthop. Res. (2017). doi:10.1002/jor.23517.

[109] K. Legerlotz, G.C. Jones, H.R.C. Screen, G.P. Riley, Cyclic loading of tendon fascicles using a novel fatigue loading system increases interleukin-6 expression by tenocytes, Scand. J. Med. Sci. Sport. 23 (2013). doi:10.1111/j.1600-0838.2011.01410.x.

[110] J. Clemmer, J. Liao, D. Davis, M.F. Horstemeyer, L.N. Williams, A mechanistic study for strain rate sensitivity of rabbit patellar tendon., J. Biomech. 43 (2010) 2785–91. doi:10.1016/j.jbiomech.2010.06.009.

[111] M.R. Buckley, J.J. Sarver, B.R. Freedman, L.J. Soslowsky, The dynamics of collagen uncrimping and lateral contraction in tendon and the effect of ionic concentration., J. Biomech. 46 (2013) 2242–9. doi:10.1016/j.jbiomech.2013.06.029.

[112] S.P. Reese, J.A. Weiss, Tendon fascicles exhibit a linear correlation between Poisson's ratio and force during uniaxial stress relaxation., J. Biomech. Eng. 135 (2013) 34501. doi:10.1115/1.4023134.

[113] L. Yin, D.M. Elliott, A biphasic and transversely isotropic mechanical model for tendon: application to mouse tail fascicles in uniaxial tension., J. Biomech. 37 (2004) 907–16. doi:10.1016/j.jbiomech.2003.10.007.

[114] H.-J. Jung, G. Vangipuram, M.B. Fisher, G. Yang, S. Hsu, J. Bianchi, C. Ronholdt, S.L.-Y. Woo, The effects of multiple freeze-thaw cycles on the biomechanical properties of the human bone-patellar tendon-bone allograft, J. Orthop. Res. 29 (2011) 1193–1198. doi:10.1002/jor.21373.

[115] K.L. Goh, Y. Chen, S.M. Chou, A. Listrat, D. Bechet, T.J. Wess, Effects of frozen storage temperature on the elasticity of tendons from a small murine model., Animal. 4 (2010) 1613–7. doi:10.1017/S1751731110000698.

[116] D.K. Moon, S.L.-Y. Woo, Y. Takakura, M.T. Gabriel, S.D. Abramowitch, The effects of refreezing on the viscoelastic and tensile properties of ligaments, 2006. doi:10.1016/j.jbiomech.2005.02.012.

[117] G. Lee, A. Kumar, E. Berkson, N. Verma, B. Bach, N. Hallab, A Biomechanical Analysis of Bone-Patellar Tendon-Bone Grafts After Repeat Freeze-Thaw Cycles in a Cyclic Loading Model, J. Knee Surg. 22 (2009) 111–113. doi:10.1055/s-0030-1247734.

[118] E.Y. Chang, W.C. Bae, S. Statum, J. Du, C.B. Chung, Effects of Repetitive Freeze–thawing Cycles on T2 and T2* of the Achilles Tendon, 83 (2014) 349–353. doi:10.1016/j.ejrad.2013.10.014.

[119] P. Clavert, J.F. Kempf, F. Bonnomet, P. Boutemy, L. Marcelin, J.L. Kahn, Effects of Freezing/Thawing on the Biomechanical Properties of Human Tendons, Surg. Radiol. Anat. 23 (2001) 259–262. doi:10.1007/s00276-001-0259-8.

[120] C.W. Smith, I.S. Young, J.N. Kearney, Mechanical Properties of Tendons: Changes with Sterilization and Preservation, 118 (1996) 56–61.

[121] H.J. Park, K. Urabe, K. Naruse, K. Onuma, N. Nemoto, M. Itoman, The effect of cryopreservation or heating on the mechanical properties and histomorphology of rat bone-patellar tendon-bone, Cell Tissue Bank. 10 (2009) 11–18. doi:10.1007/s10561-008-9109-9.

[122] B.H. Ng, S.M. Chou, B.H. Lim, A. Chong, The Changes in the Tensile Properties of Tendons after Freeze Storage in Saline Solution, Proc. Inst. Mech. Eng. Part H J. Eng. Med. 219 (2005) 387–392. doi:10.1243/095441105X63309.

[123] S. Giannini, R. Buda, F. Di Caprio, P. Agati, A. Bigi, V. De Pasquale, A. Ruggeri, Effects of freezing on the biomechanical and structural properties of human posterior tibial tendons., Int. Orthop. 32 (2008) 145–51. doi:10.1007/s00264-006-0297-2.

[124] S.E. Szczesny, J.L. Caplan, P. Pedersen, D.M. Elliott, Quantification of Interfibrillar Shear Stress in Aligned Soft Collagenous Tissues via Notch Tension Testing., Sci. Rep. 5 (2015) 14649. doi:10.1038/srep14649.

[125] A. Ozcelikkale, B. Han, Thermal destabilization of collagen matrix hierarchical structure by freeze/thaw, PLoS One. 11 (2016) e0146660. doi:10.1371/journal.pone.0146660.

[126] S. Park, A. Seawright, S. Park, J. Craig Dutton, F. Grinnell, B. Han, Preservation of tissue microstructure and functionality during freezing by modulation of cytoskeletal structure, J. Mech. Behav. Biomed. Mater. 45 (2015) 32–44. doi:10.1016/j.jmbbm.2015.01.014.

[127] Z. Guo, J.W. Freeman, J.G. Barrett, R. De Vita, Quantification of Strain Induced Damage in Medial Collateral Ligaments, J. Biomech. Eng. 137 (2015) 071011. doi:10.1115/1.4030532.

[128] A. Arampatzis, A. Peper, S. Bierbaum, K. Albracht, Plasticity of human Achilles

tendon mechanical and morphological properties in response to cyclic strain., J. Biomech. 43 (2010) 3073–9. doi:10.1016/j.jbiomech.2010.08.014.

[129] A. Bruneau, N. Champagne, P. Cousineau-Pelletier, G. Parent, E. Langelier, Preparation of Rat Tail Tendons for Biomechanical and Mechanobiological Studies, J. Vis. Exp. 41 (2010) e2176–e2176. doi:10.3791/2176.

[130] R.W. Rowe, The structure of rat tail tendon., Connect. Tissue Res. 14 (1985) 9–20.

[131] R. Strocchi, L. Leonardi, S. Guizzardi, M. Marchini, A. Ruggeri, Ultrastructural aspects of rat tail tendon sheaths., J. Anat. 140 (Pt 1 (1985) 57–67.

[132] H. Hori, T. Fukutani, H. Nakane, S. Iino, Y. Nojyo, Participation of ventral and dorsal tail muscles in bending movements of rat tail, Anat. Sci. Int. 86 (2011) 194–203. doi:10.1007/s12565-011-0110-1.

[133] A.J. Schwartz, D.C. Sarver, K.B. Sugg, J.T. Dzierzawski, J.P. Gumucio, C.L. Mendias, p38 MAPK signaling in postnatal tendon growth and remodeling., PLoS One. 10 (2015) e0120044. doi:10.1371/journal.pone.0120044.

[134] J.P. Gumucio, M.A. Korn, A.L. Saripalli, M.D. Flood, A.C. Phan, S.M. Roche, E.B. Lynch, D.R. Claflin, A. Bedi, C.L. Mendias, Aging-associated exacerbation in fatty degeneration and infiltration after rotator cuff tear., J. Shoulder Elb. Surg. 23 (2014) 99–108. doi:10.1016/j.jse.2013.04.011.

[135] D. Lambertz, C. Pérot, M.I. Almeida-Silveira, F. Goubel, Changes in stiffness induced by hindlimb suspension in rat Achilles tendon, Eur. J. Appl. Physiol. 81 (2000) 252–257. doi:10.1007/s004210050039.

[136] P. Eliasson, T. Andersson, P. Aspenberg, Rat Achilles tendon healing: mechanical loading and gene expression, J. Appl. Physiol. 107 (2009) 399–407. doi:10.1152/japplphysiol.91563.2008.

[137] P. Eliasson, A. Fahlgren, B. Pasternak, P. Aspenberg, Unloaded rat Achilles tendons continue to grow, but lose viscoelasticity, J. Appl. Physiol. 103 (2007) 459–463. doi:10.1152/japplphysiol.01333.2006.

[138] M.N. van Sterkenburg, G.M.M.J. Kerkhoffs, R.P. Kleipool, C. Niek van Dijk, The plantaris tendon and a potential role in mid-portion Achilles tendinopathy: an observational anatomical study, J. Anat. 218 (2011) 336–341. doi:10.1111/j.1469-7580.2011.01335.x.

[139] M.N. van Sterkenburg, G.M.M.J. Kerkhoffs, C.N. van Dijk, Good outcome after stripping the plantaris tendon in patients with chronic mid-portion Achilles tendinopathy, Knee Surgery, Sport. Traumatol. Arthrosc. 19 (2011) 1362–1366. doi:10.1007/s00167-011-1514-0.

[140] F. Lintz, A. Higgs, M. Millett, T. Barton, M. Raghuvanshi, M.A. Adams, I.G. Winson, The role of Plantaris Longus in Achilles tendinopathy: A biomechanical study, Foot Ankle Surg. 17 (2011) 252–255. doi:10.1016/j.fas.2010.08.004.

[141] Y. Nakagawa, M. Totsuka, T. Sato, Y. Fukuda, K. Hirota, Effect of disuse on the

ultrastructure of the achilles tendon in rats, Eur. J. Appl. Physiol. Occup. Physiol. 59 (1989) 239–242. doi:10.1007/BF02386194.

[142] R.S. Bear, The Structure of Collagen Fibrils, Adv. Protein Chem. 7 (1952) 69–160. doi:10.1016/S0065-3233(08)60018-2.

[143] M. Benjamin, E. Kaiser, S. Milz, Structure-function relationships in tendons: a review., J. Anat. 212 (2008) 211–28. doi:10.1111/j.1469-7580.2008.00864.x.

[144] C.T. Thorpe, G.P. Riley, H.L. Birch, P.D. Clegg, H.R.C. Screen, Fascicles and the interfascicular matrix show adaptation for fatigue resistance in energy storing tendons, Acta Biomater. 56 (2017) 58–64. doi:10.1016/j.actbio.2016.06.012.

[145] J.H.-C. Wang, Mechanobiology of tendon, J. Biomech. 39 (2006) 1563–1582. doi:10.1016/j.jbiomech.2005.05.011.

[146] C.M. McNeilly, A.J. Banes, M. Benjamin, J.R. Ralphs, Tendon cells in vivo form a three dimensional network of cell processes linked by gap junctions., J. Anat. (1996) 593–600. doi:10.1046/j.1469-7580.1997.19030477.x.

[147] J.R. Ralphs, M. Benjamin, A.D. Waggett, D.C. Russell, K. Messner, J. Gao, Regional differences in cell shape and gap junction expression in rat Achilles tendon: relation to fibrocartilage differentiation., J. Anat. (1998) 215–22. doi:10.1046/j.1469-7580.1998.19320215.x.

[148] N.S. Kalson, Y. Lu, S.H. Taylor, T. Starborg, D.F. Holmes, K.E. Kadler, A structure-based extracellular matrix expansion mechanism of fibrous tissue growth, Elife. 4 (2015) e05958. doi:10.7554/eLife.05958.

[149] A.H. Lee, D.M. Elliott, Freezing does not alter multiscale tendon mechanics and damage mechanisms in tension., Ann. N. Y. Acad. Sci. 1409 (2017) 85–94. doi:10.1111/nyas.13460.

[150] X. Chen, O. Nadiarynkh, S. Plotnikov, P.J. Campagnola, Second harmonic generation microscopy for quantitative analysis of collagen fibrillar structure, Nat. Protoc. 7 (2012) 654–669. doi:10.1038/nprot.2012.009.

[151] X. Pang, J.-P. Wu, G.T. Allison, J. Xu, J. Rubenson, M.-H. Zheng, D.G. Lloyd, B. Gardiner, A. Wang, T.B. Kirk, Three dimensional microstructural network of elastin, collagen, and cells in Achilles tendons, J. Orthop. Res. (2017). doi:10.1002/jor.23240.

[152] D.T. Fung, J.B. Sereysky, J. Basta-Pljakic, D.M. Laudier, R. Huq, K.J. Jepsen, M.B. Schaffler, E. Flatow, Second harmonic generation imaging and Fourier transform spectral analysis reveal damage in fatigue-loaded tendons., Ann. Biomed. Eng. 38 (2010) 1741–51. doi:10.1007/s10439-010-9976-7.

[153] S.L. Simpson, M.S. Hertzog, R.H. Barja, The plantaris tendon graft: An ultrasound study, J. Hand Surg. Am. 16 (1991) 708–711. doi:10.1016/0363-5023(91)90198-K.

[154] A.J. Freeman, N.A. Jacobson, Q.A. Fogg, Anatomical variations of the plantaris

muscle and a potential role in patellofemoral pain syndrome, Clin. Anat. 21 (2008) 178–181. doi:10.1002/ca.20594.

[155] F.J. Harvey, G. Chu, P.M. Harvey, Surgical availability of the plantaris tendon., J. Hand Surg. Am. 8 (1983) 243–7. doi:10.1016/S0363-5023(83)80151-8.

[156] S.R. Nayak, A. Krishnamurthy, L. Ramanathan, A. V Ranade, L. V Prabhu, P.J. Jiji, R. Rai, G.K. Chettiar, B.K. Potu, Anatomy of plantaris muscle: a study in adult Indians., Clin. Ter. 161 (2010) 249–52.

[157] A. Saxena, D. Bareither, Magnetic resonance and cadaveric findings of the incidence of plantaris tendon., Foot Ankle Int. 21 (2000) 570–2.

[158] M.A. dos Santos, J.A. Bertelli, P.R. Kechele, H. Duarte, Anatomical study of the plantaris tendon: reliability as a tendo-osseous graft, Surg. Radiol. Anat. 31 (2009) 59–61. doi:10.1007/s00276-008-0391-9.

[159] J. Bojsen-Møller, S.P. Magnusson, Heterogeneous Loading of the Human Achilles Tendon In Vivo, Exerc. Sport Sci. Rev. 43 (2015) 190–197. doi:10.1249/JES.0000000000000062.

[160] P. Szaro, G. Witkowski, R. Śmigielski, P. Krajewski, B. Ciszek, Fascicles of the adult human Achilles tendon – An anatomical study, Ann. Anat. - Anat. Anzeiger. 191 (2009) 586–593. doi:10.1016/j.aanat.2009.07.006.

[161] M. dos S. de Almeida, K.M. de Freitas, L.P. Oliveira, C.P. Vieira, F.D.R. Guerra, M.A.H. Dolder, E.R. Pimentel, Acupuncture increases the diameter and reorganisation of collagen fibrils during rat tendon healing., Acupunct. Med. 33 (2015) 51–7. doi:10.1136/acupmed-2014-010548.

[162] M. Franchi, A. Trirè, M. Quaranta, E. Orsini, V. Ottani, Collagen Structure of Tendon Relates to Function, Sci. World J. 7 (2007) 404–420. doi:10.1100/tsw.2007.92.

[163] V.M. Savage, A.P. Allen, J.H. Brown, J.F. Gillooly, A.B. Herman, W.H. Woodruff, G.B. West, Scaling of number, size, and metabolic rate of cells with body size in mammals., Proc. Natl. Acad. Sci. U. S. A. 104 (2007) 4718–23. doi:10.1073/pnas.0611235104.

[164] M.S.C. Godinho, C.T. Thorpe, S.E. Greenwald, H.R.C. Screen, Elastin is Localised to the Interfascicular Matrix of Energy Storing Tendons and Becomes Increasingly Disorganised With Ageing, Sci. Rep. 7 (2017) 9713. doi:10.1038/s41598-017-09995-4.

[165] C.T. Thorpe, C.P. Udeze, H.L. Birch, P.D. Clegg, H.R.C. Screen, Capacity for sliding between tendon fascicles decreases with ageing in injury prone equine tendons: a possible mechanism for age-related tendinopathy?, Eur. Cell. Mater. 25 (2013) 48–60. doi:10.22203/eCM.v025a04.

[166] J.C. Patterson-Kane, D.L. Becker, T. Rich, The Pathogenesis of Tendon Microdamage in Athletes: the Horse as a Natural Model for Basic Cellular Research, J. Comp. Pathol. 147 (2012) 227–247. doi:10.1016/J.JCPA.2012.05.010.

[167] J.M. Rijkelijkhuizen, G.C. Baan, A. de Haan, C.J. de Ruiter, P.A. Huijing, Extramuscular myofascial force transmission for in situ rat medial gastrocnemius and plantaris muscles in progressive stages of dissection., J. Exp. Biol. 208 (2005) 129–40. doi:10.1242/jeb.01360.

[168] C.A. Goodman, D.M. Mabrey, J.W. Frey, M.H. Miu, E.K. Schmidt, P. Pierre, T.A. Hornberger, Novel insights into the regulation of skeletal muscle protein synthesis as revealed by a new nonradioactive *in vivo* technique, FASEB J. 25 (2011) 1028–1039. doi:10.1096/fj.10-168799.

[169] T.J. Kirby, J.J. McCarthy, C.A. Peterson, C.S. Fry, Synergist Ablation as a Rodent Model to Study Satellite Cell Dynamics in Adult Skeletal Muscle, in: Methods Mol. Biol., 2016: pp. 43–52. doi:10.1007/978-1-4939-3810-0_4.

[170] S.M.L. Terena, K.P.S. Fernandes, S.K. Bussadori, A.M. Deana, R.A. Mesquita-Ferrari, Systematic review of the synergist muscle ablation model for compensatory hypertrophy, Rev. Assoc. Med. Bras. 63 (2017) 164–172. doi:10.1590/1806-9282.63.02.164.

[171] G.G. Handsfield, J.M. Inouyea, L.C. Slane, D.G. Thelen, G.W. Miller, S.S. Blemkera, A 3D model of the Achilles tendon to determine the mechanisms underlying nonuniform tendon displacements, J. Biomech. 51 (2017) 17–25. doi:10.1152/japplphysiol.01249.2013.

[172] L.C. Slane, D.G. Thelen, Non-uniform displacements within the Achilles tendon observed during passive and eccentric loading, J. Biomech. 47 (2014) 2831–2835. doi:10.1016/j.jbiomech.2014.07.032.

[173] J.R. Franz, L.C. Slane, K. Rasske, D.G. Thelen, Non-uniform in vivo deformations of the human Achilles tendon during walking, Gait Posture. 41 (2015) 192–197. doi:10.1016/j.gaitpost.2014.10.001.

[174] D. Rowson, M.M. Knight, H.R.C. Screen, Zonal variation in primary cilia elongation correlates with localized biomechanical degradation in stress deprived tendon, J. Orthop. Res. 34 (2016) 2146–2153. doi:10.1002/jor.23229.

[175] S.E. Szczesny, C. Aeppli, A. David, R.L. Mauck, Fatigue loading of tendon results in collagen kinking and denaturation but does not change local tissue mechanics, J. Biomech. 71 (2018) 251–256. doi:10.1016/J.JBIOMECH.2018.02.014.

[176] A.H. Lee, D.M. Elliott, Comparative Multi-scale Hierarchical Structure of the Tail, Plantaris and Achilles Tendons in the Rat, J. Anat. (in press) (2018).

[177] P. Szaro, G. Witkowski, B. Ciszek, Anatomy of the common calcaneal tendon in rat (Rattus norwegicus), Polish J. Nat. Sci. 27 (2012) 339–346.

[178] T. Finni, M. Bernabei, G.C. Baan, W. Noort, C. Tijs, H. Maas, Non-uniform displacement and strain between the soleus and gastrocnemius subtendons of rat Achilles tendon, Scand. J. Med. Sci. Sports. 28 (2018) 1009–1017. doi:10.1111/sms.13001.

[179] O.A. Komolafe, T.C. Doehring, Fascicle-Scale Loading and Failure Behavior of

the Achilles Tendon, J. Biomech. Eng. 132 (2010) 021004. doi:10.1115/1.4000696.

[180] S. Rigozzi, R. Müller, A. Stemmer, J.G. Snedeker, Tendon glycosaminoglycan proteoglycan sidechains promote collagen fibril sliding-AFM observations at the nanoscale., J. Biomech. 46 (2013) 813–8. doi:10.1016/j.jbiomech.2012.11.017.

[181] W.M. Han, S.-J. Heo, T.P. Driscoll, L.J. Smith, R.L. Mauck, D.M. Elliott, Macro- to microscale strain transfer in fibrous tissues is heterogeneous and tissue-specific., Biophys. J. 105 (2013) 807–17. doi:10.1016/j.bpj.2013.06.023.

[182] G.W. Hess, Achilles tendon rupture: a review of etiology, population, anatomy, risk factors, and injury prevention., Foot Ankle Spec. 3 (2010) 29–32. doi:10.1177/1938640009355191.

[183] S.P. Magnusson, M. Kjaer, The impact of loading, unloading, ageing and injury on the human tendon, J. Physiol. (2018). doi:10.1113/JP275450.

[184] Y. Nakagawa, K. Hayashi, N. Yamamoto, K. Nagashima, Age-related changes in biomechanical properties of the Achilles tendon in rabbits, Eur. J. Appl. Physiol. Occup. Physiol. 73 (1996) 7–10. doi:10.1007/BF00262803.

[185] G.A. Johnson, D.M. Tramaglini, R.E. Levine, K. Ohno, N.-Y. Choi, S. L-Y. Woo, Tensile and viscoelastic properties of human patellar tendon, J. Orthop. Res. 12 (1994) 796–803. doi:10.1002/jor.1100120607.

[186] C.M. Flahiff, A.T. Brooks, J.M. Hollis, J.L. Vander Schilden, R.W. Nicholas, Biomechanical Analysis of Patellar Tendon Allografts as a Function of Donor Age, Am. J. Sports Med. 23 (1995) 354–358. doi:10.1177/036354659502300319.

[187] K. Kubo, H. Kanehisa, M. Miyatani, M. Tachi, T. Fukunaga, Effect of low-load resistance training on the tendon properties in middle-aged and elderly women, Acta Physiol. Scand. 178 (2003) 25–32. doi:10.1046/j.1365-201X.2003.01097.x.

[188] J.I. Quinlan, C.N. Maganaris, M. V Franchi, K. Smith, P.J. Atherton, N.J. Szewczyk, P.L. Greenhaff, B.E. Phillips, J.I. Blackwell, C. Boereboom, J.P. Williams, J. Lund, M. V Narici, Muscle and Tendon Contributions to Reduced Rate of Torque Development in Healthy Older Males, Journals Gerontol. Ser. A. 73 (2018) 539–545. doi:10.1093/gerona/glx149.

[189] L. Stenroth, J. Peltonen, N.J. Cronin, S. Sipilä, T. Finni, Age-related differences in Achilles tendon properties and triceps surae muscle architecture in vivo, J. Appl. Physiol. 113 (2012) 1537–1544. doi:10.1152/japplphysiol.00782.2012.

[190] K.L. Goh, D.F. Holmes, H.-Y. Lu, S. Richardson, K.E. Kadler, P.P. Purslow, T.J. Wess, Ageing changes in the tensile properties of tendons: influence of collagen fibril volume fraction., J. Biomech. Eng. 130 (2008) 021011. doi:10.1115/1.2898732.

[191] C.T. Thorpe, G.P. Riley, H.L. Birch, P.D. Clegg, H.R.C. Screen, Fascicles from energy-storing tendons show an age-specific response to cyclic fatigue loading., J R Soc Interface. 11 (2014). doi:10.1098/rsif.2013.1058.

[192] C.T. Thorpe, G.P. Riley, H.L. Birch, P.D. Clegg, H.R.C. Screen, Fascicles and the interfascicular matrix show decreased fatigue life with ageing in energy storing tendons, Acta Biomater. 56 (2017) 58–64. doi:10.1016/J.ACTBIO.2017.03.024.

[193] Y. NAKAGAWA, T. MAJIMA, K. NAGASHIMA, Effect of ageing on ultrastructure of slow and fast skeletal muscle tendon in rabbit Achilles tendons, Acta Physiol. Scand. 152 (1994) 307–313. doi:10.1111/j.1748-1716.1994.tb09810.x.

[194] J. Kohler, C. Popov, B. Klotz, P. Alberton, W.C. Prall, F. Haasters, S. Müller-Deubert, R. Ebert, L. Klein-Hitpass, F. Jakob, M. Schieker, D. Docheva, Uncovering the cellular and molecular changes in tendon stem/progenitor cells attributed to tendon aging and degeneration, Aging Cell. 12 (2013) 988–999. doi:10.1111/acel.12124.

[195] J. Zhang, J.H.-C. Wang, Moderate Exercise Mitigates the Detrimental Effects of Aging on Tendon Stem Cells, PLoS One. 10 (2015) e0130454. doi:10.1371/journal.pone.0130454.

[196] S.B. Bruehlmann, J.R. Matyas, N.A. Duncan, ISSLS Prize Winner: Collagen Fibril Sliding Governs Cell Mechanics in the Anulus Fibrosus, Spine (Phila. Pa. 1976). 29 (2004) 2612–2620. doi:10.1097/01.brs.0000146465.05972.56.

[197] E.M. Spiesz, C.T. Thorpe, P.J. Thurner, H.R.C. Screen, Structure and collagen crimp patterns of functionally distinct equine tendons, revealed by quantitative polarised light microscopy (qPLM), Acta Biomater. 70 (2018) 281–292. doi:10.1016/J.ACTBIO.2018.01.034.

[198] E.M. Spiesz, C.T. Thorpe, S. Chaudhry, G.P. Riley, H.L. Birch, P.D. Clegg, H.R.C. Screen, Tendon extracellular matrix damage, degradation and inflammation in response to in vitro overload exercise, J. Orthop. Res. 33 (2015) 889–897. doi:10.1002/jor.22879.

[199] C. Woodyard, Exploring the therapeutic effects of yoga and its ability to increase quality of life., Int. J. Yoga. 4 (2011) 49–54. doi:10.4103/0973-6131.85485.

[200] P. Page, Current concepts in muscle stretching for exercise and rehabilitation., Int. J. Sports Phys. Ther. 7 (2012) 109–19.

[201] K.J. Sherman, D.C. Cherkin, R.D. Wellman, A.J. Cook, R.J. Hawkes, K. Delaney, R.A. Deyo, A Randomized Trial Comparing Yoga, Stretching, and a Self-care Book for Chronic Low Back Pain, Arch. Intern. Med. 171 (2011) 2019. doi:10.1001/archinternmed.2011.524.

[202] R.D. Herbert, A.M. Moseley, J.E. Butler, S.C. Gandevia, Change in length of relaxed muscle fascicles and tendons with knee and ankle movement in humans., J. Physiol. 539 (2002) 637–45. doi:10.1113/JPHYSIOL.2001.012756.

[203] C.I. Morse, H. Degens, O.R. Seynnes, C.N. Maganaris, D.A. Jones, The acute effect of stretching on the passive stiffness of the human gastrocnemius muscle tendon unit., J. Physiol. 586 (2008) 97–106. doi:10.1113/jphysiol.2007.140434.

[204] H. Chtourou, A. Aloui, O. Hammouda, A. Chaouachi, K. Chamari, N. Souissi, Effect of static and dynamic stretching on the diurnal variations of jump performance in soccer players., PLoS One. 8 (2013) e70534. doi:10.1371/journal.pone.0070534.

[205] S.J. Pearson, G.N.L. Onambele, Acute Changes In Knee-Extensors Torque, Fiber Pennation, and Tendon Characteristics, Chronobiol. Int. (2009).

[206] K. Gardner, M. Lavagnino, M. Egerbacher, S.P. Arnoczky, Re-establishment of cytoskeletal tensional homeostasis in lax tendons occurs through an actin-mediated cellular contraction of the extracellular matrix., J. Orthop. Res. 30 (2012) 1695–701. doi:10.1002/jor.22131.

[207] A.S. Liu, H. Wang, C.R. Copeland, C.S. Chen, V.B. Shenoy, D.H. Reich, E. Al, Matrix viscoplasticity and its shielding by active mechanics in microtissue models: experiments and mathematical modeling, Sci. Rep. 6 (2016) 33919. doi:10.1038/srep33919.

[208] H. Mohammadi, P.D. Arora, C.A. Simmons, P.A. Janmey, C.A. McCulloch, Inelastic behaviour of collagen networks in cell–matrix interactions and mechanosensation, J. R. Soc. Interface. 12 (2014). doi:10.1098/rsif.2014.1074.

[209] S.E. Szczesny, R.L. Mauck, The Nuclear Option: Evidence Implicating the Cell Nucleus in Mechanotransduction, J. Biomech. Eng. 139 (2017) 021006. doi:10.1115/1.4035350.

[210] K.M. Riching, B.L. Cox, M.R. Salick, C. Pehlke, A.S. Riching, S.M. Ponik, B.R. Bass, W.C. Crone, Y. Jiang, A.M. Weaver, K.W. Eliceiri, P.J. Keely, 3D collagen alignment limits protrusions to enhance breast cancer cell persistence., Biophys. J. 107 (2014) 2546–58. doi:10.1016/j.bpj.2014.10.035.

[211] J.R. Lange, B. Fabry, Cell and tissue mechanics in cell migration., Exp. Cell Res. 319 (2013) 2418–23. doi:10.1016/j.yexcr.2013.04.023.

[212] P. Maiuri, J.-F. Rupprecht, S. Wieser, V. Ruprecht, O. Bénichou, N. Carpi, M. Coppey, S. De Beco, N. Gov, C.-P. Heisenberg, C. Lage Crespo, F. Lautenschlaeger, M. Le Berre, A.-M. Lennon-Dumenil, M. Raab, H.-R. Thiam, M. Piel, M. Sixt, R. Voituriez, Actin Flows Mediate a Universal Coupling between Cell Speed and Cell Persistence, Cell. 161 (2015) 374–386. doi:10.1016/J.CELL.2015.01.056.

[213] D.E. Discher, P. Janmey, Y.-L. Wang, Tissue cells feel and respond to the stiffness of their substrate., Science. 310 (2005) 1139–43. doi:10.1126/science.1116995.

[214] M. Prager-Khoutorsky, A. Lichtenstein, R. Krishnan, K. Rajendran, A. Mayo, Z. Kam, B. Geiger, A.D. Bershadsky, Fibroblast polarization is a matrix-rigidity-dependent process controlled by focal adhesion mechanosensing, Nat. Cell Biol. 13 (2011) 1457–1465. doi:10.1038/ncb2370.

[215] P.M. Gilbert, V.M. Weaver, Cellular adaptation to biomechanical stress across length scales in tissue homeostasis and disease, Semin. Cell Dev. Biol. (2016).

doi:10.1016/j.semcdb.2016.09.004.

[216] C.M. Lo, H.B. Wang, M. Dembo, Y.L. Wang, Cell movement is guided by the rigidity of the substrate., Biophys. J. 79 (2000) 144–52. doi:10.1016/S0006-3495(00)76279-5.

[217] T. Yeung, P.C. Georges, L.A. Flanagan, B. Marg, M. Ortiz, M. Funaki, N. Zahir, W. Ming, V. Weaver, P.A. Janmey, Effects of substrate stiffness on cell morphology, cytoskeletal structure, and adhesion, Cell Motil. Cytoskeleton. 60 (2005) 24–34. doi:10.1002/cm.20041.

[218] N. Hammer, D. Huster, S. Fritsch, C. Hädrich, H. Koch, P. Schmidt, F. Sichting, M.F.-X. Wagner, A. Boldt, Do cells contribute to tendon and ligament biomechanics?, PLoS One. 9 (2014) e105037. doi:10.1371/journal.pone.0105037.

[219] G. Zhang, Evaluating the viscoelastic properties of biological tissues in a new way., J. Musculoskelet. Neuronal Interact. 5 (2005) 85–90. doi:10.1038/srep00316.

[220] X.T. Wang, R.F. Ker, Creep rupture of wallaby tail tendons., J. Exp. Biol. 198 (1995) 831–845.

[221] A. Öchsner, Continuum Mechanics of Plasticity, in: Elasto-Plasticity Fram. Struct. Elem., Springer Berlin Heidelberg, Berlin, Heidelberg, 2014: pp. 5–35. doi:10.1007/978-3-662-44225-8_2.

Appendix A

MECHANICAL TESTING DATA OF RAT TAIL TENDON

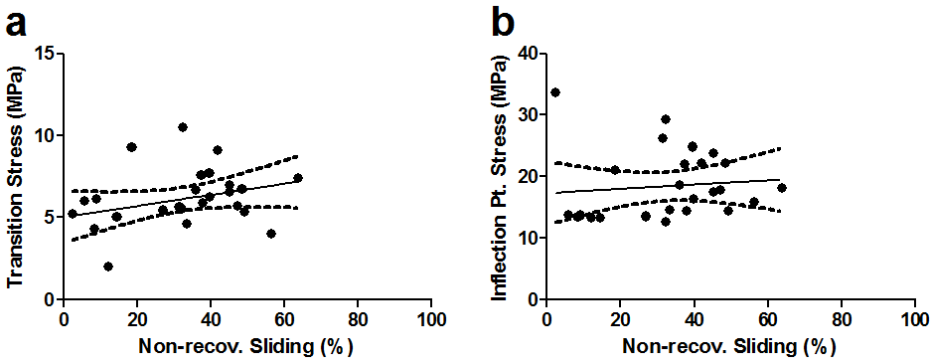

Figure A.1: Transition stress and inflection point stress correlated with non-recoverable sliding. As seen here, the correlations are not significant, suggesting these parameters may be as good as other parameters suggested in the main text.

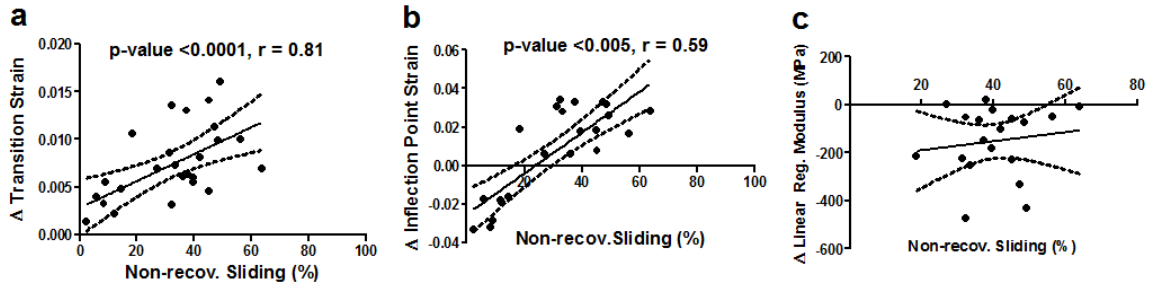

Figure A.2: Δ transition strain, inflection point, strain and linear region modulus correlated with non-recoverable sliding. The Δ transition strain and inflection point strain correlated, but not Δ linear region modulus.

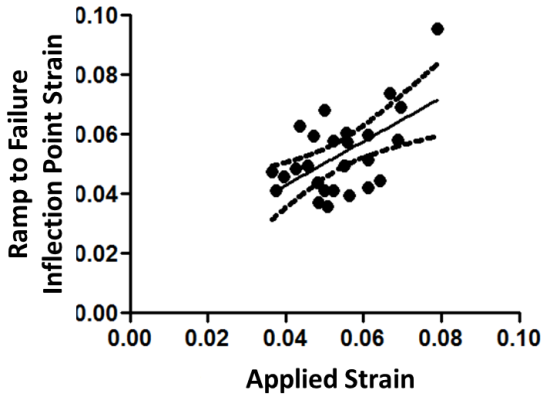

Figure A.3: Relationship between ramp to failure inflection point strain and applied strain. The correlation between applied strain and Ramp to Failure inflection point strain of rat tail tendon (Chapter 3) was significant (p-value <0.005). In addition, the slope was close to 1 (0.73). This relationship suggests that the damage threshold can increase depending on the loading history (i.e., applied strain).

Appendix B

EFFECT OF FREEZING ON RAT TAIL TENDON MECHANICS

Table B.1: Fresh and Frozen tissue-scale parameters. There was no statistical difference between the two groups except for peak strain. However, not all samples failed in the mid-substance and some failure started at the grip, so we decided not to emphasize this difference in the main text.

	Fresh	**Frozen**
Transition Strain		
Initial Ramp	0.017 ± 0.009	0.014 ± 0.006
Ramp to Failure	0.025 ± 0.011	0.020 ± 0.011
Transition Stress (MPa)		
Initial Ramp	6.28 ± 4.75	4.75 ± 1.82
Ramp to Failure	7.70 ± 3.18	6.56 ± 4.43
Linear Reg. Mod (MPa)		
Initial Ramp	1109 ± 323	1166 ± 424
Ramp to Failure	980 ± 298	982 ± 492
Inflection Pt. Strain		
Initial Ramp	0.024 ± 0.012	0.023 ± 0.009
Ramp to Failure	0.037 ± 0.014	0.034 ± 0.010
Inflection Pt. Stress (MPa)		
Initial Ramp	14.5 ± 5.7	15.7 ± 5.8
Ramp to Failure	18.5 ± 5.0	18.9 ± 7.5
Peak Strain	0.071 ± 0.006	0.061 ± 0.007
Peak Stress (MPa)	44.7 ± 13.0	37.3 ± 14.7

Appendix C

HIERARCHICAL STRUCTURE OF RAT TENDONS

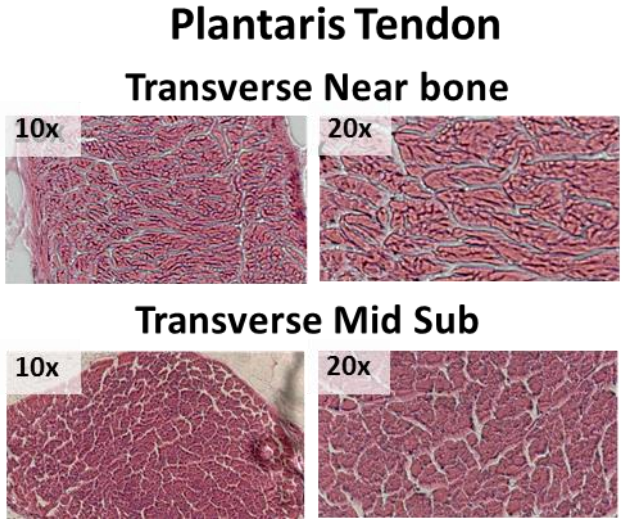

Figure C.1: Transverse sections of plantaris tendon. The histology shows that the microstructure and hierarchical structure (fiber diameter) of plantaris tendon may vary along the length.

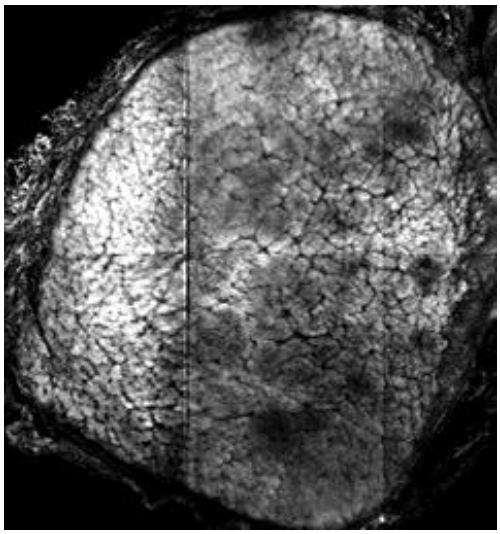

Figure C.2: Transverse SHG signal of plantaris tendon without any fixation. This was to demonstrate that the separation observed in the transverse direction is not a fixation artifact.

Appendix D

TISSUE-SCALE MECHANICS OF RAT TENDONS

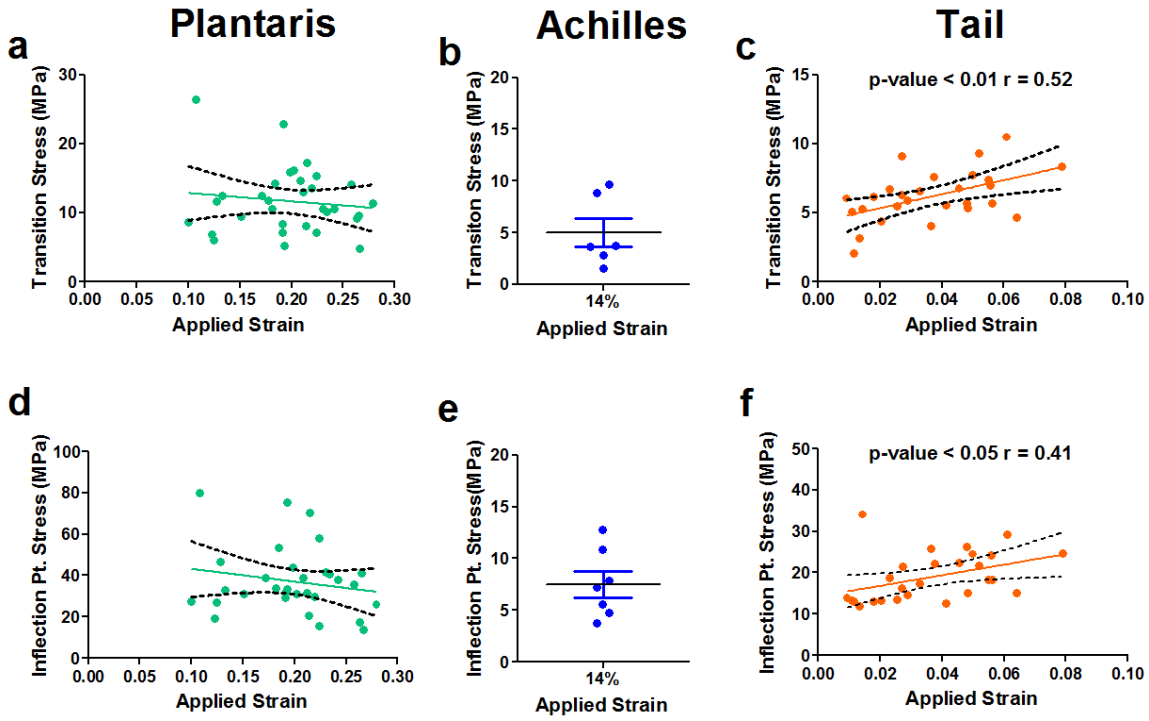

Figure D.1: Tissue-scale parameter of transition and inflection point stresses. As shown in Chapter 3, only the rat tail tendon correlated with the transition and inflection point stresses.

Appendix E

SUPPORTING EVIDENCE FOR FUTURE DIRECTIONS

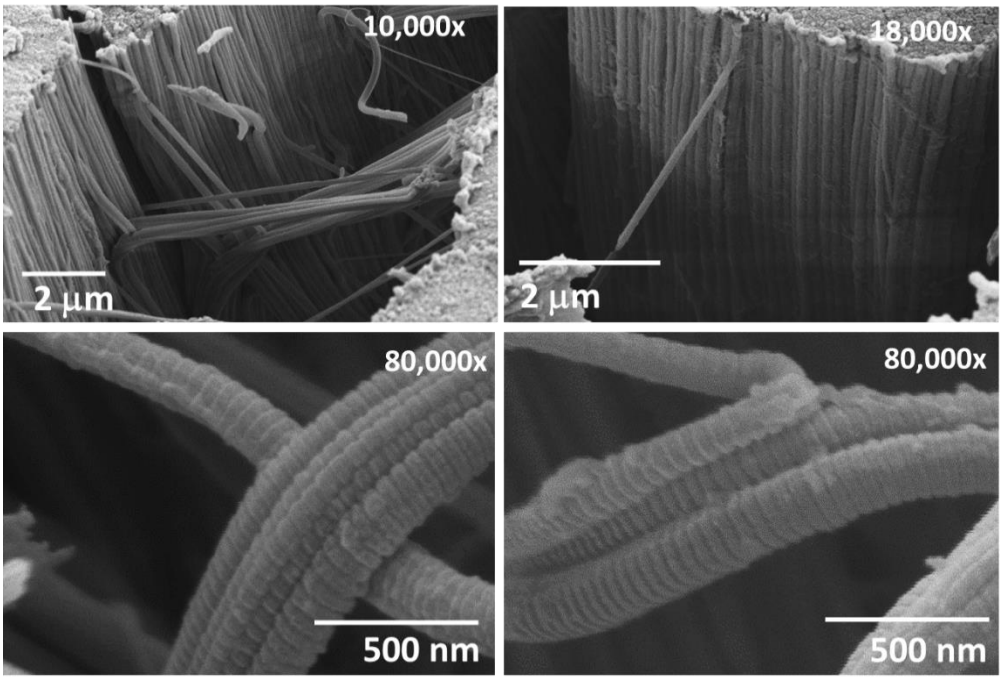

Figure E.1: SEM of bundle of fibrils. In a pilot study, we identified bundles of fibrils bridging between fibers. Analogous to the observation of smaller diameter fibrils bridging larger diameter fibrils, smaller diameter fibers may bridge larger diameter fibers. These structures were observed in a control group, but these connections may be compromised and damaged after mechanical loading.

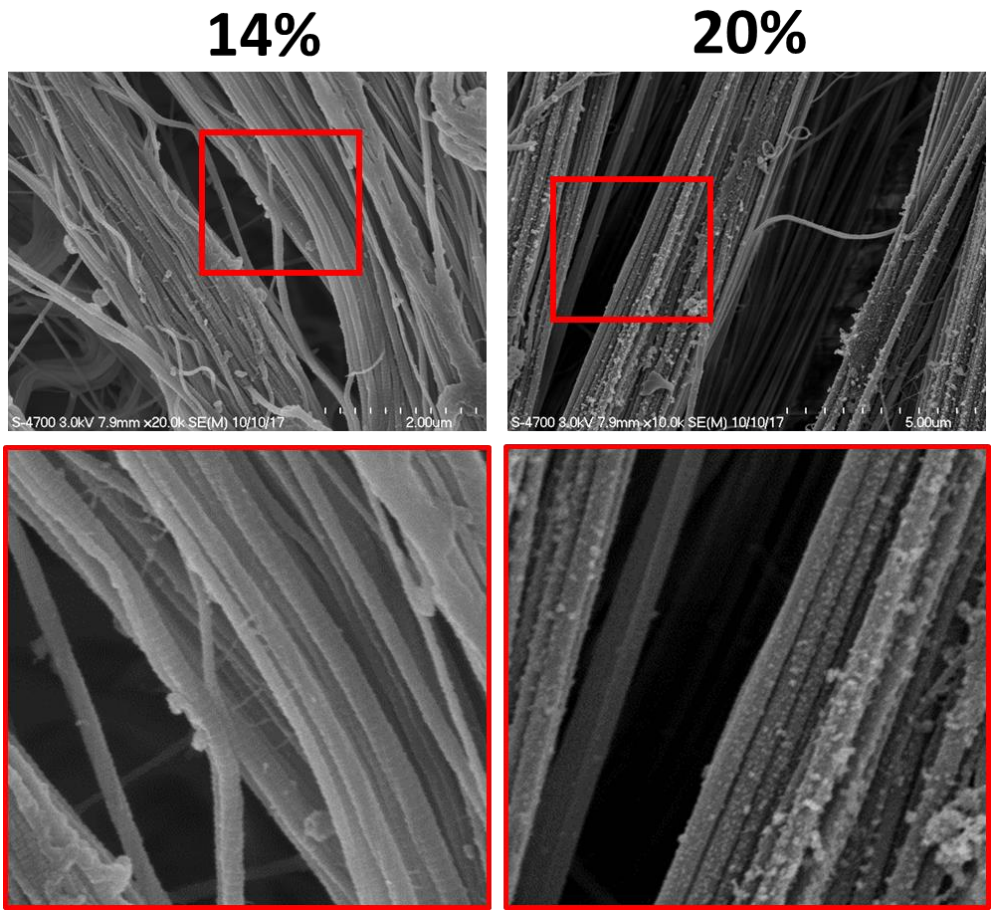

Figure E.2: SEM of plantaris tendon loaded to 14% and 20%. The SEM images show that D-period was absent for the tendon that was loaded to 20%, but not for the one that was loaded to 14%. This pilot study emphasizes the need to find the relationship between fibril deformation and micro-scale deformation measured as photobleached lines.

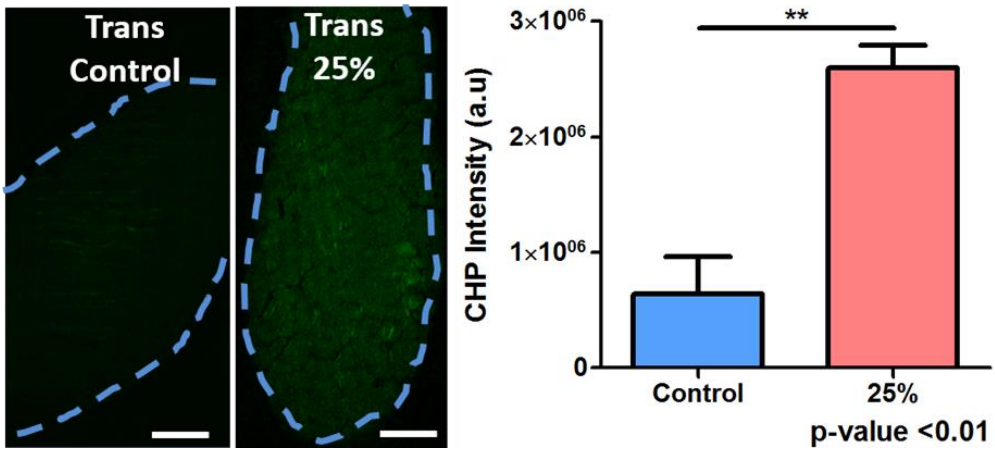

Figure E.3: CHP staining of transverse sections. The CHP intensity of the control section was statistically lower than the section of the tendon that was loaded to 25% The CHP intensity was about 3 times higher for the 25% group compared to the control. This suggests that the CHP intensity increases with mechanical loading. Scale bar: 100 μm.

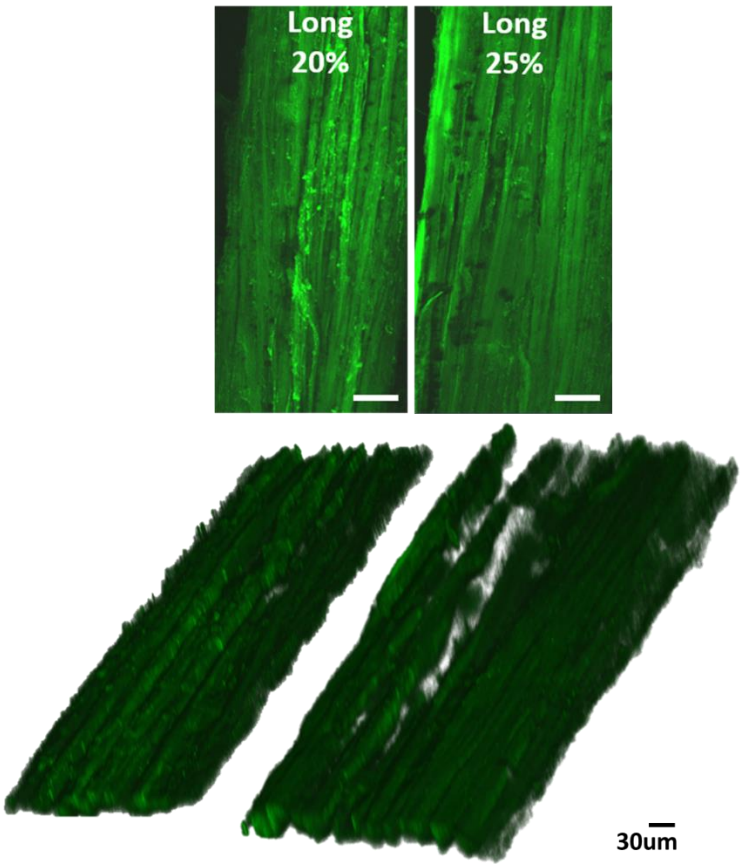

Figure E.4: CHP staining of longitudinal sections. The CHP staining of tendons that were loaded to either 20% and 25% strain showed high CHP intensity. Scale bar: 100 μm. When the longitudinal sections were rendered in 3D, you can make out the microstructure of the tendon, which is speculated to be fiber based on the diameter.